DOKUZ EYLÜL UNIVESITY

GRADUATE SCHOOL OF NATURAL AND APPLIED SCIENCES

PERFORMANCE EVALUATION OF INTERMEDIATE TEMPERATURE SOLID OXIDE FUEL CELL INTEGRATED WITH ADVANCED SUPERCRITICAL CARBON DIOXIDE BRAYTON CYCLES

by

Semanur BEYGÜL

February, 2024

İZMİR

PERFORMANCE EVALUATION OF INTERMEDIATE TEMPERATURE SOLID OXIDE FUEL CELL INTEGRATED WITH ADVANCED SUPERCRITICAL CARBON DIOXIDE BRAYTON CYCLES

A Thesis Submitted to the
Graduate School of Natural and Applied Sciences of Dokuz Eylül University
In Partial Fulfillment of the Requirements for the Degree of Master of Science
in Mechanical Engineering, Thermodynamics Program

by

Semanur BEYGÜL

February, 2024

İZMİR

M.Sc THESIS EXAMINATION RESULT FORM

We have read the thesis entitled **"PERFORMANCE EVALUATION OF INTERMEDIATE TEMPERATURE SOLID OXIDE FUEL CELL INTEGRATED WITH ADVANCED SUPERCRITICAL CARBON DIOXIDE BRAYTON CYCLES"** completed by **SEMANUR BEYGÜL** under supervision of **ASSOC. PROF. DR. YILDIZ KALINCI** and we certify that in our opinion it is fully adequate, in scope and in quality, as a thesis for the degree of Master of Science.

.....

Assoc. Prof. Dr. Yıldız KALINCI

Supervisor

.....	.....
Prof. Dr. Can Özgür ÇOLPAN	Prof. Dr. Zuhal COŞKUN
Jury Member	Jury Member

Prof. Dr. Okan FISTIKOĞLU

Director

Graduate School of Natural and Applied Sciences

ACKNOWLEDGEMENTS

I want to show my sincere appreciation to my advisor, Assoc. Prof. Dr. Yıldız KALINCI, for her invaluable guidance, and deep expertise in developing and shaping this thesis. Her patience, encouragement, and insightful feedback have been invaluable in this research journey.

I extend my heartfelt appreciation to my husband, Hüseyin BEYGÜL, for his unwavering support and understanding during this academic endeavour; his patience and belief have been a tremendous source of strength and motivation for me.

Semanur BEYGÜL

PERFORMANCE EVALUATION OF INTERMEDIATE TEMPERATURE SOLID OXIDE FUEL CELL INTEGRATED WITH ADVANCED SUPERCRITICAL CARBON DIOXIDE BRAYTON CYCLES

ABSTRACT

This thesis examines the investigation of the incorporation of solid oxide fuel cells operating at intermediate temperatures through three different configurations of supercritical carbon dioxide Brayton cycles. The primary objective is to elevate the overall system efficiency by emphasizing the evaluation of waste heat recovery and energy conversion processes. Through the EES program, various operating parameters including temperature, current density, and heat exchanger effectiveness are examined to ascertain their impact on system performance. The investigation spans various aspects, from the impact of characteristics of supercritical carbon dioxide fluid on cycle efficiency to evaluating the performance and efficiency of the intermediate temperature solid oxide fuel cell and hybrid systems. In final part, the research comparatively analyses the efficiencies, and power shares, of solid oxide fuel cell/supercritical carbon dioxide Brayton cycle hybrid systems. The findings offer insights into thorough comprehension of the potential of different hybrid systems.

Keywords: Hybrid system, intermediate temperature solid oxide fuel cell, supercritical carbon dioxide Brayton cycle, waste heat,

GELİŞMİŞ SÜPERKRİTİK KARBONDİOKSİT BRAYTON ÇEVRİMLERİ İLE ENTEGRE ORTA SICAKLIK KATI OKSİT YAKIT HÜCRESİNİN PERFORMANS DEĞERLENDİRMESİ

ÖZ

Bu tez, atık ısı geri kazanımı ve enerji dönüşümünü değerlendirmeye odaklanarak genel sistem verimliliğini artırmak için orta sıcaklıktaki katı oksit yakıt hücresinin üç farklı süperkritik karbon dioksit Brayton döngüsü konfigürasyonuyla entegrasyonunu araştırmaktadır. EES programı aracılığıyla sıcaklık, akım yoğunluğu ve ısı eşanjörü verimliliği gibi çeşitli çalışma parametreleri, sistem performansı üzerindeki etkilerini belirlemek için incelenmektedir. Araştırma, süperkritik karbon dioksit sıvısının özelliklerinin çevrim verimliliği üzerindeki etkisinden, orta sıcaklıktaki katı oksit yakıt hücresi ve hibrit sistemlerin performansının ve verimliliğinin değerlendirilmesine kadar çeşitli yönleri kapsamaktadır. Araştırmanın son bölümünde katı oksit yakıt hücresi/süperkritik karbon dioksit Brayton çevrimi hibrit sistemlerinin verimlilikleri ve güç paylaşımları karşılaştırmalı olarak analiz edilmektedir. Bulgular, farklı hibrit sistemlerin potansiyelinin kapsamlı bir şekilde anlaşılmasına dair bilgiler sunmaktadır.

Anahtar kelimeler: Hibrit sistem, orta sıcaklık katı oksit yakıt hücresi, süperkritik karbon dioksit Brayton çevrimi, atık ısı

CONTENTS

Page

LIST OF FIGURES

Page

LIST OF TABLES

Page

LIST OF SYMBOLS

i_{cell} : Current density (A/cm^2)

T_{SOFC} : SOFC operating temperature (K)

$\dot{m}$: Mass flow rate (kg/s)

T : Temperature (K)

P : Pressure (kPa)

T_0 : Ambient temperature (K)

P_0 : Ambient pressure (atm)

F : Faraday constant (C/mol)

$\overline{R}$: Universal gas constant (J/mol.K)

k_a : Anode pre-exponential factor (S/m^2)

k_c : Cathode pre-exponential factor (S/m^2)

E_a : Anode activation energy (J/mol)

E_c : Cathode activation energy (J/mol)

K_i : Ionic conductivity pre-exponential factor (S.K/m)

R_{cont} : Area-specific contact resistance ($\Omega.m^2$)

l_a : Thickness of the anode (m)

l_c : Thickness of the cathode (m)

l_{el} : Thickness of the electrolyte (m)

σ_a : Electronic conductivity of the anode (S/m)

σ_c : Electronic conductivity of the cathode (S/m)

$D_{eff,a}$: Anode effective diffusivity (m^2/s)

$D_{eff,c}$: Cathode effective diffusivity (m^2/s)

A_{cell} : Active cell area (cm^2)

U_f : Fuel utilization factor

U_o : Oxygen utilization factor

N_{cell} : Number of cells

ΔT : The pinch point temperature difference

ΔG : Gibbs free energy

ΔH : Enthalpy change

ΔS : Entropy change

V_{th} : Thermal voltage (V)

n : Number of moles of the electrons transferred

V_{max} : Maximum possible reversible voltage of an electrochemical cell (V)

v : Stoichiometric coefficients of the balanced electrochemical reaction

a : Thermodynamic activity coefficients for the reacting species

P_i : Partial pressure of the species of interest

P° : Reference pressure (Pa)

V_n : Nernst voltage (V)

V_{cell} : Cell voltage (V)

V_{act} : Activation polarization (V)

$V_{act,a}$: Anode activation polarization (V)

$V_{act,c}$: Cathode activation polarization (V)

$i_{0,a}$: Anode exchange current density

$i_{0,c}$: Cathode exchange current density

V_{ohm} : Ohmic polarization (V)

R_{ohm} : Resistance

V_{con} : Concentration polarization (V)

$V_{con,a}$: Anode concentration polarization (V)

$V_{con,c}$: Cathode concentration polarization (V)

LHV : Lower heating value (kJ/kg)

η	: Efficiency
h	: Enthalpy (kJ/kg)
$\dot{W}$	: Power rate (kW)
$\dot{Q}$	: Heat transfer rate (kW)
f	: Split rate
ε	: Effectiveness

ABBREVIATIONS

WEO	: The World Energy Outlook
STEPS	: The Stated Policies Scenario
APS	: Announced Pledges Scenario
NZE	: Net Zero Emissions by 2050
EV	: Electric Vehicle
SOFC	: Solid Oxide Fuel Cell
S-CO_2	: Supercritical Carbon Dioxide
IT-SOFC	: Intermediate-temperature Solid Oxide Fuel Cell
AFC	: Alkaline Fuel Cell
PEMFC	: Polymer Electrolyte Membrane Fuel Cell
DMFC	: Direct Methanol Fuel Cell
MCFC	: Molten Carbonate Fuel Cell
PAFC	: Phosphoric Acid Fuel Cell
CHP	: Combined Heat and Power Systems
YSZ	: Yttria Stabilized Zirconia
CFD	: Computational Fluid Dynamics
LSM	: Lanthanum Strontium Manganite
MSR	: Methane Shift Reaction
LT-SOFC	: Low-temperature Solid Oxide Fuel Cell
CGO	: Cerium Gadolinium Oxide
SOFC/GT	: SOFC/Gas Turbine Power Plants
TIT	: Turbine Inlet Temperature
LNG	: Liquefied Natural Gas
ORC	: Organic Rankine Cycle

CCGT	: Combined Cycle Gas Turbine
HEX	: Heat Exchanger
SBBC	: S-CO_2 Basic Brayton Cycle
SRBC	: S-CO_2 Regenerative Brayton Cycle
SRCBC	: S-CO_2 Recompression Brayton cycle
LTR	: Low-temperature Recuperator
HTR	: High-temperature Recuperator
RC	: Re-compressor
MC	: Main Compressor
TPB	: Three Phase Boundary

CHAPTER ONE
INTRODUCTION

The intricate balance between energy consumption and environmental sustainability has emerged as a paramount concern in an era marked by rapid industrialization and escalating energy demand. The growing global population, coupled with growing economies, has intensified the reliance on conventional energy sources, leading to an unprecedented energy crisis. The reckless depletion of fossil fuels has not only made energy security precarious but has also caused severe ecological consequences, most notably the worsening of global warming (Intergovernmental Panel on Climate Change [IPCC], 2022).

1.1 Problem Outline

The World Energy Outlook (WEO) delves into three distinct scenarios shaped by governmental policies. The Stated Policies Scenario (STEPS) captures the current policy landscape, while the Announced Pledges Scenario (APS) envisions the attainment of all declared targets. Meanwhile, the Net Zero Emissions by 2050 (NZE) Scenario pursues a trajectory aiming for a 1.5°C temperature increase and universal energy access by 2030 (International Energy Agency [IEA], 2022). The Industrial Revolution brought economic development to countries, but it also led to an increase in fossil fuel consumption. Changing this trend to make it more environmentally sustainable while still maintaining a strong economy represents a critical moment in the history of energy (British Petroleum [BP], 2023). Although fossil fuels have long dominated, making up roughly 80% of global energy for decades, the STEPS scenario predicts a drop to below 75% by 2030 and just above 60% by 2050 (IEA, 2022). In this scenario limiting of the temperature increase is to about 2.5°C by 2100. However, the STEPS scenario's modest 13% cut in annual CO_2 emissions by 2050 falls short of effectively addressing the severe impacts of climate change (IEA, 2022).

The need to reduce carbon emissions and combat climate change adds to the energy challenge. It has led to a strong focus on clean and renewable energy sources in research and technology to meet energy demands while protecting ecosystems

(IPCC, 2022). Investing in clean electricity, electrification, and modernized grids is a cost-effective way to reduce emissions and lower electricity costs. If current growth rates in solar energy, wind, electric vehicles (EV), fuel cells, and batteries continue, they could accelerate the transformation beyond what's predicted in the STEPS scenario (IEA, 2022). Supply chains for key technologies like batteries, fuel cells, solar energy, and electrolyzes are growing to meet global ambitions. Clean energy emerges as a substantial growth and employment opportunity, creating a focal point for international economic competition.

In the NZE Scenario, decarbonizing transportation relies on two key changes: firstly, a shift to electricity, including hydrogen fuel cell vehicles and EVs, secondly, the utilization of fuels with minimal emissions like hydrogen-based fuels and biofuels, both blended and direct (IEA, 2022). Furthermore, fuel cell hybrid systems applications in the fields of stationary and transportation systems will make a significant contribution to supporting this transition. Advancements in these areas will not only accelerate decarbonization in various industries but also have positive ripple effects in the marine, aerospace, and automotive sectors (BP, 2023).

In brief, as the world grapples with the dual challenge of meeting energy needs and combatting climate change, the exploration of efficient and environmentally benign energy conversion technologies has gained paramount importance. Solid oxide fuel cells (SOFC) are promising in this regard. With hydrogen as a fuel source, these high-efficiency devices have the potential to revolutionize energy generation through electrochemical reactions, presenting an environmentally friendly alternative to traditional combustion-based technologies. On the other hand, a substantial amount of low- to medium-level waste heat is continually released into the environment from industrial operations, necessitating efficient waste heat management. Studies in this field have predominantly concentrated on thermodynamic cycles capable of recovering waste heat, such as the supercritical CO_2 (S-CO_2) Brayton cycle and organic Rankine cycle. Integrating these cycles with renewable energy sources and fuel cells presents a compelling strategy for optimizing energy utilization while minimizing environmental impact. Given this backdrop, exploring the potential of SOFCs and their innovative integration with

advanced power cycles that efficiently harness system waste heat while maximizing power output becomes a significant matter.

1.2 Objectives

The urgency of achieving sustainable and clean energy systems has catalyzed the integration of advanced technologies and scientific insights. The focus extends beyond novel energy sources to effective handling of waste heat, as the energy crisis deepens, and climate change mitigation intensifies.

This research is aimed at comprehensively analyzing the integration of intermediate temperature SOFCs (IT-SOFC) with various S-CO_2 Brayton cycle configurations. This study endeavors to achieve the following objectives:

- The foremost goal of this study is to contribute to the general understanding of efficient and environmentally friendly energy conversion systems. The study enhances understanding sustainable energy technologies by providing insight into incorporating IT-SOFCs with Brayton cycle configurations.
- This research evaluates the performance and efficiency of IT-SOFC/S-CO_2 Brayton cycle hybrid systems. By conducting an in-depth analysis, the study aims to reveal the complex interaction of these hybrid systems about energy production and medium-temperature waste heat utilization.
- This study intends to explore the influence of essential factors, for instance, SOFC current density and operating temperature on efficiency of the hybrid system. The research aims to discover the crucial elements that affect the performance of the system by thoroughly analyzing these variables.
- The study's goal is to identify the most efficient and pragmatic SOFC/S-CO_2 hybrid system capable of effectively harnessing intermediate temperature waste heat generated by SOFCs. Through comparative evaluations, the research endeavors to determine the configuration that maximizes energy conversion efficiency.

Through rigorous analysis, simulation, and assessment, this research endeavors to provide valuable insights into the potential of hybrid systems, thus paving the way for enhanced energy conversion efficiency and a more sustainable energy landscape.

CHAPTER TWO
FUEL CELLS

The fuel cell operates differently compared to power station. The primary factor behind this distinction is that in thermal power station, fuel undergoes oxidation through combustion before being converted into energy. Chemical energy is transformed to mechanical energy, which is then further transformed into electrical energy in thermal power plant. Conversely, in a fuel cell, the energy conversion process directly transforms chemical energy into electrical energy, without the efficiency limitations typically associated with thermodynamic cycles. Natural gas and hydrogen are generally fuel sources utilized in fuel cells, although other hydrocarbon-based fuels and ammonia can also be utilized (Andersson, 2009; Ferrari, Damo, Turan, & Sánchez, 2017; Kalinci & Dincer, 2018).

2.1 Historical Background of Fuel Cell

The description of inverse electrolysis was introduced by Christian Friedrich Schönbein in the late 1830s. Shortly thereafter, fuel cells considered energy conversion devices were conceptualized by Sir William Grove in 1839 (Ferrari, Damo, Turan, & Sánchez, 2017; Weber & Lipman, 2019). In 1894, W. Ostwald conducted the first analysis demonstrating the advantages of fuel cells over thermal engines. In 1900, W. Nernst constructed both a redox cell and a fuel cell, and the electrolyte utilized in those pioneering experiments remains a fundamental component in modern leading SOFCs. The noteworthy efforts of Bacon from 1932 to 1952 in improvement of 5-kW fuel cell system played a pivotal role in its subsequent advancement and application. This fuel cell system, initially conceived via the United Technologies Corporation, was designed as an auxiliary power source for NASA's Apollo Flights (Srinivasan, 2006).

2.2 Basic Operating Principles

The general components of a fuel cell, as depicted in Figure 2.1, include diffusion media, composite structures comprising a membrane, a gas-diffusion layer, bipolar

plates or flow fields, and catalyst layers (Da Rosa & Ordóñez, 2021; Mench, 2008; Weber & Lipman, 2019).

Electrochemical oxidation of the fuel generates electrons that flow across interconnect into external circuit at anode electrode. Simultaneously, ions produced pass into electrolyte, completing circuit. These electrons are produced at anode by employing the external circuit and can be utilized for work previously their eventual consumption at cathode. Cathode receives oxidants, typically oxygen derived from the atmosphere, through the cathode flow field (Srinivasan, 2006). The resulting products of the fuel cell process encompass three aspects: end products, heat, and power.

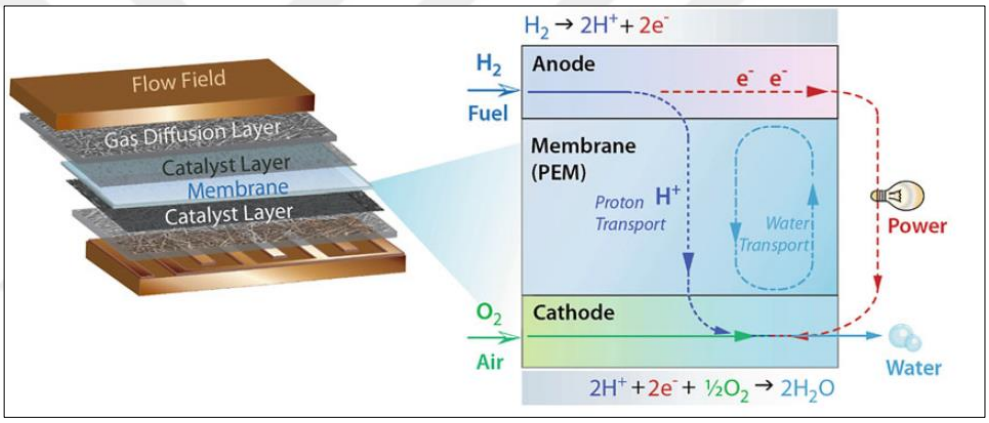

Figure 2.1 Fuel cell structure and electrochemical energy conversion (Weber & Lipman, 2019)

2.3 Classification of Fuel Cells

Fuel cells are generally categorized according to operating temperature or electrolyte material used. Each type of fuel cell offers distinct advantages that make them suitable for various applications. Alkaline fuel cells (AFC) and polymer electrolyte membrane fuel cells (PEMFC) fall under low-temperature fuel cells. Lower temperatures provide benefits such as quicker start-up and higher efficiency (Da Rosa & Ordóñez, 2021). The narrow temperature differential between the environment necessitates using larger heat exchangers and higher-priced catalysts to dissipate waste heat in these systems. Recent research aims to increase the temperature range of aqueous OH^- and H^+ transmission over 100˚C, motivated by

technological factors, for instance, the platinum-based catalysis's carbon monoxide resistance and heat management in automobiles. (Weber & Lipman, 2019). A common focus of research in this field is to enable SOFCs to operate at lower temperatures to increase durability, reduce costs, and shorten startup times. It's important to note a temperature gap in electrolyte availability between 100˚C and 600˚C. Current research endeavors are directed towards achieving fuel cells operation within this intermediate temperature range.

2.3.1 Polymer Electrolyte Membrane Fuel Cell

PEMFCs typically operate at temperatures between 20-100 °C and use a catalyst made of noble metal platinum on both the cathode and anode. The high specific and volumetric power density, cold start capabilities, and rapid load-following capabilities of this type of hydrogen-fed fuel cell are gaining considerable attention (Da Rosa & Ordóñez, 2021; Weber & Lipman, 2019). The PEMFC is perceived as a promising option for inner combustion engines and as a possible alternative to batteries in portable power applications and vehicles (Sazali, Wan Salleh, Jamaludin, & Mhd Razali, 2020). The PEMFC's performance and control are hindered by numerous technical problems, such as frozen-start capability, freeze-thaw cycles, water-heat management, and durability (Mench, 2008). Additionally, the market uptake, manufacturing process, and auxiliary system components of PEMFCs remain subjects of scrutiny.

2.3.2 Direct Methanol Fuel Cell

Direct methanol fuel cells (DMFC), among the most appropriate for portable electronics, are widely regarded as a feasible substitute for lithium-ion batteries. Although DMFCs and PEMFCs have similar design characteristics, DMFCs use a liquid solution of methanol and water for fuel instead of hydrogen gas (Mench, 2008; Sazali, Wan Salleh, Jamaludin, & Mhd Razali, 2020). Operating at low temperatures, DMFCs exhibit high conversion efficiencies and minimal emissions (Ramli, Shaari, & Saharuddin, 2022). The main technical issues affecting performance that have lately been treated with nanotechnology are high catalyst loading, poor catalyst

activity, methanol crossover, and two-phase flow managing in cathode and anode (Mench, 2008).

2.3.3 Solid Oxide Fuel Cell

The SOFC, electrolyte comprises thin ceramic body that serves as an oxide material conducting O^{2-} or H^{+}. SOFC systems can employ hydrocarbons as a source of fuel utilizing reforming procedures while functioning within a temperature interval of roughly 500-1000°C, a circumstance that proves advantageous. (Timurkutluk B. , 2007). SOFCs can be integrated with cogeneration systems because of their elevated operating temperature. The main focus of SOFC technology enhancement is on stationary power plants, which usually exceed 100 kW, along with small power generation for residence. (Ferrari, Damo, Turan, & Sánchez, 2017; Weber & Lipman, 2019). The primary technical challenges for SOFCs encompass achieving intermediate operating temperatures, managing start-up times, ensuring durability, and achieving effective cell sealing (Andersson, Yuan, & Sunden, 2011; Boaro & Aricò, 2017; Shao & Tadé, 2016).

2.3.4 Molten Carbonate Fuel Cell

The temperature range at which molten carbonate fuel cells (MCFCs) operate is generally 650°C. The electrolyte commonly consists of lithium and potassium carbonates (McVay, 2014). A significant advantage of MCFCs is their reduced dependence on precious metal catalysts, resulting in substantial reductions in raw material costs. However, MCFCs face certain challenges, including intricate electrolyte management due to finite vapor pressure and loss, extended start-up times, durability concerns, and the requirement to inject CO_2 into the anode to ensure electrolyte stability (Mench, 2008).

2.3.5 Phosphoric Acid Fuel Cell

The utilization of a high-concentration phosphoric acid as the mobile (liquid) electrolyte characterizes phosphoric acid fuel cell (PAFC) (Sammes, Bove, & Stahl,

2004). Operating at temperatures typically ranging between 150 and 200°C, the PAFC found its initial installations in the 1970s, and since then, numerous units have been deployed worldwide. Prominent developers of PAFC technology include United Technologies Corporation (UTC) Fuel Cells, Toshiba, and Fuji Electric (Sammes, Bove, & Stahl, 2004). Numerous 200 kW fuel cell power units designed for co-generation have been introduced in the market over the last 20 years, with UTC Power being the main contributor (Weber & Lipman, 2019). A noteworthy advantage of the PAFC lies in its simplified water management compared to PEMFCs, given that the highly concentrated acid electrolyte does not rely on water for conductivity. However, the substantial system cost remains a significant drawback (Sammes, Bove, & Stahl, 2004).

2.3.6 Alkaline Fuel Cell

The liquid alkaline electrolyte used by AFCs is based on solution of potassium hydroxide in water, chosen for its superior conductivity among all alkaline hydroxides. (Mench, 2008; Merle, Wessling, & Nijmeijer, 2011). The initial stages of fuel cell development greatly benefited from the less demanding requirements for electrocatalysts that alkaline electrolytes offered. In the 1950s, the AFC systems were utilized by the NASA Apollo space program to supply both potable water and power to astronauts aboard the Space Shuttle orbiter, a technology that is still used in modern space applications (Merle, Wessling, & Nijmeijer, 2011). Recent significant advancements in scientific knowledge, particularly regarding PEMFCs, have renewed interest in AFCs over the last two decades. AFCs hold distinct advantages, such as the ease of operation at temperatures relatively lower (23–70°C) and the enhanced reaction kinetics at the electrodes in comparison to acidic circumstances (Merle, Wessling, & Nijmeijer, 2011). However, a notable drawback of AFCs is their susceptibility to even minor levels of CO_2 present in the air. CO_2 reacts with the alkaline electrolyte, forming potassium carbonate (K_2CO_3) and significantly degrading performance over time (Mench, 2008). The KOH solution exhibits high sensitivity to the presence of CO_2 (Merle, Wessling, & Nijmeijer, 2011).

2.4 Comparison of Fuel Cells and Heat Engines

Heat engines that rely on fossil fuel combustion, dating back to the industrial revolution, have resulted in significant environmental issues. Nevertheless, fuel cells are addressing the demands of modern conditions by offering enhanced efficiency, eco-friendliness, and applicability with alternative fuels and renewable energy sources (Li X. , 2007).

The fuel and oxidizer's chemical energy is initially converted into mechanical work in thermal power station. This mechanical work is subsequently converted to electrical energy. In fuel cell, this energy conversion process only involves the conversion from chemical energy to electrical energy (Boaro & Aricò, 2017). The maximum efficiency of a fuel cell is not restricted within Carnot efficiency much the same in thermal cycles, meaning that fuel cells can exceed the maximum efficiency of a Carnot engine operating at the same temperatures (Haseli Y. , 2018). The A comparison of the fuel cell's ideal thermodynamic efficiency and the efficiency achieved in the Carnot process is shown in Figure 2.2.

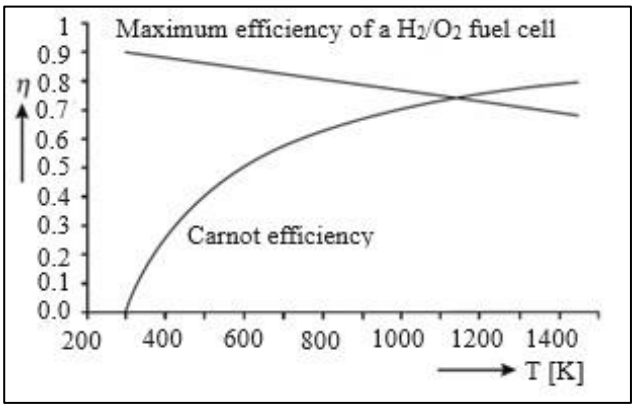

Figure 2.2 A comparative diagram of temperature-dependent efficiency between Carnot cycle and fuel cells (Weber & Lipman, 2019)

2.5 Comparison of Fuel Cells and Batteries

Rechargeable batteries and fuel cells represent advanced electrochemical systems for storing and converting energy, thereby offering the benefits of substantial theoretical energy density and environmental friendliness. The distinction among fuel cell and battery can be attributed to concepts of open system and closed system. A battery functions as a thermodynamically closed system, wherein the movement of mass is prohibited across the boundaries of the system. It converts and stores electrical energy within the same compartment (Weber & Lipman, 2019). Conversely, a fuel cell operates as an open system with mass flux permitted across its boundaries. The fuel cell operates as a steady-state device by ensuring a consistent supply of oxidizer and fuel, thus maintaining an uninterrupted flow (Mench, 2008; Srinivasan, 2006).

Batteries are categorized into two different groups, namely primary batteries, and secondary batteries. Primary batteries, unlike their counterparts, are incapable of being recharged. They store chemical energy internally, and their discharging reactions are irreversible (Weber & Lipman, 2019). Secondary batteries are rechargeable and undergo reversible discharging reactions, though recharging is notably lengthier compared to refueling a fuel cell (Mench, 2008). Hydrogen fuel cells prove well-suited for long-range EVs due to their rapid refueling, grid compatibility, and fuel flexibility. Lithium-ion batteries possess the necessary attributes for electric mobility applications. However, combining a hybrid system of batteries and fuel cells can yield clean, low-carbon transportation (Cano, et al., 2018). The higher cost of fuel-cell systems currently renders conventional fuel cell EVs more expensive than battery EVs. Furthermore, a drawback of fuel cells lies in their slower electrochemical and thermodynamic responses, making them susceptible to poor water management and reactant shortages during sudden load changes (Fedakar, 2012).

2.6 Fuel Cell Applications

Fuel cell applications are evaluated in three fields: portable, transportation, and stationary applications. Each type of fuel cell tends to be suited to a specific market

segment. Fuel cell technology's versatility in terms of size allows it to cover a broad spectrum, ranging from systems delivering a few watts to megawatts (Ferrari, Damo, Turan, & Sánchez, 2017).

2.6.1 Portable Applications of Fuel Cell

Fuel cells find application in portable contexts, involving units integrated into or charged up, as well as products designed for mobility, such as small auxiliary power units. In portable applications, the priority is to ensure simplicity and high system power density rather than focusing on cost and efficiency. A typical micro-fuel cell, generating around 300 mW, is sufficient for maintaining a cell phone battery charge (Kundu & Dutta, 2016). More substantial power outputs can be attained through fuel cell stack design. Table 2.1 showcases various prototype fuel cells in the industry.

Table 2.1 Overview of prototype fuel cells in the industry

Companies	**Application**	**Type of fuel**	**Power (W)**
SFC Energy-(EFOY)	Power generator	Methanol	40-125
BOC-(HYMERA)	Power generator	Hydrogen	175
Bramble Energy-(SDX)	Power generator	Hydrogen	60
Ultracell-(XX55)	Power generator	Methanol	50
Horizon-(MiniPak)	Power bank	Hydrogen	1.5–2

The portable fuel cells possess the potential to be employed to power a variety of devices:

- Telecommunications satellites
- Small personal electronics (mobile phones, video cameras and, laptop computers)
- Biological applications
- Military applications

2.6.2 Stationary Applications of Fuel Cell

Stationary fuel cell applications encompass devices that furnish electrical power, and occasionally, thermal energy, however, they lack the purpose of being mobile. The scope of application for stationary fuel cells varies depending on their characteristics, ranging from 1 kW small-scale stationary power plants to 20 MW large-scale stationary power plants. For stationary applications, the focus is on extended lifespan, durability, and high efficiency (Wilberforce, Alaswad, Palumbo, Dassisti, & Olabi, 2016). Table 2.2 showcases various existing fuel cell power systems.

Table 2.2 Overview of different existing fuel cell power systems

Companies	**Application**	**Type of fuel**	**Efficiency**	**Power (kW)**
ENE-FARM	Fuel cell system for practical home use	LPG	60%	1
Elcogen-(E3000)	Stationary power unit	Biogas/natural gas/hydrogen	75%	3
Panasonic	Fuel cell-CHP	Hydrogen	56%	5
Ceres Power	Stationary power unit	Natural Gas	60%	5
Convion	Stationary power unit	Natural Gas	60%	60
Toshiba-(H2REX)	Fuel cell-CHP	Hydrogen	55%	100
Fuji Electric-(FP-100i)	Fuel cell-CHP	City gas 13A	42%	100
Bloom Energy- (Bloom Box)	Stationary power unit	Hydrogen	52%	300
DOOSAN-(Pure Cell Model 400 NG)	Stationary power plant	Natural Gas	43%	440
Mitsubishi Power	Fuel cell-CHP	Natural gas	57%	1000

The usage areas of fuel cells for stationary application are listed below:

- Remote area supply
- Uninterruptible power supplies

- Emergency backup power supply
- Distributed power CHP generation (Combined Heat and Power Systems)
- Larger auxiliary power units for ships, trucks, etc.

2.6.3 Transportation Applications of Fuel cell

Transportation applications encompass units that furnish the propulsive power or extension of range for vehicles. Essential features sought in transportation applications include optimal efficiency, fast charging, rapid start-up, power grid compatibility, portable size, and durability (Da Rosa & Ordóñez, 2021; Mench, 2008).

Table 2.3 Overview of existing fuel cell transportation applications

Companies	**Application**	**Filling time (min.)**	**Driving range (km)**	**Power (kW)**
Hyundai-(Nexo)	Automobile	5	756	120
Toyota-(Mirai)	Automobile	5	650	120
Hyzon-(Class8)	Semi-trucks	15	800	450
Nikola-(TRE-FCEV)	Semi-trucks	20	800	400
PEUGEOT e-Expert Hydrogen	Van	3	400	100
WrightBus-(StreetDeck)	Bus	8	450	172
Hyzon	Bus	15	400	195
Texys-(H2K compact)	Racing motorbike	-	45	100

In the present day, oil predominantly covers transportation fuel consumption. However, with the advancement of EVs, fuel demand has diversified to include natural gas, electricity, hydrogen, and biofuels (Olabi, Wilberforce, & Abdelkareem, 2021). The advancement of fuel-cell EVs, although having the potential to be eco-friendlier and more effective compared to Hybrid EVs, has not yet reached degree of

progress that is adequate for extensive commercialization (Olabi, Wilberforce, & Abdelkareem, 2021).

On the other hand, the NZE goals of countries are compelling the global economy to reduce dependence on the oil industry, acting as a strong impetus for fuel cell vehicle development. Table 2.3 presents the current fuel cell vehicles.

Transport applications include in follows:

- Private transport
- Public transport
- Railway vehicles
- Aviation
- Buses and trucks

CHAPTER THREE
SOLID OXIDE FUEL CELL

The electrolyte used in SOFCs is solid one, as the name implies. They represent a potentially clean and highly efficient technology that directly turns chemical energy of fuel to electrical energy. The inception of SOFC advancement can be attributed to the 1890s, during which German chemist Walter Nernst made a significant revelation. Nernst's discovery revealed that stabilized zirconia (ZrO_2) displayed the capability of ion conductivity at particular temperatures. Consequently, this finding demonstrated the potential of zirconia as an efficacious electrolyte (Ferrari, Damo, Turan, & Sánchez, 2017). Baur and Preis were the pioneers who successfully constructed the initial SOFC prototype in the year 1943. Their study showcased the capability of zirconia to effectively operate as an electrolyte, facilitating the conduction of oxygen-ions in fuel cells (Boaro & Aricò, 2017).

A standard SOFC unit includes a permeable anode, a dense electrolyte, and a permeable cathode. Generally, cathode employs Sr-doped $LaMnO_3$, anode is constructed from Ni–ZrO_2 composite material, and the electrolyte is comprised of yttria-stabilized zirconia (YSZ) (Cicek, 2015). An essential consideration in this context pertains to the utilization of a robust electrolyte, which serves to inhibit material corrosion as well as the challenges associated with managing liquid electrolytes (Ferrari, Damo, Turan, & Sánchez, 2017). Furthermore, nickel is employed as a catalyst due to its high stability, conductivity, and cost-effectiveness.

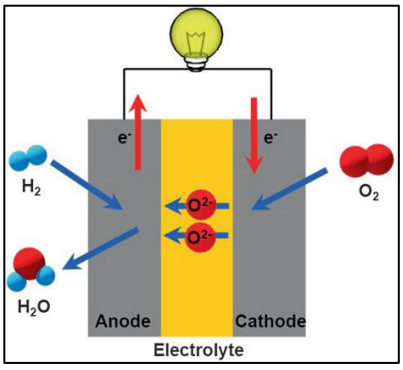

Figure 3.1 Basic SOFC arrangement (Shao & Tadé, 2016)

The operating principle of the SOFC is summarized in Figure 3.1. Molecular oxygen is steadily diffused from cathode to cathode surface, where it undergoes reduction to form oxygen ions. Once situated at interface among electrolyte and anode, these ions interact with hydrogen ions to produce H_2O, which is subsequently eliminated through exhaust stream. Electrons are discharged at anode and traverse external load to reach cathode, that they are employed in reduction of oxygen molecules (Shao & Tadé, 2016).

A customary SOFC stack is comprised of a pair of electrodes, namely cathode and anode, additionally a frame, electrolyte, interconnect plates, and seals (Figure 3.2). Because of relatively low power and voltage output of single SOFC, it is common practice to stack individual cells together in order to create a device that operates at approximately 50V. This allows for the production of power values that exceed 1 kW, with typical SOFC stack sizes ranging from 100 kW to 250 kW. By stacking one cell element on top of another, planar cells can be assembled easily (Ferrari, Damo, Turan, & Sánchez, 2017).

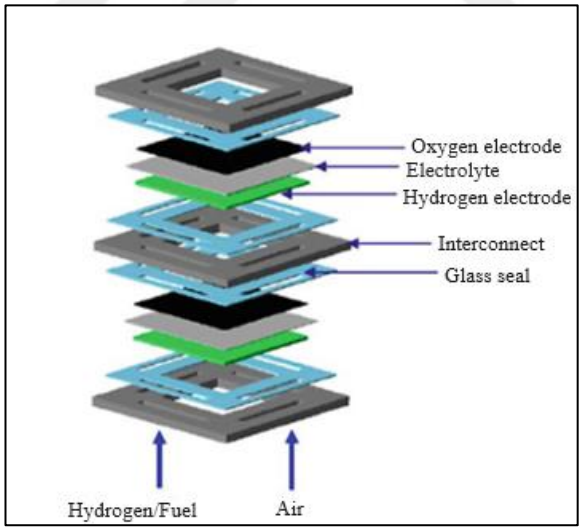

Figure 3.2 Typical SOFC stack configuration (Weber & Lipman, 2019)

SOFCs are designed to operate within the temperature range of 500-1000˚C. Historically, the focus of studies was on high temperatures (800-1000°C); however, the costs associated with these high operating temperatures have prompted recent

research efforts to decrease temperature range to 500-800°C, thereby significantly lowering costs.

The operational temperatures of SOFCs present the opportunity for the utilization of a bottoming cycle to exploit waste heat. Additionally, these fuel cells can directly utilize natural gas or other hydrocarbon fuel sources (Schöffer, Klein, Aravind, & Pecnik, 2021). While various studies have explored the application of SOFCs in different vehicle power systems (particularly for larger vehicles), their primary use is in power plants and industrial settings. Fuel cell efficiencies typically range from 30% to 60%, which can rise to 50% to 85% in cogeneration applications. As is known, reliability and sustainability are important parameters of stationary power generation applications. SOFC systems are seen as reliable systems, particularly for off-grid systems. Ritchie (2016) demonstrated that a SOFC system with a reliability factor of 0.97 can meet the reliability requirements of a data center aiming for 0.999 reliability.

However, the endeavor to maintain a low operating temperature for SOFCs has redirected some research toward proton conducting SOFCs (Kalinci & Dincer, 2018). In SOFCs that utilize proton conduction, hydrogen fuel undergoes oxidation, resulting in the formation of hydrogen ions at the anode. These ions subsequently traverse the proton conductor, where they react by oxygen at cathode, ultimately forming H_2O (Rashid, et al., 2019). The electrical efficiency and ionic conductivity of proton conducting electrolytes are more than that of ion-conducting electrolytes in SOFCs operating temperature range (Rashid, et al., 2019). The reason for this is that H^+ transport often has lower activation energy than O^{2-} (Rashid, et al., 2019). In this study, ion conducting SOFC was examined.

3.1 SOFC Geometries

SOFCs generally come in two main geometries: planar and tubular configurations.

3.1.1 Planar SOFC

Due to the more compact design of planar SOFC, it provides a higher current density compared to other configurations (Canavar, 2013). Examples of planar SOFCs with different areas are illustrated in Figure 3.3. Planar SOFCs are simpler to manufacture and more adaptable in terms of shaping compared to other design types. Internal stresses in cell components caused by fuel leakage and temperature changes are the main problems in cell design (Andersson, 2009). Ilbas et al. (2021) analyzed the performance of planar and micro-tubular type SOFCs with the same thicknesses of electrolyte and electrode. Their study revealed that temperature increases had a lesser impact on micro-tubular SOFCs than on planar SOFCs. Additionally, they concluded that planar SOFCs outperformed micro-tubular SOFCs under the same operating conditions.

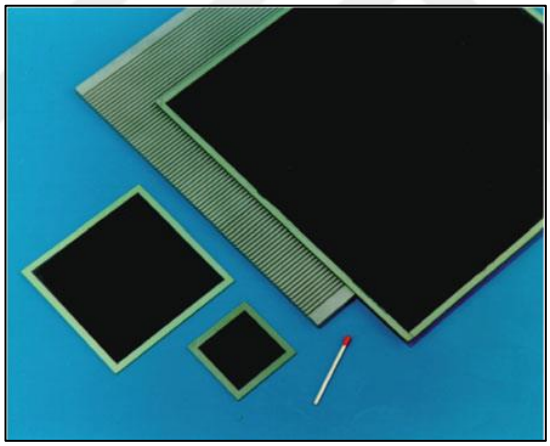

Figure 3.3 Planar SOFCs with different areas (Kupecki, 2018)

In the literature, studies on planar SOFCs have explored various aspects including materials, performance, polarization losses, and manufacturing. Yakabe et al. (2001) developed a mathematical modeling for planar SOFC operating at 900-1000˚C. An abrupt decline in fuel temperature near the inlet, ascribed to internal reforming, resulted in considerable tensile stresses within the electrolytes. Timurkutluk (2007) investigated the performance of a SOFC by assessing its membrane electrode group, which had been developed under various parameters. These parameters encompassed

the thickness of the electrolyte, the temperature at which sintering occurred, and the operational temperature. Theoretical and experimental results from the study showed that the highest current density at 640ºC was measured at 0.21 A/cm^2, corresponding to 0.47 W/cm^2. Li et al. (2017) employed comprehensive mathematical modelling to analyze behavior of production-scale 30-cell planar SOFC stacks. The study explored various operational scenarios, employing methane as the primary fuel source. The computational analysis of the multiphysics stack simulation yielded notable results, including power of 1.2 kW and total current output of 57.6 A. Celik (2018) developed a multiphysics model for the planar SOFCs, which included computational fluid dynamics (CFD) solutions. This comprehensive approach also considered the intricate dynamics of heat transfer involving convection, conduction, and radiation. In the current study, planar SOFC was used.

3.1.2 Tubular SOFC

The tubular SOFC exhibits a distinct geometry, as depicted in Figure 3.4. Typically, the initial stage involves a porous electrode tube, which is surrounded by the other components of the cell. Consequently, these configurations often consist of either cathode or anode-supported structures (Sarı, 2017). Tubular SOFCs with a diameter of 5 mm or less are referred to as micro-tube SOFCs. Volumetric power density of micro-tube SOFC stack increases as diameter of the micro-tubes decreases (Aydın U. , 2018). A tubular SOFC presents a range of benefits in comparison to planar SOFC, including enhanced rapid start-up and shutdown capabilities, thermal shock resistance, and stability during long-term operation (Canavar, 2013). However, disadvantages of tubular SOFCs include increased ohmic losses with longer current lines and potential manufacturing challenges (Aydın U. , 2018).

Tubular SOFC studies in the literature primarily focus on performance improvement. Campanari and Iora (2004) formulated mathematical modeling of a tubular SOFC. An examination of sensitivities was conducted to assess the effects of hydrocarbon reforming reactions, internal cell heat exchange processes, as well as cell losses. Soydan (2015) developed a 100 W micro-tube SOFC system consisting of 50 micro-tube SOFCs. Performance tests conducted at 750°C yielded power

densities of 0.45 W/cm^2 for a single cell, 0.41 W/cm^2 for 5 cells, 0.39 W/cm^2 for 10 cells, and 0.35 W/cm^2 for 50 cells. This indicated that power density per unit cell number decreases with increasing cell number due to rising total resistance. Aydın (2018) analyzed the production of anode-supported micro-tube SOFCs and characterized the microstructure of the produced micro-tube SOFCs. Performance tests resulted in 920 mW of power being generated at 1.84 A current and 500 mV voltage, with a pure hydrogen flow of 150 mL/min at 800°C. Timurkutluk (2019) investigated the numerical and experimental optimization of anode-supported micro-tube SOFCs, determining YSZ as the electrolyte material. Through numerical optimization at constant cell voltage of 0.7 V at 800°C, base cell's maximum power density of 0.136 W/cm^2 was increased to 0.489 W/cm^2, resulting in more than a twofold performance improvement.

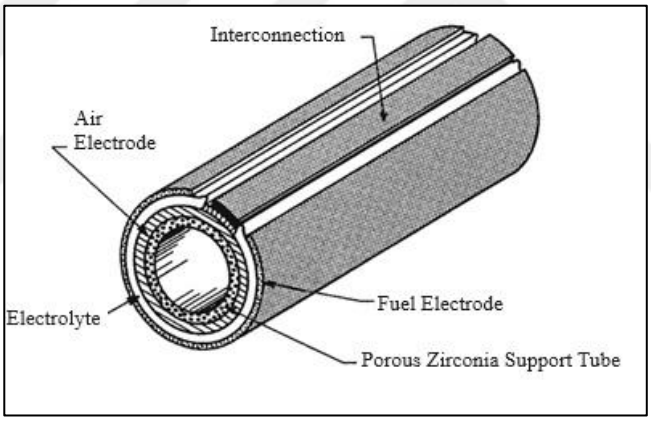

Figure 3.4 Tubular SOFC configuration (Weber & Lipman, 2019)

3.2 SOFC Types by Temperature

Most companies and researchers have generally developed SOFCs in temperature range of 800–1000°C. Nonetheless, presently, there exists an increasing inclination toward investigating the feasibility of operating SOFCs under lower temperatures, primarily driven by the potential to achieve reduced operational costs. SOFCs are classified into three groups based on their temperatures: high-temperature, intermediate-temperature, and low-temperature.

3.2.1 High-temperature SOFCs

High temperature SOFCs represent conventional kinds of SOFCs, characterized by YSZ electrolytes. These operate at elevated temperatures (800-1000°C) to ensure efficient ionic conductivity within YSZ (Ni M. , 2012). The anode commonly consists of Ni-YSZ, and cathode comprise Lanthanum Strontium Manganite (LSM). Nickel is a widely used anode material because it has notable electrical conductivity and stability even under chemically reducing circumstances. Moreover, nickel is chosen for its cost-effectiveness in comparison to platinum, which is a preferred metal in fuel cells operating at lower temperatures (Ferrari, Damo, Turan, & Sánchez, 2017).

High-temperature SOFCs achieve exceptional efficiency and power density values owing to their operation at elevated temperatures. Higher operating temperatures lead to increased reaction rates and decreased polarization losses within the cell. However, these high temperatures also result in shorter cell lifetimes and the need for more expensive materials (Andersson, 2009; Khan, 2019). Additionally, the large thermal stresses induced during heating and cooling processes compromise the structure's durability, hindering widespread commercialization of SOFCs. Current research focuses on solutions that aim to decrease operating temperatures significantly to achieve cost reductions (Andersson, Yuan, & Sunden, 2011; Sarı, 2017).

Much of the literature is dedicated to mitigating the drawbacks associated with high-temperature operation. Yılmaz (2010) modeled and analyzed an SOFC stack fueled by natural gas. The study examined velocity distribution, polarization curves, power-voltage relationships, and power-current curves within the cell. Anode, cathode, and electrolyte materials chosen were Ni-YSZ, Sr-$LaMnO_3$, and Y_2O_3-ZrO_2, respectively, with operating temperature of 1000°C. Maximum power output reached current density of 650 A/m² at cell voltage of 0.65 V. Luo and Fong (2016) improved 2D dynamic model of high-temperature SOFC. Hydrogen and natural gas (30% pre-reformed methane) were employed as fuels. The study proposed the application of methane fed SOFCs, utilizing electrochemical reaction heat in SOFC as a source of heat for methane shift reaction (MSR) reaction, providing convenience with a

provision of biogas or natural gas. The Bloom Energy Server, a SOFC power generator about the size of a refrigerator, produces 100 kW of power output using hydrocarbon fuel such as methane, biogas, or gasoline for electricity generation. The server's maximum operating temperature is 980°C. A single cell consists of three ceramic layers, measuring 100 mm × 100 mm, and generates 25 watts. The expected lifespan of one server is ten years. These servers are utilized by corporations such as eBay, Google, Yahoo, and Walmart (Deepika, Kumar, & Sivasankar, 2018).

3.2.2 Intermediate/Low-temperature SOFCs

In studies aimed at developing SOFCs, the primary focus is on lowering the operating temperature, reducing expense, and enhancing cell lifetime. IT-SOFCs have been designed to function within the temperature range of 600-800˚C, whereas low-temperature SOFCs (LT-SOFCs) target temperatures under 600˚C. Reducing the operational temperature to an intermediate level result in elevated ohmic and polarization losses within the electrodes. Due to these losses, the rise in electrode polarization resistance, especially at the cathode, leads to reduced power output from the cell. To address this limitation, it is necessary to create an exceptionally active electrolyte that exhibits minimal polarization loss at intermediate temperatures (Andersson, 2009; Khan, 2019). One potential approach involves utilizing doped ceria or doped lanthanum gallate as electrolyte materials to enhance ionic conductivity within the electrolyte (Andersson, 2009).

The interconnect and sealant components play crucial roles in constructing IT-SOFC stacks. Operating at lower temperatures reduces thermal stresses on active ceramic structures, increasing system longevity and enabling the use of cost-effective interconnect materials (Khan, 2019). For instance, metallic interconnects can be employed, significantly reducing material costs compared to the high-cost ceramic interconnects used in high-temperature SOFCs (Shao & Tadé, 2016). Metal-supported cells offer robustness against both mechanical and thermal stresses, improving handling during manufacturing and delivery over conventional anode (Ni-YSZ) supported cells (Blennow, et al., 2009; Leah, et al., 2011). Moreover, the

lower operating temperature reduces the impact of thermal expansion rate mismatches between sealant and cell components (Shao & Tadé, 2016).

Numerous studies aim to enhance the performance of low-temperature SOFCs. R. Doshi et al. (1999) demonstrated that doped ceria serves as a viable electrolyte for operation at 500°C with fuels like liquid methanol or hydrogen-containing gases. They achieved maximum power density of 140 mW/cm^2 at 500°C. In study conducted by Oishi et al. (2005), an investigation was carried out to examine the response of the open circuit voltage (OCV) at a temperature of 550˚C. This investigation specifically focused on a cell that consisted of a cerium gadolinium oxide (CGO) electrolyte, which was supported by a NiO-CGO support. The findings of this investigation revealed that the reduction of NiO-CGO at the temperature of 550˚C resulted in NiO-CGO support being able to effectively function considered anode. Additionally, it was observed that cell achieved maximum power density of approximately 130 mW/cm^2 at the temperature of 550˚C, under wet conditions with a 10% concentration of Hydrogen. Hui et al. (2007) conducted a study on metal supported SOFC. This cell utilized a bilayer electrolyte consisting of SDC/ScSZ. The metal-supported SOFC that was constructed, attained remarkable power density of 0.161 W/cm^2 when operated at a temperature of 600°C. Salogni et al. (2009) formulated a dynamic model for 5 kW IT-SOFC which comprises stack of fuel cells related to control valves, combustor, and heat exchangers. Stout (2015) proposed a design process and considerations for a high-volumetric-power-density IT-SOFC, featuring a novel hexagonal honeycomb shape. The design successfully achieved power density of 2 W/cm^2 at 650°C. Sarı (2017) utilized a methodology in order to fabricate cathode substances that would effectively reduce operating temperatures of SOFCs to a range of 500-600°C. Evcimen (2019) endeavored to augment the efficacy of cells and diminish the operational temperature (600-800°C). Different samples were examined using ScSZ as the electrolyte and Gadolinium-doped ceria (GDC) as the electrode. The SOFC that was fabricated resulted in power density of 800 mW/cm^2 at 800°C. Table 3.1 features IT-SOFC studies. In the current study, IT-SOFC was considered.

Table 3.1 A summary of studies of IT-SOFCs

Ref	**Geometry**	**Operating temperature**	**Fuel**
(Doshi, Richards, Carter, Wang, & Krumpelt, 1999)	Planar	500 ˚C	Methanol, gasoline, hydrogen
(Cheddie & Munroe, 2007)	Planar	750˚C	Hydrogen
(Hui, et al., 2007)	Planar	400-600 ˚C	Hydrogen
(Tseronis, Kookos, & Theodoropoulos, 2008)	Planar	750˚C	Hydrogen
(Blennow, et al., 2009)	Planar	655 ˚C	Hydrogen
(Leah, et al., 2011)	Planar	570 ˚C	Hydrogen, natural gas
(Spallina, Mastropasqua, Iora, Romano, & Campanari, 2015)	Planar	750˚C	Hydrogen, syngas
(Stout, 2015)	Honeycomb structure	650 ˚C	Hydrogen
(Li, Song, & Lin, 2017)	Planar	750˚C	Methane

3.3 Types of SOFC Support

Mechanical support for the cell is crucial to ensure its structural integrity and withstand various mechanical stresses during handling, mounting, changes in gas pressure, and different operational modes. Resistances of membrane are influenced by layer's thickness, thus one of constituents must possess an adequate thickness to offer mechanical reinforcement for the cell (Kupecki, 2018; Sarı, 2017). There are four main alternatives for providing this support in fuel cell designs: cathode supported, anode supported, electrolyte supported, and metal supported SOFCs.

3.3.1 Anode Supported SOFC

SOFCs commonly use anodes composed of a blend of nickel oxide and electrolyte material. The selection of nickel as the anode material stems from its enduring

stability in chemically reducing circumstances, elevated electrical conductivity, lower cost, and transport properties. (Ferrari, Damo, Turan, & Sánchez, 2017; Kupecki, 2018):

- High electrical conductivity to facilitate current flow.
- Electrochemical and fuel conditioning reactions exhibit a substantial level of activity.
- High porosity (20–40%).

In an anode-supported SOFC design, overall resistances tend to be lower, and efficiency is generally higher compared to electrolyte-supported SOFCs. This design permits the use of a very thin electrolyte, reducing ohmic losses and allowing for lower temperatures, typically ranging between 600-800°C (Andersson, 2009). Kaya (2012) conducted an evaluation of performance of tubular anode supported SOFC using COMSOL. The cell utilized $LaMnO_3$/LSM as cathode, NiO/YSZ considered anode, and YSZ as electrolyte. H_2-H_2O mixture was employed as fuel on the anode side. The model was optimized through parameter examination, yielding an optimum variable current density of 5300 A/m² for the anode and 2000 A/m² for the cathode. Njodzefon et al. (2013) created a zero-dimensional model of anode supported SOFC. Their findings emphasized influence of rising polarization losses due to Knudsen diffusion and declining reaction rates, particularly at elevated current densities in electrolysis model. Their study also indicated a strong coupling of gas diffusion and activation polarization.

3.3.2 Cathode Supported SOFC

The porous structure of the cathode facilitates effective mass transfer. LSM is commonly utilized as the cathode material in current SOFC designs (Ferrari, Damo, Turan, & Sánchez, 2017). The cathode materials need to possess certain characteristics, as highlighted by Ilbas and Kumuk (2019):

- High catalytic activity at lower operating temperatures,
- ionic–electronic conductivity.

In cathode-supported SOFCs, the cathodes are engineered to possess sufficient thickness, acting as a supportive substrate during cell manufacturing, usually falling within the range of 0.3 to 1.5 millimeters. These designs present benefits compared to anode-supported SOFCs, including the use of cost-effective cathode-supporting materials and mitigating carbon deposition in thin anode during operation with hydrocarbon fuels. However, production of cathode-supported SOFCs can be challenging due to the high sintering temperatures required (Ilbas & Kumuk, 2019). Shi and Xue (2010) developed a 2-D CFD model using COMSOL to examine the performance of bi-electrode-supported cells. Their discoveries indicated which performance of cell is considerably impacted from distribution of porous microstructures within the electrodes. Additionally, operating conditions can affect cell performance, especially gas and fuel pressure losses throughout electrodes, depending on porosity distribution of the electrode. Kumuk (2018) conducted an investigation into the factors affecting SOFC performance. According to the results, cathode supported SOFC performs preferable than electrolyte supported SOFC. Furthermore, increasing temperature and pressure values, along with using pure oxygen as the oxidant, positively influenced the performance of cathode supported SOFC.

3.3.3 Electrolyte Supported SOFC

Currently, the predominant electrolyte material used in SOFCs is YSZ. At temperatures exceeding 800˚C, YSZ-based electrolytes exhibit good conductivity for oxygen ions while demonstrating minimal electrical conductivity. Consequently, an electrolyte-supported SOFC typically operates optimally in temperature range of 800-1000°C. Electrolyte serves three primary functions within SOFCs (Kupecki, 2018):

- The electrolyte facilitates ion conduction, allowing chosen ions to react at anode and cathode.
- It behaves considered barrier among fuel and oxidizer sections, preventing any unintended mixing of fuel and oxidant.

- It functions as an electric insulator, directing electrons to alternate pathways and enabling their capture as useful direct electric current.

Electrolyte-supported SOFCs are primarily employed with solid fuels like coal or char. They offer characteristics conducive to hybrid systems, particularly due to their operation at high temperatures. This temperature range is advantageous for integration into hybrid systems.

3.3.4 Metal Supported SOFC

Thermal shock can be a significant concern for the structural integrity of ceramics used in SOFCs, potentially leading to ceramic breakage. To mitigate this issue, the utilization of metallic supports has been explored. Positioned on the anode side, the support layer typically comprises highly porous, reduction-resistant metals, commonly presented as a metal mesh. This layer serves as a foundation for other components while facilitating fuel accessibility (Blennow, et al., 2009; Kupecki, 2018). The incorporation of metal substrates offers several advantages:

- Metal substrates enhance the efficiency of the cell by improving ionic and electronic conductivity.
- The overall structural stability of the SOFC is enhanced by the good mechanical strength provided by metal substrates.
- They exhibit satisfactory ductility, allowing for some flexibility and resilience against mechanical stress.
- Thermal expansion coefficients of ceramics are aligned with those of electrolyte materials, reducing the likelihood of cracking due to thermal stress.
- Both anode, cathode, and electrolyte layers can be thinner in metal-supported SOFCs, enabling more efficient ion and electron transport.
- Metal substrates contribute to advanced ionic and electronic conductivity, enhancing the efficiency of the cell.
- Metal-supported SOFCs are more easily integrated with interconnectors, facilitating their connection in the stack.

- The adoption of metal supports can lead to a reduction in materials cost compared to traditional ceramic supports.

In summary, the integration of metallic supports in SOFC design addresses issues related to thermal shock and introduces benefits that span from improved structural stability to enhanced efficiency and cost-effectiveness.

3.4 Flow Configurations of SOFC

SOFCs can be configured with different flow patterns, including cross flow, co-flow, and counter flow designs, it is depicted in Figure 3.5. Each of these configurations has its own advantages and considerations. In a counter flow design, maintaining proximity among fuel inlet temperature and air outlet temperature is crucial to mitigate potential temperature gradients within this area. This helps reduce thermal stresses and gradients within the cell. On the other hand, the co-flow configuration is known for promoting a more uniform temperature distribution within the cell or stack (Andersson, 2009; Khan, 2019).

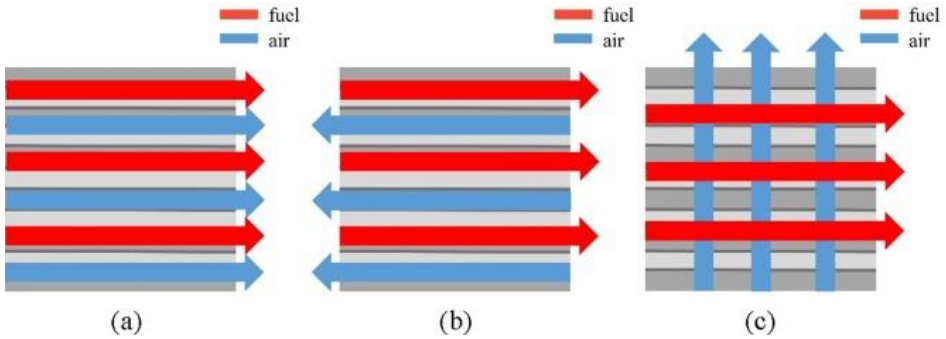

Figure 3.5 Flow configurations in SOFC (Lee, Han, Kim, Kim, & Kim, 2022)

Researchers have explored various aspects of these flow configurations. Yakabe et al. (2001) conducted a study involving a planar SOFC model operating at 900-1000°C. The results of their research indicated that the utilization of co-flow patterns was observed to alleviate the occurrence of temperature variations and internal stress. Colpan et al. (2010) formulated a heat transfer model for co-flow and counter flow

direct internal reforming SOFCs in the process of warming up and commencing operation. Their observations demonstrated that the counter-flow arrangement yielded increased power density and current density, yet reduced efficiency. Furthermore, they discerned maximum stress occurring near to fuel inlet and interface between the electrolyte and anode. Marra et al. (2015) developed a one-dimensional model for co-flow and counter-flow SOFC arrangements. They utilized a symmetrical cell cross-section to investigate the distribution of temperature and the efficiency of these arrangements. Ranasinghe and Middleton (2017) developed a three-dimensional model for SOFCs that are supported by an anode and feature gas flow patterns in both counter-flow and radial configurations. Their investigation showcased that the radial flow pattern displayed superior performance in contrast to the counter flow pattern across varying operational temperatures. Isık (2019) investigated the distribution of temperature and the performance of SOFCs by employing both parallel and counter-flow configurations. The findings of their study unveiled that although the counter-flow design displayed marginally superior performance, the co-flow configuration presented a more homogeneous temperature distribution. In summary, the choice of flow configuration in SOFCs significantly impacts temperature distribution, stress generation, and overall performance. Researchers have undertaken various studies to optimize these factors and enhance the efficiency and reliability of SOFC systems.

3.5 Types of Fuel Used in SOFC

SOFCs demonstrate a remarkable capacity to adapt to different fuel sources, enabling their operation not only with hydrogen but also with a diverse array of hydrocarbon fuels, such as methane, coal gas, bioethanol, ammonia, and more. This inherent adaptability allows for a broad spectrum of applications and potential uses. However, the utilization of hydrocarbon fuels can present certain challenges, specifically regarding carbon deposition on anode, that ultimately leads to deactivation and diminished durability (Staniforth & Ormerod, 2002). To address this, fuel reformers can be employed, either externally or internally, to convert hydrocarbons like CH_4 into hydrogen. Internal reforming offers the advantage of

supplying extra cooling to SOFC and reducing the need for an external reformer, as steam reforming is an endothermic reaction (Akroot, 2018). However, ensuring effective thermal management is crucial to prevent inadequate cooling of SOFC system (Bove & Ubertini, 2008).

Numerous studies have investigated the impact of various fuels on SOFC performance. Chan et al. (2002) modeled SOFC systems that use methane and hydrogen. Their analysis emphasized that cathode activation and ohmic overpotentials are significant contributors to losses within the fuel cell. At 800°C, the efficiency of an H_2-fed system was 50.97%, while the efficiency of a CH_4-fed system was 62.19%. Staniforth and Ormerod (2002) demonstrated the feasibility of running an SOFC directly on biogas, showcasing the wide compositional range (15% to 85% methane) that can be accommodated. Ni (2013) developed a 2D thermo-electrochemical model for SOFCs fueled by CO_2/CH_4 mixtures, examining effect of different operational variables on SOFC. Liu et al. (2013) investigated SOFC system fueled by gasification syngas, reporting increased electrical efficiency and absence of carbon deposition or nickel oxidation. Aydın (2017) investigated variations in current and temperature using hydrogen and syngas as fuels in anode-supported micro-tubular SOFCs. The study highlighted differences in performance and current distribution between the two fuels. Rabuni et al. (2018) fabricated a micro-tube SOFC using CH_4 as fuel. Experimental data revealed lower power density for CH_4 compared to H_2, attributed to catalytic limitations and more complex reactions. Kalinci and Dincer (2018) considered NH_3 as an alternative fuel for a proton-conducting electrolyte-based SOFC, calculating maximum power densities for H_2 and NH_3. Lv et al. (2019) investigated the secure attributes and load efficiency of hybrid system comprising IT-SOFC and gas turbine, which utilized gasified biomass gas. They found system efficiency changes with variations in fuel composition. These studies collectively emphasize the wide range of fuel options for SOFCs and the significance of understanding their impact on performance, efficiency, and durability.

CHAPTER FOUR
SOFC HYBRID SYSTEMS AND S-CO_2 BRAYTON CYCLE

In recent times, there has been an escalating focus on the advancement of innovative and effective sustainable technologies that strive to diminish investment expenses while attaining enhanced power concentration. Technologies such as wind, solar, and hydro-based energies have gained prominence and are often integrated with backup units to create hybrid systems that are both efficient and environmentally friendly. Among these technologies, SOFCs have received significant attention over the past decade due to their exceptional efficiency.

SOFCs possess several features that make them well-suited for integration into hybrid systems. These include their ability to operate on a variety of fuels, their inherent modularity, and their potential for use in bottoming cycles due to their versatile operating temperature range. As evidenced in existing literature, SOFC stacks have been successfully integrated into combined power plants, gas turbine systems, and other renewable energy systems, showcasing their adaptability and potential for synergistic applications (Buonomano, Calise, d'Accadia, Palombo, & Vicidomini, 2015).

4.1 SOFC/Gas Turbine Hybrid Systems

In recent years, researchers have shown a strong interest in SOFC/Gas Turbine power plants (SOFC/GT) as exemplars of energy conversion systems renowned for their high efficiency. These hybrid systems are notable for their ability to achieve low emissions, high efficiency, and compatibility with hydrogen fuels. The analysis of the SOFC/GT system necessitates consideration of numerous variable parameters. These parameters can be explored from various perspectives, including the type of fuel utilized, temperature, pressure, the subsystem type, and heat recovery methods (Buonomano, Calise, d'Accadia, Palombo, & Vicidomini, 2015; Ferrari, Damo, Turan, & Sánchez, 2017).

In the literature, numerous studies have focused on investigating operating variables to advance performance of SOFC/GT hybrid systems. These systems

demonstrate impressive efficiency, ranging from 55% to 60% for smaller systems in 250-1000 kW and reaching approximately 68% at larger 5-10 MW systems (Calise, Palombo, & Vanoli, 2006; Cheddie & Murray, 2010; Van Biert, Woudstra, Godjevac, Visser, & Aravind, 2018). The overall efficiency, combining thermal and electrical outputs, can even surpass 85%. Importantly, emissions from these systems are significantly lower compared to conventional gas turbine (Damo, Ferrari, Turan, & Massardo, 2019; Massardo & Lubelli, 2000).

Numerous studies have explored SOFC/GT hybrid systems by employing diverse approaches. An example of this is the pressurized system engineered by Siemens-Westinghouse Power Corporation, which produces 220 kW power and boasts 55% net efficiency. Chan et al. (2003) provided evidence of an SOFC/GT system that utilized natural gas and achieved an electrical efficiency surpassing 60% and an overall system efficiency surpassing 80%. Haseli et al. (2008) developed an SOFC hybrid system integrated to recuperative gas turbine (GT) cycle. The investigation concluded that thermal efficiency of SOFC/GT system declined due to an elevation in turbine inlet temperature (TIT). Moreover, it was demonstrated that the SOFC/GT configuration exhibited an average performance enhancement of 27.8% in terms of thermal efficiency compared to a conventional gas turbine facility. Kaya (2021) developed a model of the SOFC/GT which consists of 250 cells. The outcomes from this comprehensive investigation divulged that the quintessential variable for augmenting the system's efficacy was the operational pressure exerted upon the fuel cell stack. The system demonstrated power output of 138 kW and achieved peak electrical conversion efficiency of 65.19%. Additional studies have investigated different designs, including internal reforming tubular SOFC stacks and various hybrid cycles, all contributing to the understanding of system efficiencies, emissions reduction, and thermal performance (Akroot, 2018; Arabacı, 2008; Eyiler, 2008; Faleh, Khir, & Ben Brahim, 2017; Huang & Turan, 2020; Khan, 2019; Krüger, 2019; McVay, 2014; Pirkandi, Mahmoodi, & Ommian, 2017; Saebea, Authayanun, Patcharavorachot, & Arpornwichanop, 2016); (Tarroja, Mueller, Maclay, & Brouwer, 2010; Welaya, Mosleh, & Ammar, 2013; Yari, Mehr, Mahmoudi, & Santarelli, 2016).

Efforts to optimize SOFC/GT hybrid systems have led to insights into the impact of parameters like operating pressure, temperature, fuel utilization, and turbine design. These studies have provided valuable insights into the capacity of these systems to achieve notable efficiency gains and markedly reduce emissions, positioning them as promising contenders for future energy generation applications.

4.2 Supercritical CO_2 Brayton Cycle

The advancement of power generation technology has consistently focused on energy conservation, emission reduction, increased efficiency, and cost reduction. The S-CO_2 Brayton cycle has garnered substantial interest considered advanced technology for converting energy, aiming to tackle the emerging worldwide issues associated with environmental contamination and the scarcity of energy resources (Zhang, Liao, Jiaqiang, Chen, & Leng, 2021). S-CO_2 Brayton cycle emerges considered viable option for a bottoming cycle owing to its inherent benefits of notable efficacy and compact equipment sizes within intermediate temperatures (450-750˚C) (Mehrpooya, Bahramian, Pourfayaz, & Rosen, 2016).

Figure 4.1 presents a visual representation of the thermal efficiencies exhibited by a range of heat sources and power systems across varying TIT ranges. These heat sources include liquefied natural gas (LNG), coal, solar thermal energy, geothermal energy, nuclear energy, and use of waste heat. Power conversion systems encompass Rankine cycle, organic Rankine cycle (ORC), combined cycle gas turbine (CCGT), GT, and S-CO_2 Brayton cycles (Ahn, et al., 2015). The steam Rankine cycle demonstrates heightened efficiency at lower TITs as a result of the compression of the working fluid while in a liquid state. Conversely, gas turbines employ a compressible fluid, requiring significant work for the compression process. As a result, gas turbine compressors demand substantial energy input. Despite the much higher TITs, gas turbines do not significantly outperform steam Rankine cycles in terms of thermal efficiency. However, higher TITs with gas turbines give rise to material-related challenges. Figure 4.2 displays the critical condition of CO_2 at 30.98˚C and 7.38 MPa, wherein CO_2 approaches an incompressible fluid state, leading to reduced compression work requirements. The variation in specific heat

ratio of CO_2 is more prominent in vicinity of critical point, and temperature at which the maximum specific heat occurs increases as the pressure rises. (Liu, Wang, & Huang, 2019). Consequently, the S-CO_2 Brayton cycle achieves heightened efficiency within intermediate temperature ranges (Ahn, et al., 2015). However, there are two notable drawbacks to consider. Firstly, as the compressor's inlet parameters approach critical area, potentially inducing two-phase field because of acceleration at blade's leading edge, leading to a drop in pressure and temperature in specific fields under critical point. Secondly, the property transition of S-CO_2 close its critical point exhibits non-smooth behavior, leading to localized overlap within the flow field (Liu, Wang, & Huang, 2019).

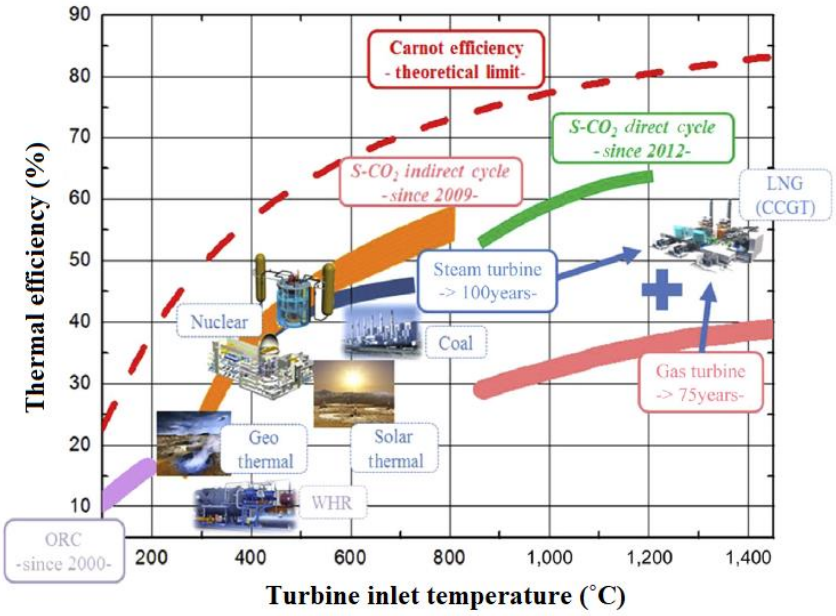

Figure 4.1 The efficiencies of various power systems (Ahn, et al., 2015)

To short, S-CO_2 properties can be summarized as follows (Liu, Wang, & Huang, 2019):

- As CO_2 nears its critical point, it exhibits properties close to an incompressible fluid, subsequently diminishing the demands for compression work.

- The critical temperature of CO_2 permits the utilization of air, rather than water, considered a heat sink by lower temperatures in cooling process, thereby mitigating environmental impact.
- The critical pressure of CO_2, being one-third that of water, facilitates operation at comparatively lower pressure levels.
- In the context of the Brayton cycle, the CO_2 temperature glide near its critical point proves advantageous for heat sources, effectively circumventing pinch issues in heat exchangers. The temperature profile of S-CO_2, devoid of phase variation, exhibits improved compatibility with the heat source.
- The heightened fluid density inherent in S-CO_2 facilitates the use of smaller-scale equipment. This reduction in volumetric flow rate due to the elevated S-CO_2 density yields turbomachinery sizes approximately one-tenth that of a steam Rankine cycle, thereby offering space-saving advantages and cost reductions.

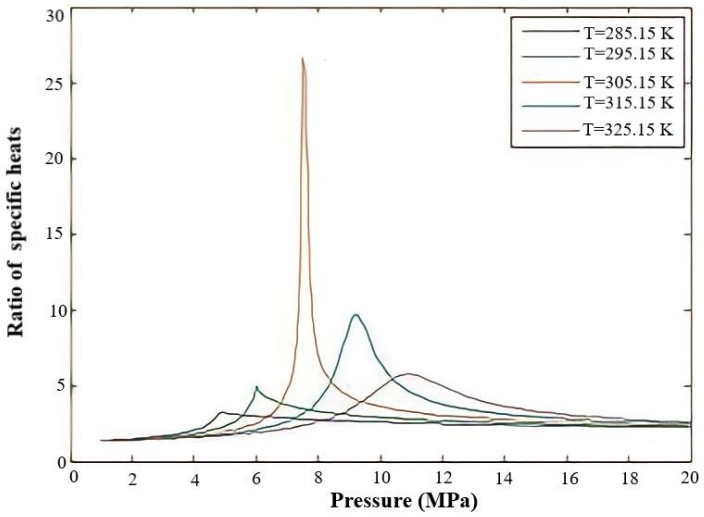

Figure 4.2 Specific heat ratio of CO_2 around critical point (Lee, Lee, Yoon, & Cha, 2014)

S-CO_2 Brayton cycle has undergone thorough investigation across numerous studies in the literature, encompassing a spectrum of heat sources and cycle configurations. Sarkar (2009) performed exergetic analyses and optimization of S-CO_2 recompression cycle. The study emphasized impact of the minimum

temperature on cycle efficiencies and compressor pressure ratio. This influence primarily stems from the substantial impact of specific heat capacity variations around the critical point. Sandia National Laboratories conducted a comprehensive exploration into Brayton cycles utilizing supercritical working fluids, applicable to spectrum of heat sources, with the inclusion of renewable energy and thermal power plant. Their focus on S-CO_2 model development supports systems, components, operations, and commercial strategies to establish a 10 MWe S-CO_2 power conversion system (Wright, Conboy, & Suo-Anttila, 2011). Sandia National Laboratories researchers designed a highly recuperated closed Brayton cycle power system operating on S-CO_2, subjected to various operational conditions. The findings revealed a cycle efficiency of 32% under design conditions of 811 K TIT (Pasch, Fleming, & Rochau, 2012). Utamura et al. (2012) exhibited power generation employing an S-CO_2 regenerative Brayton cycle via a test facility. Their study obtained 110 W power with turbine inlet conditions at 10.6 MPa and 533 K. The regenerative heat exchangers demonstrated remarkable thermal performance, showcasing a regenerative efficiency surpassing 0.95. Le Moullec (2013) analyzed a conceptual model for coal power plant incorporating an S-CO_2 power cycle and 90% CO_2 capture. This concept revealed a net efficiency of 50% for coal power station utilizing an S-CO_2 Brayton cycle without carbon capture while operating at maximal temperatures and pressures reaching 620˚C and 300 bar, respectively. Al-Sulaiman and Atif (2015) conducted a thermodynamic assessment comparing various S-CO_2 Brayton cycles integrated with solar energy system. Among power systems examined, recompression Brayton cycle demonstrated higher efficiency, reaching 52%, accompanied by a system efficiency of 40%. Deng et al. (2017) analyzed exergy efficiency and net power output of S-CO_2 recompression Brayton cycles by optimizing thermodynamic parameters. The investigation unveiled that augmenting the turbine, and compressor isentropic efficiency, temperature of heat source, and TIT, within specific pressure ratios, leads to a notable improvement in cycle exergy efficiency. Sharma et al. (2017) analyzed a waste heat recovery system employing an S-CO_2 regenerative recompression Brayton cycle designed for shipboard applications. Their findings underscored notably elevated exergy destruction within heat exchangers compared to turbomachinery. Cheng et al. (2017) delved into

parameters influencing ultimate cycle efficiency via thermodynamic modeling of the recompression S-CO_2 Brayton cycle. Optimization analysis highlighted the paramount influence of split ratio and pressure in maximizing efficiency of cycle. At heat source temperature of 600°C, efficiency of 0.447 was achieved. Gumus (2019) demonstrated that S-CO_2 power cycles could serve as alternatives to diesel engines, achieving a cycle efficiency of 44.6%. Arnaiz del Pozo et al. (2019) investigated regenerative Brayton cycle with solar based that utilized two distinct working fluids, CO_2 and helium. According to their study, CO_2 has advantages over helium as a preferred working fluid for lower TIT from an efficiency perspective. Wang et al. (2019) presented a novel S-CO_2 recompression power cycle to alleviate temperature sensitivity. Their investigation illustrated which diminished temperature sensitivity were found to be a diminutive flow split ratio, high compressor inlet pressure. Marchionni et al. (2019) advanced numerical model representing regenerative S-CO_2 Brayton cycle of limited capacity intended for the purpose of recuperating waste heat at intermediate temperatures. This system exhibits the potential to generate electricity reaching a maximum of 75 kW. Ceylan and Ozgur (2021) conducted a comparative examination of the thermodynamic analysis of power cycles utilizing air and S-CO_2, thereby unveiling the commendable viability of the S-CO_2 Brayton cycle in relation to other gas-fluid power cycles. Zhang et al. (2021) investigated improvement of the performance of recompression S-CO_2 Brayton cycle through integration by two innovative cycles. Their research emphasized the viability of recompression S-CO_2 Brayton cycle considered potential alternative for medium-temperature heat sources. Cao et al. (2021) analyzed utilization of hybrid solar and biomass waste heat in recompression S-CO_2 Brayton cycle and regenerative GT cycle. The results indicated notable enhancements in overall energy efficiency. Que et al. (2022) conducted a thermodynamic analysis on a power generation system that consisted of a recompression S-CO_2 Brayton cycle with solar-geothermal hybrid systems, resulting in notable power generation and efficiency. Jin et al., (2022) applied finite-time thermodynamics to establish a regenerative S-CO_2 Brayton model, showcasing high cycle thermal efficiency and net power output. Li et al. (2022) designed novel He/S-CO_2 combined Brayton cycles for temperature concentrating solar power, outperforming typical He cycles in terms of performance. Jin et al. (2023) introduced

novel recompression S-CO_2 power cycle which integrates the benefits of preheated S-CO_2 power cycle to effectively recover waste heat from gas turbines, resulting in a noteworthy enhancement in system thermal efficiency.

4.3 Supercritical CO_2 Brayton Cycle and Fuel Cell Hybrid Systems

The use of the waste heat produced by fuel cell system within thermodynamic cycle presents a feasible approach to augment the overall efficiency of the system. The integration of the S-CO_2 Brayton cycle considered option thermodynamic cycle for waste heat recovery has attracted attention in the literature, leading to several studies examining the synergy between these systems.

Sánchez et al. (2009) conducted an analysis of hybrid systems incorporating SOFC or MCFC coupled with S-CO_2 power cycle. They contrasted these systems with conventional cycles employing air as the working fluid. Their investigation notably showcased that the CO_2-MCFC hybrid system exhibited superior performance compared to air-based systems across a broad spectrum of operational conditions. Furthermore, the inclusion of an S-CO_2 bottoming cycle notably enhanced the performance of atmospheric fuel cell-based hybrid systems. Interestingly, as temperatures decreased, turbine power exhibited an increase for both fuel cell types. Mehrpooya et al. (2016) proposed an innovative hybrid system integrating a MCFC with a S-CO_2 Brayton cycle. Their analysis yielded an impressive overall thermal efficiency of 78%, suggesting the thermodynamic viability of suggested hybrid system. Liu et al. (2019) developed a comprehensive mathematical model for a novel power system predicated on integration of SOFC, GT, and CO_2 cycle. The attained energy efficiencies amounted to roughly 79.81%, with efficiency of SOFC standing at 50.96%, accompanied by a CO_2 capture rate of 79.2 kg/h. Schöffer et al. (2021) explored design concepts for SOFC/S-CO_2 Brayton cycle hybrid systems, examining various configurations. Their research highlighted the beneficial effects of cathodic air recirculation on system efficiency and the reduction in heat exchanger size, despite an increase in system complexity. In study investigated by Sadeghi et al. (2022), an assessment was made regarding waste heat recovery systems in a plant using SOFC. The researchers compared two layouts of S-

CO_2 Brayton cycle, taking into consideration the thermodynamic and economic aspects. Their results indicated that, under optimized conditions, a straightforward S-CO_2 cycle exhibited 30.86% higher heat recovery capability from the SOFC compared to a recompression S-CO_2 layout.

Combining S-CO_2 Brayton cycles with fuel cell technologies is crucial for enhancing overall system efficiency. Challenges persist, especially regarding system complexity, yet optimized S-CO_2 cycles demonstrate notable efficiency gains and heat recovery potential. Despite limited studies on this subject, these collective findings emphasize the capacity of S-CO_2 Brayton cycle/Fuel cell hybrid system to enhance efficiency and ensure environmental sustainability. However, the existing literature on SOFC/S-CO_2 hybrid systems remain limited, offering insufficient understanding of the system. This study focuses on evaluating and analyzing the waste heat of a SOFC operating at medium temperatures within different S-CO_2 Brayton cycles.

CHAPTER FIVE
MATHEMATICAL MODELLING OF SYSTEM

This study focuses on a hybrid system comprising an IT-SOFC stack and an S-CO_2 Brayton cycle. The waste heat produced via IT-SOFC stack is efficiently transferred to S-CO_2 Brayton cycle, which serves as a bottoming cycle, facilitated by a heat exchanger (HEX).

5.1 System Configurations

Three distinct hybrid systems were examined in this study. Initially, the integration involves SOFC with S-CO_2 basic Brayton cycle (SBBC). Secondly, a recuperator is incorporated into the standard Brayton cycle, resulting in S-CO_2 regenerative Brayton cycle (SRBC) hybrid system integrated with SOFC. Lastly, another configuration known for enhancing efficiency, the S-CO_2 recompression Brayton cycle (SRCBC), is combined with the SOFC stack, creating a SOFC/SRCBC hybrid system.

5.1.1 SOFC/SBBC Hybrid System

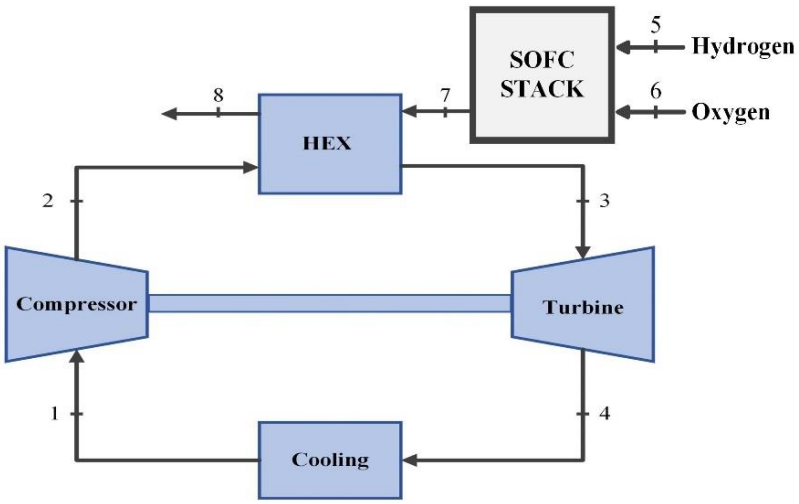

Figure 5.1 SOFC/SBBC hybrid system

An SBBC integrated with SOFC is shown in Figure 5.1. It consists of five components: compressor, HEX, SOFC stack, turbine, and cooling. The low-pressure CO_2 is pressurized by the compressor. The gases from SOFC, which is utilized as heat source, are sent directly to the HEX and there the pressurized CO_2 gains energy. The CO_2 gas exiting from the HEX expands through the turbine. Then it is cooled to the critical temperature point by means of the cooling component.

5.1.2 SOFC/SRBC Hybrid System

The differentiating factor of the SRBC from the SBBC lies in the inclusion of a recuperator within the system. The primary objective of incorporating the recuperator is to enhance efficiency by minimizing waste heat within the Brayton cycle.

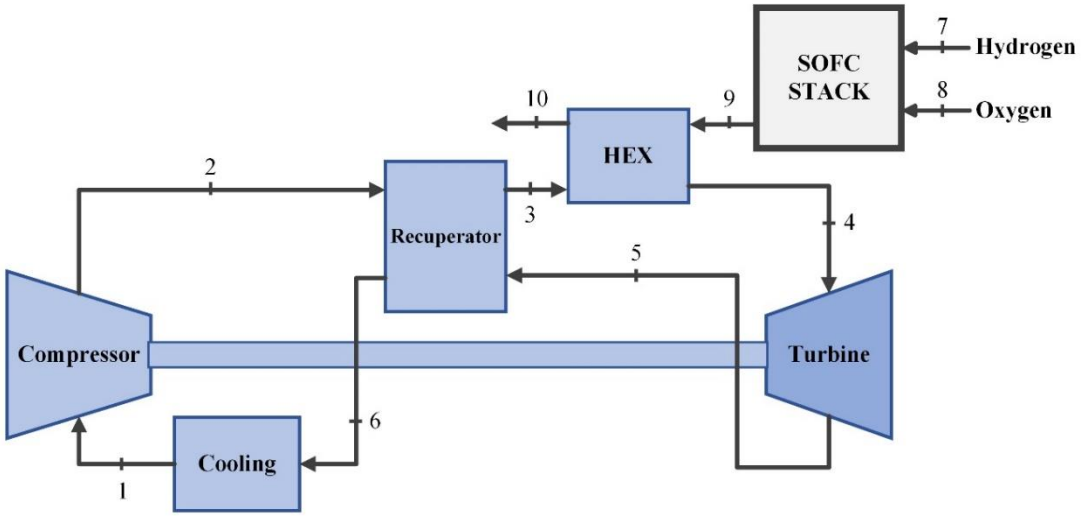

Figure 5.2 SOFC/SRBC hybrid system [modified from (Jin, Xia, Li, & Xie, 2022)]

The SOFC/SRBC hybrid system is primarily composed of essential components, including a compressor, recuperator, HEX, turbine, cooler, and SOFC stack. The low-pressure S-CO_2 undergoes pressurization through the compressor. After compression, the CO_2 stream is heated within the recuperator. Concurrently, the gases emitted from the SOFC, serving as a heat source, are directed to the HEX, where the pressurized CO_2, having received heat in the recuperator, gains additional

energy. The CO_2 stream emerging from the HEX then expands through the turbine, generating power. The turbine exhaust is directed back into the recuperator, providing heat to stream 2. Subsequently, the exhaust is cooled in preparation for the compression stage. The recuperator effectively captures surplus energy from the turbine exhaust.

5.1.3 SOFC/SRCBC Hybrid System

Another alternative system to consider is the SRCBC. In this setup, the system incorporates multiple heat recovery points, namely low temperature recuperator (LTR), high-temperature recuperator (HTR), and HEX. Additionally, a re-compressor (RC) is employed to compress a portion of the CO_2 fluid without cooling, while another portion is cooled before entering the main compressor (MC). The primary objective of this configuration is to enhance both cycle's efficiency and overall efficiency of hybrid system by effectively recovering and utilizing heat. This approach aims to maximize the utilization of available heat sources and improves total performance of system.

The investigated SOFC/SRCBC hybrid system is structured with key components including a MC, LTR, RC, HTR, HEX, turbine, cooler, and SOFC stack. The schematic diagram of the system is illustrated in Figure 5.3. Operational process begins with the pressurization of a portion of low-pressure CO_2 by MC. Subsequently, CO_2 stream is heated within LTR before being combined with the compressed CO_2 stream from the RC. Following the heat absorption in the HTR, the CO_2 flow is directed to the heat exchanger. The gases emitted by the SOFC, serving as the heat source, facilitate the transfer of energy to the pressurized CO_2 within the HEX. The CO_2, now enriched with heat, proceeds to the turbine for expansion, generating power output. The exhaust from the turbine is sent sequentially to HTR and LTR for heating of streams 3 and 2. Cooled CO_2 exiting LTR (stream 8) is divided into two distinct streams with varying mass flow rates. The majority of mass flow rate, denoted as stream 8m, undergoes cooling in the cooler to achieve an appropriate temperature before entering MC. Remaining mass flow rate, identified as flow 8r, is directed to the RC for pressurization.

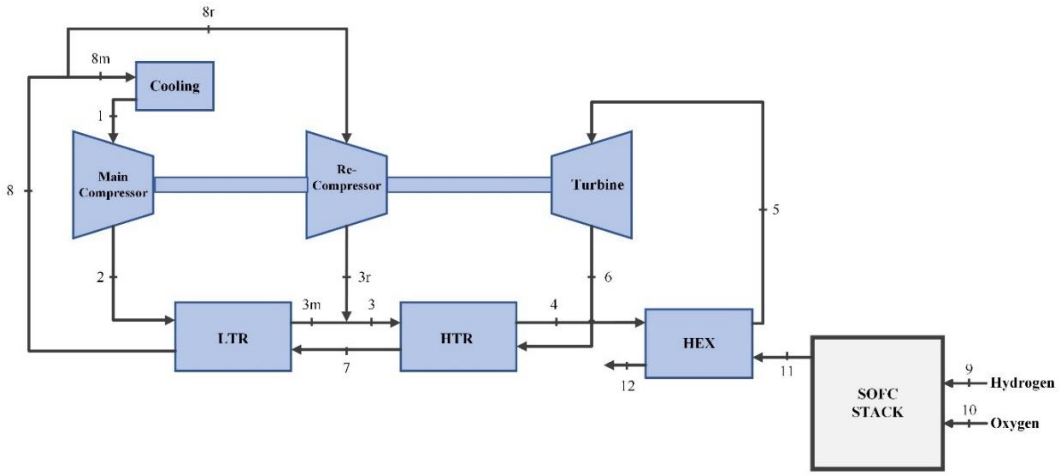

Figure 5.3 SOFC/SRCBC hybrid system [modified from (Zhang, Liao, Jiaqiang, Chen, & Leng, 2021)]

5.2 Inlet Parameters of Systems

The analysis employed Ceres Power's metal-supported IT-SOFC cell, suitable for integration into stacks and larger systems. Notably, Ceres SOFCs utilize CGO as the electrolyte material instead of YSZ. This choice leverages CGO's significantly enhanced ionic conductivity, enabling practical fuel cell operation even at lower temperatures, down to 500˚C (Leah, Brandon, & Aguiar, 2005). The examined IT-SOFC operates at typical parameters of 873 K temperature and 0.3 A/cm^2 current density. Inlet variables for SOFC are detailed in Table 5.1. In stationary power plant applications utilizing fuel cells, power capacity spans a wide range. For this system, considering applications like semi-trucks with fuel cells (e.g., Nikola-400 kW and Hyzon-450 kW) and stationary SOFC power plants (e.g., DOOSAN-440 kW), the system incorporates 20,000 cells (Hart, Jones, Houghton, Cordobes, & Lewis, 2022). The current study investigates impact of SOFC operating temperature and current density on both Brayton cycles and hybrid systems.

Table 5.1 Inlet parameters of SOFC (Leah, Brandon, & Aguiar, 2005)

Parameter	**Value**
Ambient temperature, T_0	298 K
Ambient pressure, P_0	1 atm
Faraday constant, F	96485 C/mol
Universal gas constant, $\overline{R}$	8.314 J/(mol K)
Anode pre-exponential factor, k_a	6.54×10^{11} S/m^2
Cathode pre-exponential factor, k_c	7×10^{11} S/m^2
Anode activation energy, E_a	1.294×10^{5} J/mol
Cathode activation energy, E_c	1.309×10^{5} J/mol
Ionic conductivity pre-exponential factor, K_i	2.706×10^{6} S K/m
Area-specific contact resistance, R_{cont}	8.46×10^{-6} Ω m^2
Thickness of the anode, l_a	1.5×10^{-5} m
Thickness of the cathode, l_c	5.0×10^{-5} m
Thickness of the electrolyte, l_{el}	1.5×10^{-5} m
Electronic conductivity of the anode, σ_a	8.0×10^{4} S/m
Electronic conductivity of the cathode, σ_c	8.4×10^{3} S/m
Anode effective diffusivity, $D_{eff,a}$	1.495×10^{-6} m^2/s
Cathode effective diffusivity, $D_{eff,c}$	1.495×10^{-6} m^2/s
Active cell area, A_{cell}	121 cm^2
Fuel utilization factor, U_f	0.7
Oxygen utilization factor, U_o	0.1
Number of cells, N_{cell}	20 000

The inlet parameters for the Brayton cycles were established based on an S-CO_2 Brayton cycle power system operated by Sandia National Laboratories (Pasch, Fleming, & Rochau, 2012). For each cycle in this investigation, the input parameters

detailed in Table 5.2 were employed. The selection of a pressure ratio of 3 is rooted in the current practical limitations and availability of piping equipment, heat exchangers, and circuit components. Working at pressures exceeding 300 bar is restricted and impractical due to the prevailing conditions (Dyreby, Klein, Nellis, & Reindl, 2014; Gumus, 2019; Sánchez, Chacartegui, Jiménez-Espadafor, & Sánchez, 2009).

Table 5.2 Inlet parameters of S-CO_2 Brayton cycles

Parameter	**Value**
Compressor inlet temperature (Pasch, Fleming, & Rochau, 2012)	305 K
Compressor inlet pressure (Pasch, Fleming, & Rochau, 2012)	7690 kPa
Compressor isentropic efficiency (Pasch, Fleming, & Rochau, 2012)	0.70
Turbine isentropic efficiency (Pasch, Fleming, & Rochau, 2012)	0.87
Pressure ratio (Gumus, 2019)	3
Heat exchanger effectiveness (Pasch, Fleming, & Rochau, 2012)	0.85
Heat exchanger efficiency	0.85
The split rate for the re-compression cycle (Pasch, Fleming, & Rochau, 2012)	0.4
The pinch point temperature difference (ΔT)	50 K

The heat exchanger effectiveness values specified in Table 5.2 were used for the recuperator in the SRBC, and for the LTR and HTR in the SRCBC. The heat exchanger efficiency value was used for the HEX in the SBBC, SRBC, SRCBC. No analysis of cooling has been performed; however, it is of utmost importance to emphasize that the cooler functions in a manner comparable to a heat exchanger. The isentropic efficiencies of the MC and RC in SRCBC are also equal. In order to avoid pinch point problems in current density range examined (0.05-0.8 A/cm^2), different approaches have been used for it in the literature. The TIT was kept constant at varying source temperatures (Dyreby, Klein, Nellis, & Reindl, 2014; Gumus, 2019; Li, Erqi, Qiu, Wang, & Zhang, 2022; Zhang, Liao, Jiaqiang, Chen, & Leng, 2021) or,

as in this study, the difference between turbine inlet temperature and source temperature (ΔT) was taken as constant (Cao, Habibi, Zoghi, & Raise, 2021; Garg, Kumar, & Srinivasan, 2013; Li, Erqi, Qiu, Wang, & Zhang, 2022; Ma, Liu, Yan, & Liu, 2017; Pan, et al., 2020). Additionally, ΔT is generally in the range of 10-50 K in the literature (Cao, Habibi, Zoghi, & Raise, 2021; Garg, Kumar, & Srinivasan, 2013; Li, Erqi, Qiu, Wang, & Zhang, 2022; Ma, Liu, Yan, & Liu, 2017; Pan, et al., 2020). In a study examining the S-CO_2 Brayton Cycle and SOFC hybrid system, the minimum temperature difference between TIT and SOFC operating temperature was taken as 50 K (Sadeghi, Mahmoudi, & Rosen, 2022), thus, it is assumed ΔT is a constant 50 K for this study.

5.3 Assumptions for Modeling the System

In the model, some assumptions made are given as below:

- For all components, a steady-flow operation is present and the variations in kinetic and potential energy are insignificant.
- All components are perfectly thermally insulated.
- The pressure drops in the recuperators, piping and the heat exchanger are ignored.
- The fuel supplied to the SOFC system is hydrogen.
- The pressure parameters at anode outlet in SOFC exhibit identical values to those of cathode.

5.4 Electrochemical Model of SOFC

The electrochemical processes of the SOFC commence with incoming electrons driving the reduction of oxygen at the junction of the cathode and electrolyte. These produced oxygen ions travel directly solid electrolyte to anode-electrolyte interface, that they undergo an electrochemical reaction with adsorbed hydrogen, resulting in formation of water vapor. Simultaneously, operation releases the electron charge into the external circuit (Braun, 2002). The electrochemical reactions considered are (Mench, 2008):

$$Anode: H_2+O^{2-} \rightarrow H_2O+2e^- \quad (5.1)$$

$$Cathode: {}^{1}\!/\!_{2}\, O_2+2e^- \rightarrow O^{2-} \quad (5.2)$$

$$Overall: H_2+ {}^{1}\!/\!_{2}\, O_2 \rightarrow H_2O \quad (5.3)$$

The maximum theoretical work that can be done is equivalent to change of Gibbs free energy (Mench, 2008):

$$\Delta G=\Delta H-T\cdot\Delta S \quad (5.4)$$

ΔH is enthalpy change, T is temperature and ΔS is entropy change. When considering thermal voltage, the complete amount of potential chemical energy involved in reaction is fully converted into electrical work. If this was the case, then the thermal voltage would be (Mench, 2008):

$$V_{th}=\frac{-\Delta H}{n\cdot F} \quad (5.5)$$

where F is Faraday constant and *n* is the number of moles of the electrons transferred. The expression depicting the maximum possible reversible voltage that is reversible in an electrochemical cell is shown (Mench, 2008):

$$V_{max}=\frac{-\Delta G}{n\cdot F} \quad (5.6)$$

Global redox reaction in fuel cell (Mench, 2008):

$$v_A A + v_B B \leftrightarrow v_C C + v_D D \quad (5.7)$$

the stoichiometric coefficients of the balanced electrochemical reaction can be represented by the variable '*v'*. The Nernst Voltage can be determined using the principles of thermodynamics applied to systems in equilibrium (Mench, 2008):

$$V_n = V_{max} + \frac{\overline{R} \cdot T}{n \cdot F} ln \left(\frac{a_A^{v_A} \cdot a_B^{v_B}}{a_C^{v_C} \cdot a_D^{v_D}} \right) \quad (5.8)$$

the thermodynamic activity coefficients for the reacting species are denoted by the letter '*a*'. For ideal gas (Mench, 2008):

$$a = \frac{P_i}{P^\circ} \quad (5.9)$$

where P_i is the partial pressure of the species of interest and P° is the reference pressure, 1 atm (101,325 Pa). Nernst voltage for SOFC (Mench, 2008):

$$V_n = V_{max} + \frac{\overline{R} \cdot T}{2 \cdot F} ln \left(\frac{a_{H_2} \cdot a_{O_2}^{1/2}}{a_{H_2O}} \right) \quad (5.10)$$

The different polarization losses are succinctly encapsulated within the subsequent equation, which represents the voltage of an SOFC in relation to the current density (Mench, 2008):

$$V_{cell}=V_n-V_{act}-V_{ohm}-V_{con} \quad (5.11)$$

5.4.1 Activation Polarization

Activation polarization, which is the primary cause of losses at low current density, refers to the voltage overpotential that is necessary to surpass the activation energy of the electrochemical reaction taking place on the catalytic surface. (Mench, 2008). The activation overpotential is given as:

$$V_{act}=V_{act,a}+V_{act,c} \quad (5.12)$$

where $V_{act,a}$ is the anode activation polarization and $V_{act,c}$ is the cathode activation polarization (Sadeghi, Mahmoudi, & Rosen, 2022):

$$V_{act,a}=\frac{\bar{R}\cdot T}{F}\cdot sinh^{-1}\left(\frac{i_{cell}}{2\cdot i_{0,a}}\right) \quad (5.13)$$

$$V_{act,c}=\frac{\bar{R}\cdot T}{F}\cdot sinh^{-1}\left(\frac{i_{cell}}{2\cdot i_{0,c}}\right) \quad (5.14)$$

Where i_{cell} is the cell current density, $i_{0,a}$ is the anode exchange current density, $i_{0,c}$ is the cathode exchange current density (Leah, Brandon, & Aguiar, 2005; Sadeghi, Mahmoudi, & Rosen, 2022).

$$i_{0,a}=k_a\frac{\bar{R}\cdot T}{2\cdot F}exp\left(\frac{-E_a}{\bar{R}\cdot T}\right) \quad (5.15)$$

$$i_{0,c}=k_c\frac{\bar{R}\cdot T}{2\cdot F}exp\left(\frac{-E_c}{\bar{R}\cdot T}\right) \quad (5.16)$$

Where k_a and k_c are pre-exponential factor for the anode and the cathode respectively. E_a and E_c are activation energy for the anode and the cathode respectively (Leah, Brandon, & Aguiar, 2005; Sadeghi, Mahmoudi, & Rosen, 2022).

5.4.2 Ohmic Polarization

Ohmic polarizations arise because of the electronic conduction of current and ionic conduction of oxygen anions. Ionic conductivity in main electrolyte and in catalyst layers dominate the ohmic polarization. The voltage drop due to ohmic polarizations is (Mench, 2008):

$$V_{ohm}=I\cdot R_{ohm}=i_{cell}\cdot A_{cell}\cdot R_{ohm} \quad (5.17)$$

where R_{ohm} is the resistance and A_{cell} is electrode surface area.

$$R_{ohm}=\frac{1}{A_{cell}}\cdot\left(\frac{l_a}{\sigma_a}+\frac{l_c}{\sigma_c}+\frac{l_{el}}{\sigma_{el}}+R_{cont}\right) \quad (5.18)$$

Where σ is the conductivity, l is the linear path length of ion travel to preferred fuel cell materials. R_{cont} is contact resistance. CGO electrolyte's ionic conductivity can be estimated as (Leah, Brandon, & Aguiar, 2005):

$$\sigma_{el}=K_i\frac{exp\left(-\frac{0.64}{\left(8.6173\times10^{-5}T\right)}\right)}{T} \quad (5.19)$$

Where K_i is the ionic conductivity pre-exponential factor.

5.4.3 Concentration Polarization

The occurrence of concentration polarization arises from alterations in the concentration of reactants, leading to a reduction in partial pressure for both hydrogen and oxygen within anode and cathode gas channels, respectively. The concentration polarizations are written as (Leah, Brandon, & Aguiar, 2005; Sadeghi, Mahmoudi, & Rosen, 2022):

$$V_{con} = V_{con,a} + V_{con,c} \quad (5.20)$$

$$V_{con,a} = \frac{\bar{R} \cdot T}{2 \cdot F} ln \left(\frac{P_{H_2O,TPB} \cdot P_{H_2}}{P_{H_2,TPB} \cdot P_{H_2O}} \right) \quad (5.21)$$

$$V_{con,c} = \frac{-\bar{R} \cdot T}{4 \cdot F} ln \left(\frac{P_{O_2,TPB}}{P_{O_2}} \right) \quad (5.22)$$

the partial pressure of the species of interest is denoted as 'P_i'.

$$P_{H_2O,TPB} = P_{H_2O} + \frac{i_{cell} \cdot l_a \cdot T \cdot \bar{R}}{2 \cdot F \cdot D_{eff,a}} \quad (5.23)$$

$$P_{H_2,TPB} = P_{H_2} - \frac{i_{cell} \cdot l_a \cdot T \cdot \bar{R}}{2 \cdot F \cdot D_{eff,a}} \quad (5.24)$$

$$P_{O_2,TPB} = P_c - (P_c - P_{O_2}) \cdot exp \left(\frac{i_{cell} \cdot l_c \cdot T \cdot \bar{R}}{4 \cdot F \cdot D_{eff,c} \cdot P_c} \right) \quad (5.25)$$

Where D_{eff} is the effective diffusivity of species of interest and P_c is pressure of the cathode.

5.5 SOFC Stack Energy Balance Equation

The molar conversion rate of Eq. (4.3) defined as (Timurkutluk B. , 2007):

$$x = \frac{i_{cell} \cdot N_{cell} \cdot A_{cell}}{2 \cdot F} \quad (5.26)$$

Where N_{cell} and A_{cell} are number of cells and cell active area. The cell current density is an inlet parameter. The definition of fuel utilization factor is (Sadeghi, Mahmoudi, & Rosen, 2022):

$$U_F = \frac{Fuel\ consumed}{Fuel\ supplied} = \frac{x}{\dot{n}_{H2,in}} \quad (5.27)$$

The oxygen utilization factor defined by Eq (4.28):

$$U_O = \frac{Oxygen\ consumed}{Oxygen\ supplied} = \frac{x}{2 \cdot \dot{n}_{O2,in}} \quad (5.28)$$

The SOFC stack power, which is calculated as follow:

$$\dot{W}_{SOFC} = N_{cell} \cdot A_{cell} \cdot i_{cell} \cdot V_{cell} \quad (5.29)$$

The SOFC stack energy balance equation (Haseli, Ibrahim, & Naterer, 2008):

$$\left(\dot{m}_{O_2,in} \cdot h_{O_2,in}\right) + \left(\dot{m}_{H_2,in} \cdot U_F \cdot LHV\right) + \left(\dot{m}_{H_2,in} \cdot (1 - U_F) \cdot h_{H_2,in}\right) = \dot{W}_{SOFC} + (\dot{m}_{out} \cdot h_{out})_{SOFC} \quad (5.30)$$

where $\dot{m}_i$ is mass flow rate of species of interest. SOFC efficiency which is calculated as follow (Timurkutluk B. , 2007):

$$\eta_{SOFC}=U_F \frac{V_{cell}}{V_{th}} \quad (5.31)$$

5.6 Thermodynamic Analysis of Brayton Cycles

Under the specified assumptions, energy balance of system is determined according to first law of thermodynamics, yielding the following equations:

$$\sum \dot{E}_{in} - \sum \dot{E}_{out} = 0 \quad (5.32)$$

$$\sum \dot{Q}_{in} - \sum \dot{Q}_{out} + \sum \dot{W}_{in} - \sum \dot{W}_{out} + \sum_{in} \dot{m}\, h - \sum_{out} \dot{m} h = 0 \quad (5.33)$$

Where, $\dot{E}$, $\dot{Q}$ and $\dot{W}$ means energy rate, heat rate and work rate as well as $\dot{m}$,h being mass flow rate and specific enthalpy, respectively. Under the assumptions mentioned above the general equations can be written for each equipment as given in following Table 5.3. The energy equations employed here are expressed in terms of the SRCBC, which encompasses all the equipment.

Table 5.3 Energy equation of the SRCBC

Component	**Equations**	
MC	$\dot{W}_{mc}=(1-f)\cdot\dot{m}_{CO_2}\cdot(h_2-h_1)$	(5.34)
	$\eta_{mc}=\frac{h_{s2}-h_1}{h_2-h_1}$	(5.35)
RC	$\dot{W}_{rc}=f\cdot\dot{m}_{CO_2}\cdot(h_3-h_8)$	(5.36)
	$\eta_{rc}=\frac{h_{s3}-h_8}{h_3-h_8}$	(5.37)
Turbine	$\dot{W}_t=\dot{m}_{CO_2}(h_5-h_6)$	(5.38)
	$\eta_t=\frac{h_5-h_6}{h_5-h_{6s}}$	(5.39)
HEX	$\eta_{HEX}=\frac{\dot{m}_{CO_2}(h_5-h_4)}{\dot{m}_{11}(h_{11}-h_{12})}$	(5.40)

Table 5.3 (continued)

HTR	$\varepsilon=\frac{T_6-T_7}{T_6-T_3}$	(5.41)
	$h_4-h_3=h_6-h_7$	(5.42)
LTR	$\varepsilon=\frac{T_3-T_2}{T_7-T_2}$	(5.43)
	$(1-f)\cdot(h_3-h_2)=(h_7-h_8)$	(5.44)
Energy balance	$\dot{W}_{net}=\dot{W}_t-(\dot{W}_{mc}+\dot{W}_{rc})$	(5.45)
	$\dot{Q}_{in}=\dot{m}_{CO_2}(h_5-h_4)$	(5.46)

Brayton cycles efficiency is calculated as follow:

$$\eta_{cycle}=\frac{\dot{W}_{net}}{\dot{Q}_{in}} \quad (5.47)$$

The hybrid system's net power and efficiency are written as:

$$\dot{W}_{net,hybrid}=\dot{W}_{net}+\dot{W}_{SOFC} \quad (5.48)$$

$$\eta_{hybrid}=\frac{\dot{W}_{net}+\dot{W}_{SOFC}}{\dot{m}_{H_2,in}\times LHV} \quad (5.49)$$

5.7 Hybrid Systems Features

The T-s diagrams of the specified Brayton Cycles were scrutinized under constant SOFC temperature and current density conditions, set at 873 K and 0.3 A/cm2, respectively. The input parameters outlined in Table 5.1 and Table 5.2 were employed for this analysis.

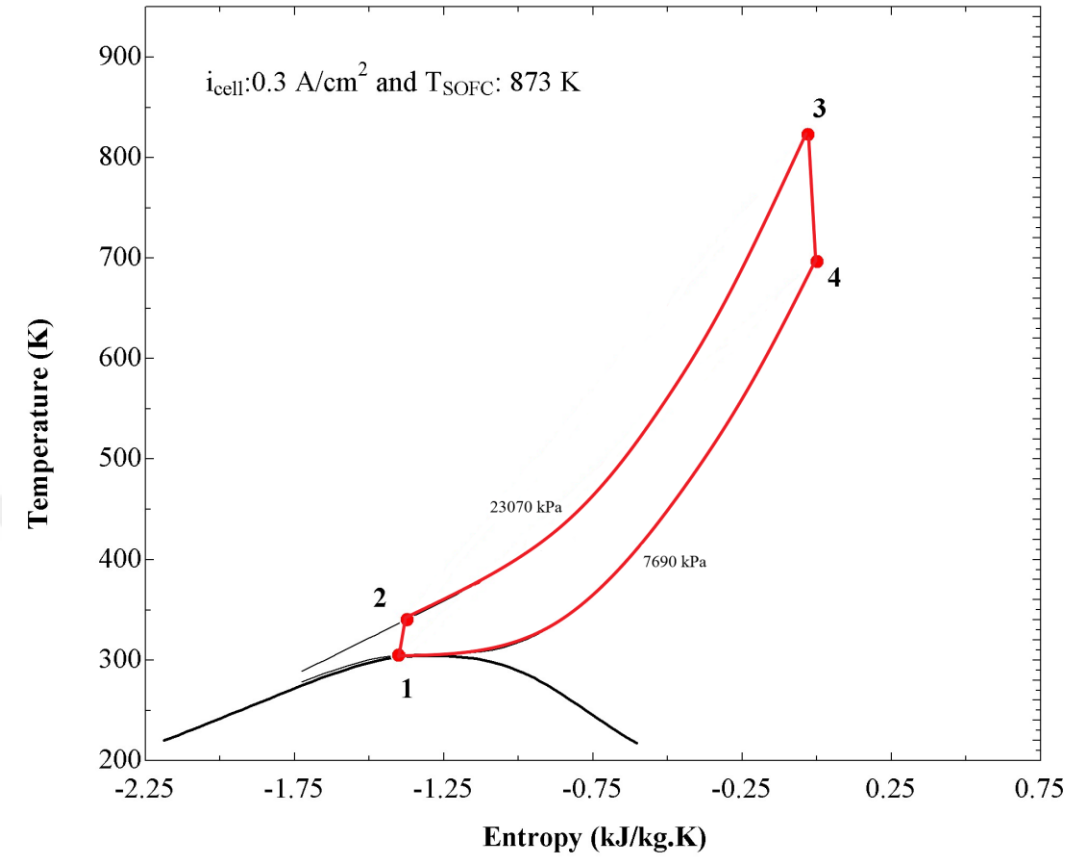

Figure 5.4 SBBC T-s diagram (i_{cell}:0.3 A/cm^2, T_{SOFC}:873 K)

Figure 5.4 illustrates T-s diagram of SBBC. The features of fluid at each state within SBBC under typical SOFC operating conditions are detailed in Table 5.4.

Table 5.4 The features at identified state points for SBBC

SBBC (i_{cell}:0.3 A/cm^2, T_{SOFC}:873 K)			
State point	**ṁ (kg/s)**	**T (K)**	**P (kPa)**
1	1.154	305	7690
2	1.154	340.7	23070
3	1.154	823	23070
4	1.154	697	7690

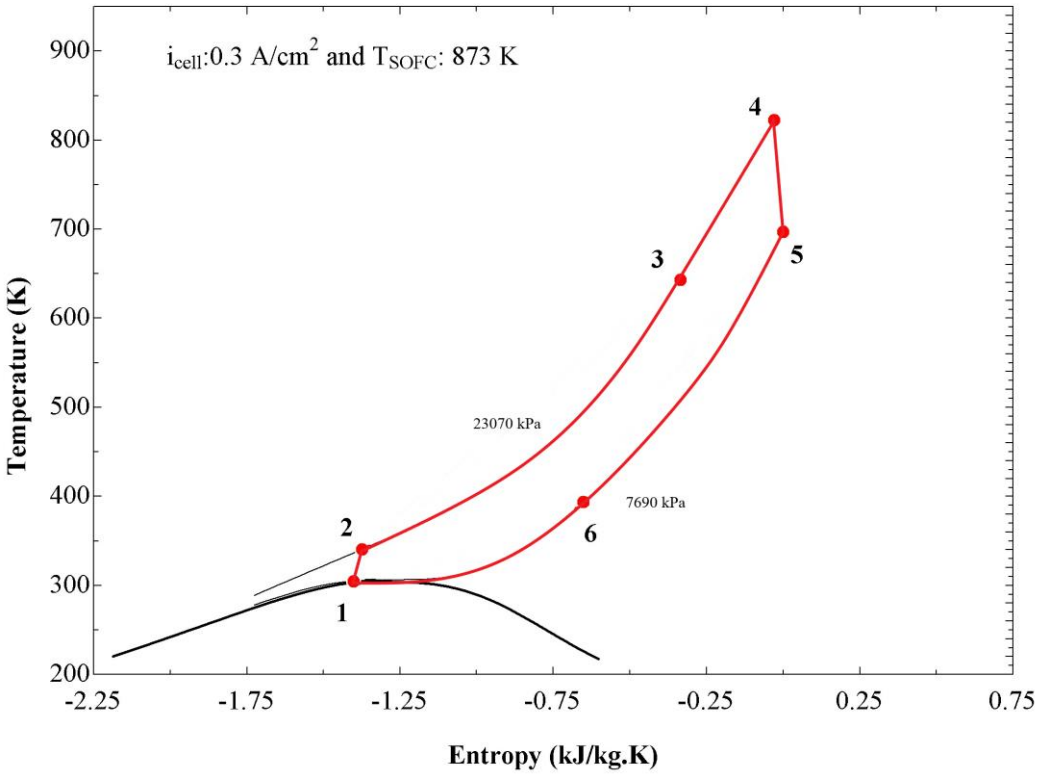

Figure 5.5 SRBC T-s diagram (i_{cell}:0.3 A/cm^2, T_{SOFC}:873 K)

Table 5.5 The features at identified state points for SRBC

SRBC (i_{cell}:0.3 A/cm^2, T_{SOFC}:873 K)			
State point	**ṁ (kg/s)**	**T (K)**	**P (kPa)**
1	2.502	305	7690
2	2.502	340.7	23070
3	2.502	643.5	23070
4	2.502	823	23070
5	2.502	697	7690
6	2.502	394.2	7690

To illustrate this configuration, Figure 5.5 presents the corresponding T-s diagram for the SRBC. Moreover, Table 5.5 provides features of fluid at each point within SRBC under these specific operational conditions.

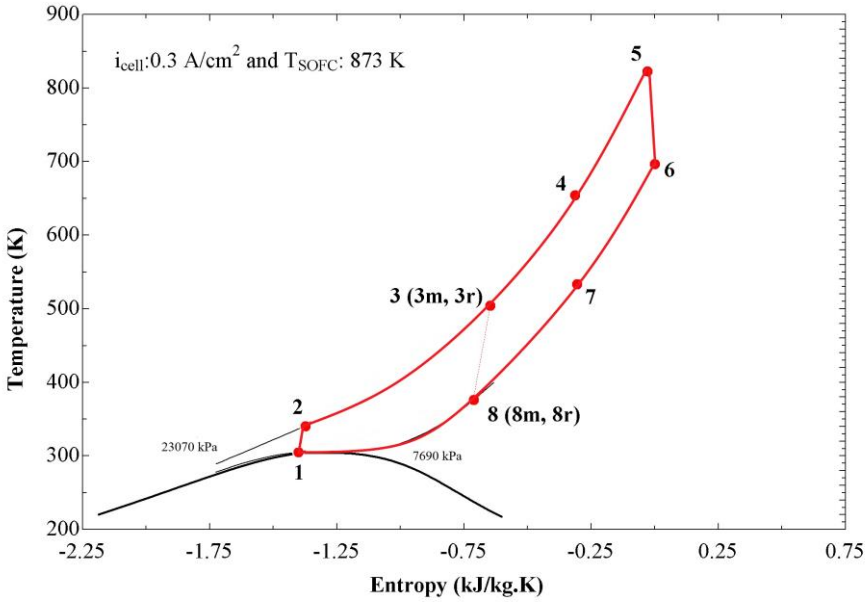

Figure 5.6 SRCBC T-s diagram (i_{cell}:0.3 A/cm^2, T_{SOFC}:873 K)

Figure 5.6 visually represents the corresponding T-s diagram for the SRCBC system, and Table 5.6 provides the fluid properties at the specified state points.

Table 5.6 The features at identified state points for SRCBC

SRCBC (i_{cell}:0.3 A/cm^2, T_{SOFC}:873 K)			
State point	**ṁ (kg/s)**	**T (K)**	**P (kPa)**
1	2.628	305	7690
2	2.628	340.7	23070
3	2.628	504.4	23070
4	2.628	654.2	23070
5	2.628	823	23070

Table 5.6 (continued)

6	2.628	697	7690
7	2.628	533.3	7690
8	2.628	376.2	7690

CHAPTER SIX
RESULTS AND DISCUSSION

The IT-SOFC system's typical operating temperature and current density are reported to be 873 K and 0.3 A/cm^2, respectively (Leah, Brandon, & Aguiar, 2005). In this study, considering the intermediate temperature range, three different temperatures were selected: 823 K, 873 K, and 923 K. The current density of the Ceres Power IT-SOFC, as mentioned in Ref. (Leah, Brandon, & Aguiar, 2005), ranges from 0.05 to 0.8 A/cm^2, which was also considered in the current study. The mass flow rate of Brayton cycle was determined based on capacity and operating conditions of the SOFC.

The primary focus of this study was to evaluate the performance and efficiency of the IT-SOFC as a foundational aspect. Subsequently, the analysis shifted to scrutinize power and efficiency features of both Brayton cycles and hybrid systems within specific system configurations. Notably, the investigation extended to the SOFC/SRBC hybrid system, where the impact of recuperator effectiveness on both the Brayton cycle and the hybrid system was thoroughly examined. Furthermore, the study delved into the SOFC/SRCBC hybrid system, elucidating impact of compressor separation ratio on both Brayton cycle and hybrid system. In the final part, the research involved a thorough comparison of the efficiency of each hybrid system, along with an examination of the SOFC's power contribution within the hybrid context.

6.1 SOFC Stack

At 873 K, the Nernst voltage of the SOFC is calculated as 1.034 V using Eq (5.8). The effect of SOFC current density and temperature on power density and voltage was determined using Eqs. (5.1-5.25). The outcomes of these calculations are presented in Figure 6.1, which demonstrates relation between current density, temperature, cell voltage, and power density.

During fuel cell operation with current flow, the observed voltage is lower than the Nernst voltage due to irreversible losses known as polarizations, resulting in a

voltage drop as depicted in Figure 6.1. Activation polarizations appear across each current density although they exhibit a more pronounced at lower values. Conversely, at medium current densities, such as those commonly used for IT-SOFCs, ohmic polarizations play a significant role. In Figure 6.1, at 0.3 A/cm^2, voltages of 0.46 V, 0.63 V, and 0.77 V were achieved at temperatures of 823 K, 873 K, and 923 K, respectively. Notably, highest voltage was attained at 923 K, indicating that voltage loss reduces as temperature increases due to decreased polarization losses.

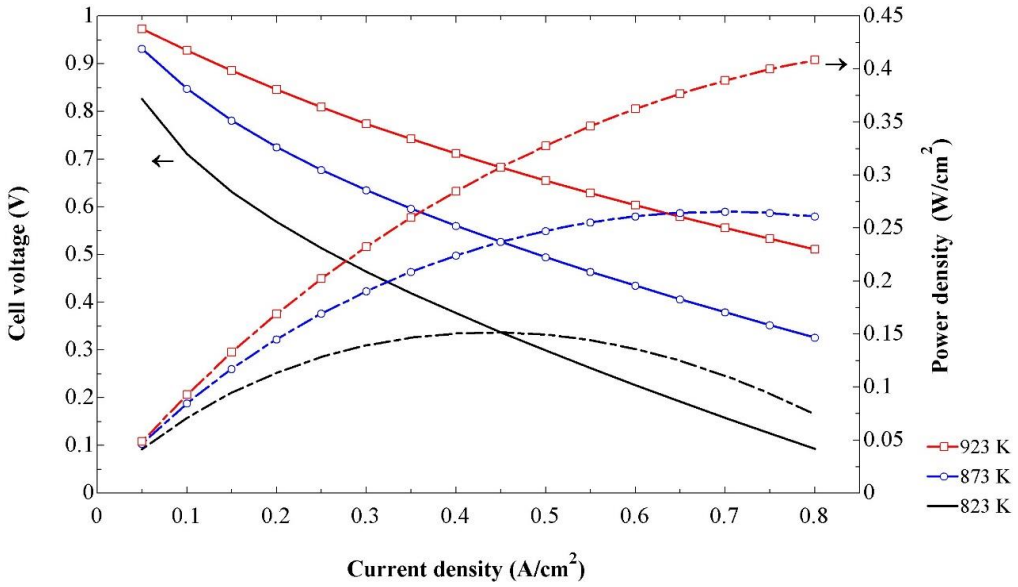

Figure 6.1 The effect of current density on cell voltage and power density at different SOFC operating temperatures

As the current density increases, power density initially rises, reaches a peak, and then starts to decline at lower temperatures. Crucially, as SOFC operating temperature rises, limiting current density also increases, allowing for a broader range of higher current densities and subsequently higher power densities. This emphasizes the benefit of operating the SOFC at higher temperatures within a specific range of current densities. For instance, at current density of 0.1 A/cm^2, power densities of 0.071 W/cm^2, 0.084 W/cm^2, and 0.093 W/cm^2 were achieved at 823 K, 873 K, and 923 K, respectively. At lower current densities where activation

polarization dominates, temperature's impact on power density is less significant (Ugartemendia, Ostolaza, & Zubia, 2013). In contrast, at 0.8 A/cm^2, power densities of 0.074 W/cm^2 at 823 K, 0.26 W/cm^2 at 873 K, and 0.41 W/cm^2 at 923 K were achieved. At higher current densities, temperature demonstrates a notable effect on power density. Rising operating temperature leads to increased power density owing to reduced polarization losses. Despite the reduced open-circuit voltage linked with higher cell temperature, improved cell efficiency and power density arise from reduced overall irreversible overpotential for the cell. This indicates that cell performance enhances as polarization losses decrease, notwithstanding the reduced open-circuit voltage related to elevated cell temperature (Chan, Ho, & Tian, 2003). Most importantly, maintaining optimal operating temperatures for SOFCs is vital to prevent adverse effects on material strength and fuel cell operation. The Ceres fuel cell employed in this system has been previously utilized in another investigation, where it demonstrated power density ranging from approximately 0.15 to 0.25 W/cm^2 at a current density of 0.3 A/cm^2, within a temperature range of 823 K to 873 K (Leah, Brandon, & Aguiar, 2005). In the present study, the power density achieved at 873 K with a current density of 0.3 A/cm^2 is recorded as 0.191 W/cm^2.

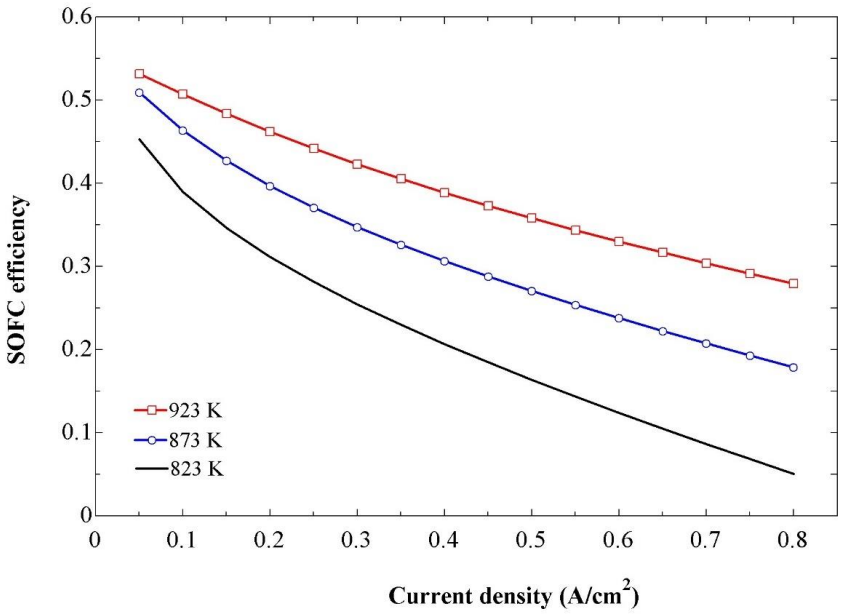

Figure 6.2 The efficiency of SOFC at different temperatures according to varying current density

The SOFC's efficiency was computed using Eq. (5.31), yielding results illustrated in Figure 6.2. This graph demonstrates how the SOFC's efficiency varies with changes in current density. Notably, increasing the SOFC's temperature has a positive effect on its efficiency, whereas efficiency decreases with higher current densities (Tarroja, Mueller, Maclay, & Brouwer, 2010). Under typical IT-SOFC operating conditions, such as a current density of 0.3 A/cm^2 and a temperature of 873 K, the SOFC's efficiency measures at 0.3475. It is important to note that as current densities increase, polarizations increasingly impact the overall efficiency of the SOFC. Consequently, optimizing the operating range of the SOFC at medium current densities is essential for maintaining cell efficiency.

6.2 SBBC and SOFC/SBBC Hybrid System

Prior to analyzing effect of SOFC current density and temperature on SBBC and SOFC/SBBC hybrid systems, an investigation was conducted to understand the characteristics of S-CO_2 fluid by studying the effects of compressor inlet pressure and temperature on efficiency, compressor work, and Brayton cycle net power. The IT-SOFC was assumed to operate under typical operating conditions (0.3 A/cm^2, 873 K). The following graphs were generated using the SOFC input parameters found in Table 5.1.

For Figure 6.3 and Figure 6.4, the input parameters of the SBBC are detailed in Table 5.2. Here the compressor inlet pressure was taken as a variable investigated within the range of 7400-9000 kPa (Saeed, Khatoon, & Kim, 2019). It's essential to highlight that, considering equipment availability, heat exchangers in the system, and overall system cost, the maximum pressure in the cycle, which is the compressor outlet pressure, should not surpass 30,000 kPa (Dyreby, Klein, Nellis, & Reindl, 2014).

Figure 6.3 presents the variations in SBBC net power and compressor work concerning the compressor inlet pressure. As the compressor inlet pressure increases, the compressor work decreases until the critical pressure point is reached. After the critical pressure, the compressor work starts to increase slightly. At approximately 7690 kPa, near the critical pressure, the compressor consumes 36.6 kW of work.

When the pressure is increased to 9000 kPa, the compressor work rises to 37.86 kW. Notably, the compressor work is minimized around the critical pressure, primarily due to the significant change in specific heat at this critical point, which helps reduce the compressor's workload. Analyzing the SBBC net power concerning changes in the compressor inlet pressure, it's evident that net power increases up to the critical pressure and then experiences a slight decrease. At approximately 7690 kPa, near the critical pressure, the cycle produces a net power of 121.9 kW, whereas at 9000 kPa, the net power is 119.4 kW. This higher net power at the around critical pressure is a result of reduced compressor work. A similar trend was observed in a referenced study (Gumus, 2019).

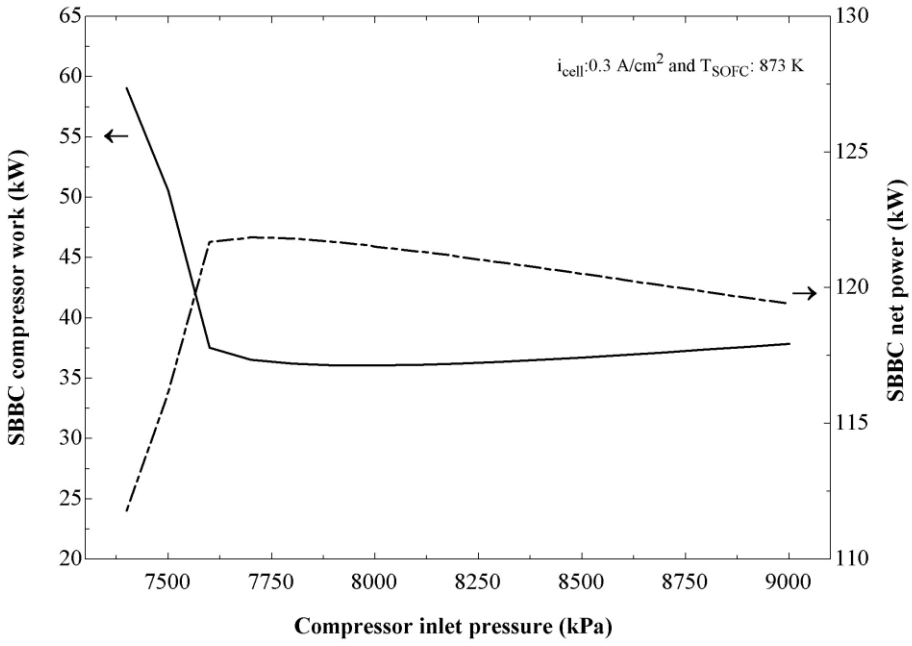

Figure 6.3 Change of SBBC net power and compressor work according to compressor inlet pressure

Figure 6.4 depicts the correlation between the thermal efficiency of the cycle and the pressure at the compressor inlet. The cycle efficiency is observed to be 0.1514 at approximately 7690 kPa (near the critical pressure) and 0.1466 at 9000 kPa. The peak efficiency of cycle is achieved at around the critical pressure due to high specific heat of the fluid at this point (Gumus, 2019; Saeed, Khatoon, & Kim, 2019).

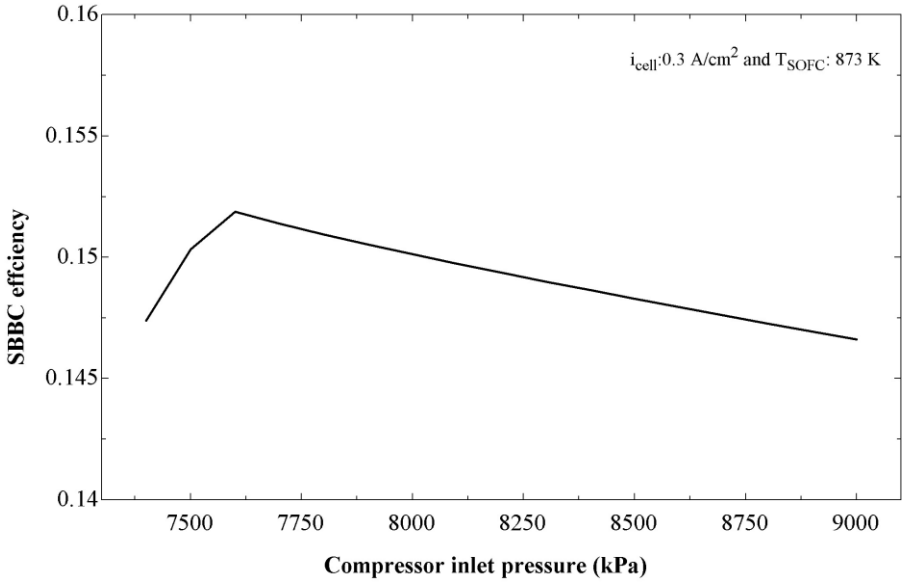

Figure 6.4 Change of SBBC efficiency according to compressor inlet pressure

For Figure 6.5 and Figure 6.6, the input parameters of the SBBC are detailed in Table 5.2. In these figures, the compressor inlet temperature was varied within the range of 303-323 K (Saeed, Khatoon, & Kim, 2019; Sharma, Kaushik, & Manjunath, 2017; Wang, et al., 2019). Figure 6.5 illustrates the variations in net power and compressor work concerning compressor inlet temperature. It's worth noting that the specific heat of S-CO_2 experiences a significant increase at critical temperature, leading to a noticeable change in compressor work at this juncture. It is also important to emphasize that compressor work increases dramatically after reaching the supercritical temperature, resulting in a decrease in net power output. Taking a closer look at this change reveals that at 305 K (near the critical temperature), the compressor work stands at 36.6 kW. At 303 K, this value drops to 33.49 kW, while at 307 K, it surges to 58.65 kW. The transition from 303 K to 305 K sees a 3.11 kW increase in compressor work, and from 305 K to 307 K, a substantial 22.05 kW increase occurs. Meanwhile, the SBBC net power registers at 122.6 kW at 303 K, 121.9 kW at 305 K, and 111.9 kW at 307 K. The shift from 303 K to 305 K results in a minor 0.7 kW decrease in SBBC net power, but from 305 K to 307 K, there's a more significant 10 kW decrease. It becomes evident how the compressor works and

SBBC net power of the system undergoes significant changes after reaching the supercritical temperature, despite the same magnitude of temperature change.

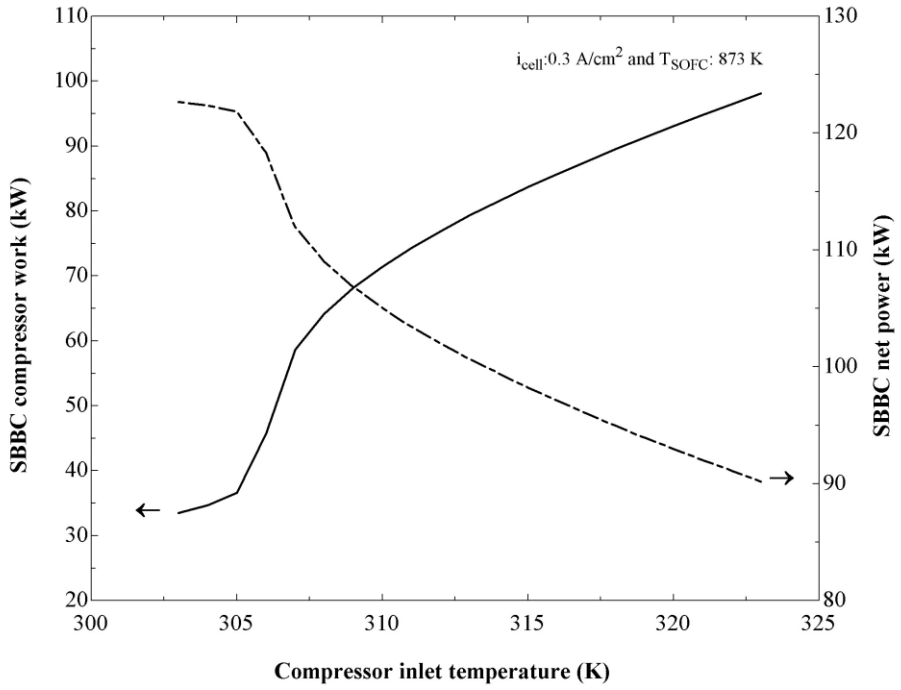

Figure 6.5 Change of net power and compressor work according to compressor inlet temperature

Figure 6.6 illustrates the change in thermal efficiency concerning the compressor inlet temperature. The impact of the high specific heat near the critical point becomes evident in the results. The Brayton cycle attains its highest efficiency at the critical temperature (Gumus, 2019; Li, Ju, & Zhang, 2022; Saeed, Khatoon, & Kim, 2019). Specifically, the SBBC exhibits efficiencies of 0.1505, 0.1514, 0.1472, and 0.1267 at 303, 305, 307, and 323 K, respectively. Furthermore, it's noticeable that higher compressor inlet temperatures have a detrimental effect on net power, as observed in Figure 6.5. Consequently, optimizing the system around the critical pressure and temperature becomes crucial for achieving superior system performance and efficiency. It is noteworthy that system performance and efficiency tend to decline for values surpassing the critical point.

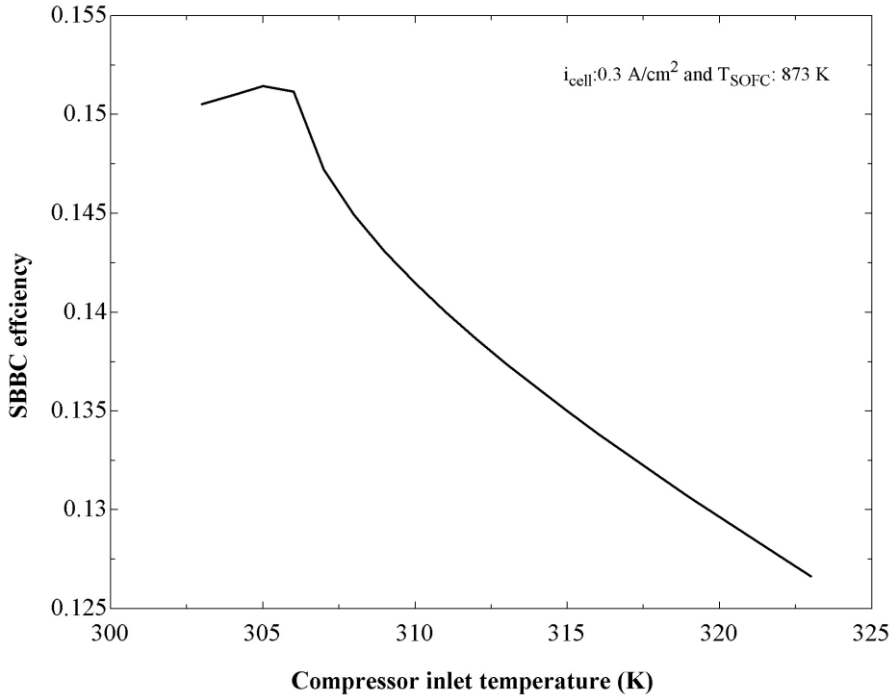

Figure 6.6 Change of SBBC efficiency according to compressor inlet temperature

Figure 6.7-Figure 6.9 were generated using the input parameters listed in Table 5.1 and Table 5.2. ΔT was set at 50 K in Table 5.2, indicating a constant turbine inlet temperature while varying current density. Consequently, changes in SOFC parameters directly impact the mass flow rate of the Brayton cycle. Figure 6.7 depicts the mass flow rate of the cycle as it responds to alterations in current density, with the mass flow rate of the SBBC ranging from 0.1486 to 3.805 kg/s at 873 K. At the specified IT-SOFC operating conditions (0.3 A/cm^2, 873 K), the SBBC exhibits a mass flow rate of 1.154 kg/s. Importantly, current density closely relates to the quantities of fuel and oxygen entering the SOFC, leading to fluctuations in mass flow rate and energy of the products within the SOFC.

A key observation is that the mass flow rate of the Brayton cycle decreases with rising temperature due to the reduction in polarizations within the SOFC at higher temperatures. The extent of irreversibility within the SOFC significantly influences the waste heat generated by the stack.

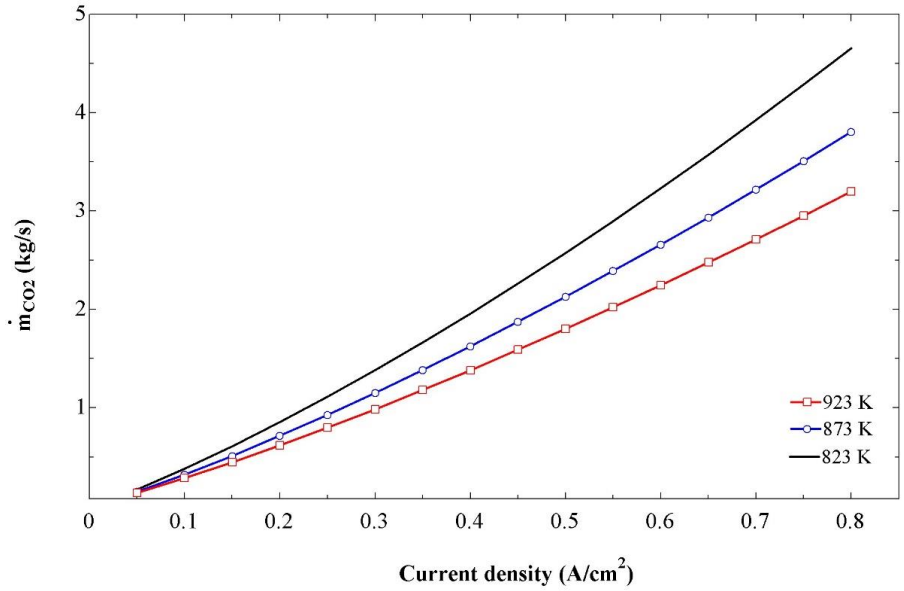

Figure 6.7 The mass flow rate of the SBBC according to the change in current density at different SOFC operating temperatures

Power generated via SBBC and SOFC/SBBC hybrid system demonstrates variability with changes in current density at various SOFC operating temperatures. Figure 6.8 presents the power outputs of both systems in response to current density adjustments, using Eq (5.48). The power output of both the SBBC and the hybrid system increases as current density rises. This correlation is due to an increased quantity of hydrogen reacting in cell, leading to greater energy in output products. Consequently, more heat is supplied to the cycle, contributing to overall power generation (Ugartemendia, Ostolaza, & Zubia, 2013). Moreover, higher current density levels lead to increased voltage losses in SOFCs. Irreversibility within the cell results in higher energy levels for the products exiting the SOFC. Thus, the increased energy of the waste products contributes to the energy of the Brayton cycle.

At low current densities, the increase in SOFC temperature has a limited effect on power produced by SBBC. At a current density of 0.1 A/cm^2, the SBBC generates a net power of 36.66 kW at 823 K, 34 kW at 873 K, and 33.02 kW at 923 K. Notably, the net powers achieved at different temperatures and low current densities exhibit

minor variations due to the strong effect of activation polarization at low current densities. Conversely, at high current density (0.8 A/cm^2), the SBBC demonstrates a more pronounced response to SOFC operating temperature variations, resulting in net powers of 447.2 kW at 823 K, 401.9 kW at 873 K, and 368 kW at 923 K. At typical IT-SOFC operating conditions (0.3 A/cm^2, 873 K), the SBBC generates 121.9 kW of power using the waste heat of the SOFC. Under the same current density, power output reaches 133 kW at 823 K and 113.4 kW at 923 K. Notably, the current density-hybrid system power curve closely resembles the SOFC power density curve, highlighting the substantial contribution of the SOFC to power output in hybrid system. The net power from the SOFC/SBBC hybrid system increases as both current density and SOFC operating temperature rise. At low current density (0.1 A/cm^2), SOFC/SBBC hybrid system produces net powers of 208.8 kW at 823 K, 239 kW at 873 K, and 257.6 kW at 923 K. At high current density (0.8 A/cm^2), the power from the hybrid system reaches 626.4 kW at 823 K, 1034 kW at 873 K, and 1357 kW at 923 K.

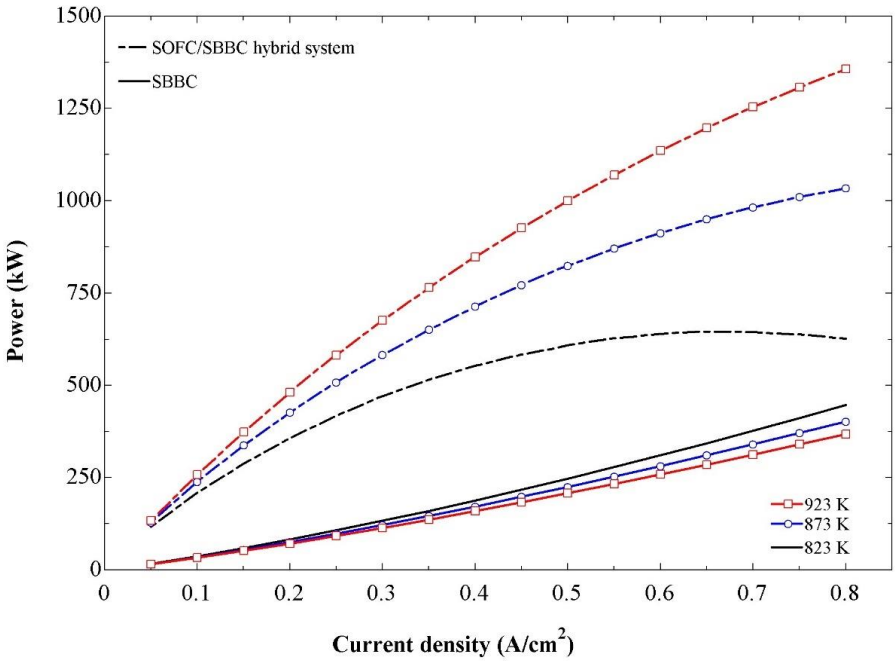

Figure 6.8 Power generated via SBBC and SOFC/SBBC hybrid system with changes in current density at different SOFC operating temperatures

In summary, temperature has a greater impact on power output at high current density compared to low current density. The SOFC/SBBC hybrid system generates 583 kW at specified SOFC operating conditions (0.3 A/cm^2, 873 K), with power outputs of 470 kW at 823 K and 675.6 kW at 923 K under the same current density.

Figure 6.9 depicts efficiency of both SBBC and SOFC/SBBC hybrid system at specified temperatures, considering varying current density with the application of Eq (5.47) and (5.49). Given that only the mass flow rate changes in the SBBC, its efficiency remains constant according to current density.

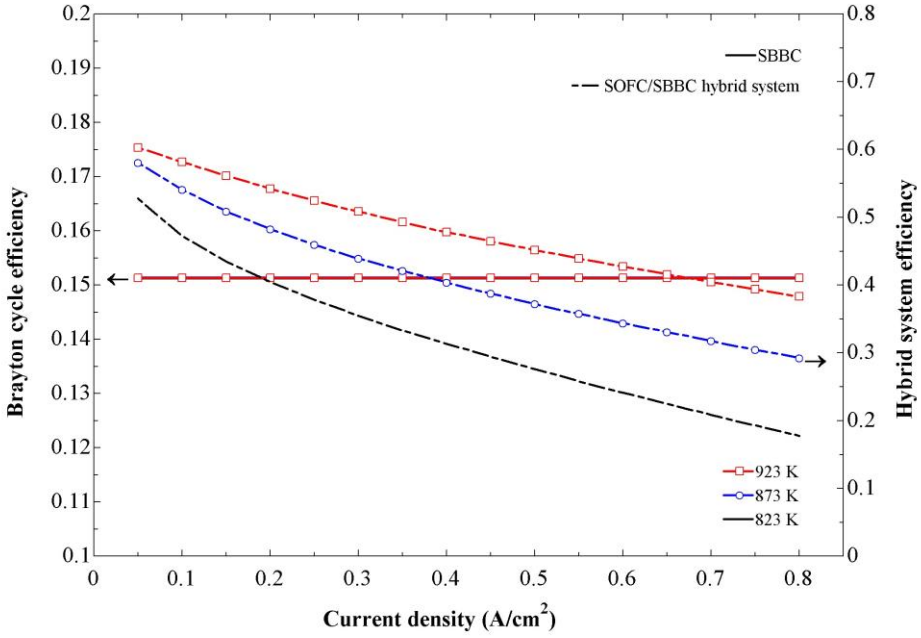

Figure 6.9 The efficiency of SBBC and SOFC/SBBC hybrid system according to current density change at different SOFC operating temperatures

The SBBC achieves efficiencies of 0.1510 at 823 K, 0.1514 at 873 K, and 0.1513 at 923 K. It's notable that a higher efficiency was achieved at 873 K compared to other temperatures, although with minimal differences. To clarify, there was a 0.003 efficiency increase from 823 K to 873 K, followed by a 0.001 efficiency decrease from 873 K to 923 K. These results are consistent with earlier research, (Beygul & Kalinci, 2022; Ceylan & Özgur, 2021). However, this increase was not of significant magnitude and did not make a substantial contribution to overall efficiency (Pan, et

al., 2020). This behavior can be linked to the significant changes in specific heat of S-CO_2 at its critical point.

Efficiency of SOFC/SBBC hybrid system varies with current density, mainly driven by the SOFC stack's behavior, which significantly influences overall system performance. For the SOFC/SBBC efficiency, an increase in current density results in a decrease, reflecting the impact of higher current densities on SOFC stack performance and polarization losses (Tarroja, Mueller, Maclay, & Brouwer, 2010). At low current density (0.1 A/cm^2), hybrid system exhibits efficiencies of 0.47 at 823 K, 0.54 at 873 K, and 0.58 at 923 K. At high current density (0.8 A/cm^2), the hybrid system's efficiencies are 0.18 at 823 K, 0.29 at 873 K, and 0.38 at 923 K.

The highest efficiency value of 0.58 is achieved at 0.1 A/cm^2 current density and 923 K temperature. However, it's important to note that at this current density, the power produced by the hybrid system is relatively low. The highest efficiency values for the hybrid system are attained at 923 K, attributed to the reduction of irreversibility in the SOFC with increasing temperature.

Under standard SOFC operating conditions (0.3 A/cm^2, 873 K), the SOFC system achieves an efficiency of 34.75%. By incorporating waste heat of SOFC and integrating SBBC, hybrid system's efficiency increases to 43.93%. This effective utilization of waste heat elevates efficiency by 9.18%.

6.3 SRBC and SOFC/ SRBC Hybrid System

As discussed earlier in section 5.1.2, the primary objective of incorporating the recuperator is to enhance the Brayton cycle's efficiency by reducing waste heat in the system. Under the typical operating conditions, the IT-SOFC was maintained at a constant current density of 0.3 A/cm^2 and a temperature of 873 K.

Based on the provided input parameters, the waste heat of the SOFC was assessed using the SRBC. The mass flow rate of SRBC behaves similarly to that of SBBC, as explained in section 6.2. At 873 K, the mass flow rate of the SRBC varies between 0.2803-8.952 kg/s. Under the typical IT-SOFC operating conditions (0.3 A/cm^2, 873 K), the SRBC exhibits a higher mass flow rate of 2.502 kg/s compared to SBBC's

mass flow rate of 1.154 kg/s. This difference in mass flow rate is attributed to distinct temperatures of CO_2 fluid entering HEX in both systems, with 340.7 K in the SBBC (Table 5.4) and 643.5 K in the SRBC (Table 5.5). Consequently, the recuperator in the SRBC system gains a substantial amount of heat.

Figure 6.10 illustrates the net power generated in the SRBC and the SOFC/SRBC hybrid system as the current density of the SOFC varies, using Eq (5.48). The current density-power curve closely resembles the SBBC power curve illustrated in Figure 6.8. Both the loop's power output and the hybrid system's power output increase with higher current density and decrease with rising temperature. At a current density of 0.1 A/cm^2, the net power from the SRBC is 77.48 kW at 823 K, 67.38 kW at 873 K, and 61.73 kW at 923 K. At high current density (0.8 A/cm^2), the net power from the SRBC reaches 1088 kW at 823 K, 945.5 kW at 873 K, and 826.2 kW at 923 K. At the specified SOFC operating conditions (0.3 A/cm^2, 873 K), the power produced by the SRBC is 264.3 kW. Under the same current density, this value is 302.5 kW at 823 K and 231.2 kW at 923 K.

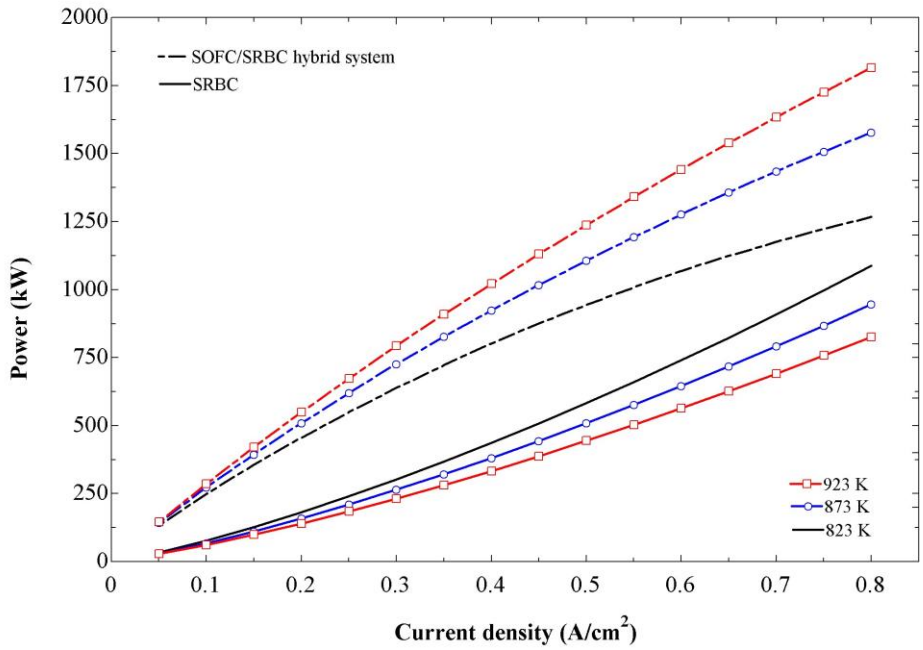

Figure 6.10 SRBC and SOFC/SRBC hybrid system power according to current density variation at different SOFC operating temperatures

Moving on to the SOFC/SRBC hybrid system, at low current density (0.1 A/cm^2), net power is 249.6 kW at 823 K, 272.5 kW at 873 K, and 286.3 kW at 923 K. At high current density (0.8 A/cm^2), the net power from the hybrid system reaches 1267 kW at 823 K, 1578 kW at 873 K, and 1816 kW at 923 K. At the determined SOFC operating conditions (0.3 A/cm^2, 873 K), the power produced by the hybrid system is 725.5 kW. Under the same current density, this value is 639.6 kW for 823 K and 793.3 kW for 923 K.

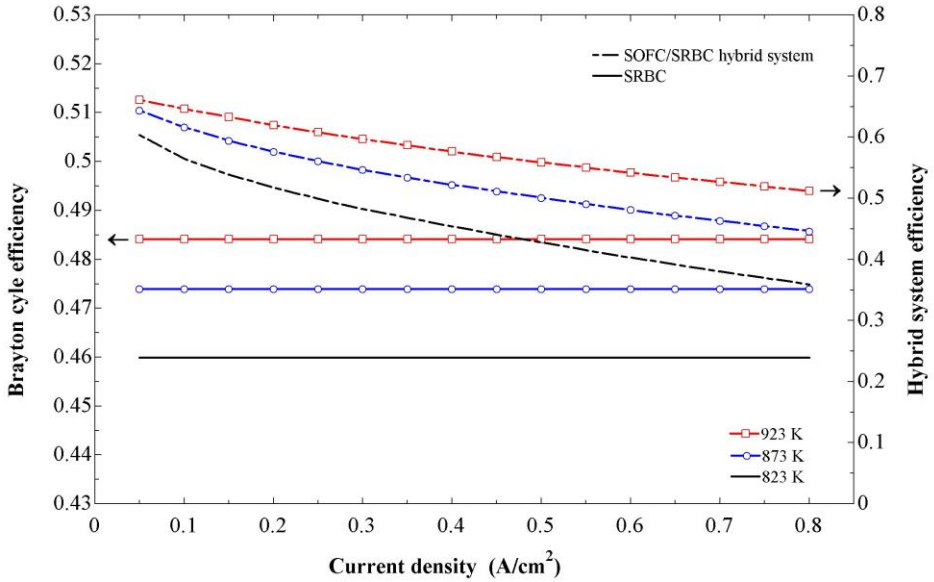

Figure 6.11 Efficiency of SRBC and SOFC/SRBC cycle hybrid system according to current density change at different SOFC operating temperatures

Figure 6.11 illustrates the efficiency of the SRBC and the SOFC/SRBC hybrid system at different temperatures, corresponding to the varying current density of the SOFC. Under the specified SOFC operating conditions (0.3 A/cm^2, 873 K), the efficiency of the SBBC is 15.14%, while the efficiency of the SRBC is 47.4%. The addition of a recuperator to SBBC increased Brayton cycle's efficiency by 32.26%. A notable distinction lies in the impact of the SOFC temperature on SRBC efficiency. The SRBC efficiency reaches 0.4599 at 823 K, 0.474 at 873 K, and 0.4842 at 923 K. The recuperator plays a crucial role in the SRBC system, where its efficiency increases with rising temperature, consequently boosting overall efficiency. For the

SRBC, the SOFC operating temperature proves to be a more important and influential parameter compared to the SBBC.

Furthermore, Figure 6.11 demonstrates the significant role of SOFC efficiency in the efficiency of the SOFC/SRBC hybrid system. The efficiency of the SOFC/SRBC hybrid system behaves similarly to the efficiency curve of the SOFC/SBBC hybrid system illustrated in Figure 6.9. The efficiency obtained from SOFC/SRBC hybrid system is 0.565 at 823 K, 0.616 at 873 K, and 0.6463 at 923 K at low current density (0.1 A/cm^2). Efficiency obtained from SOFC/SRBC hybrid system is 0.3586 at 823 K, 0.4458 at 873 K, and 0.5122 at 923 K, at high current density (0.8 A/cm^2).

Under typical SOFC operating conditions (873 K, 0.3 A/cm^2), the standalone SOFC system's efficiency is 34.75%. Utilizing the waste heat of the SOFC in the SRBC raises the newly created system's efficiency to 54.66%, resulting in a significant 19.91% increase in efficiency. In contrast, the increase in the SOFC/SBBC hybrid system was only 9.18%. This difference highlights the substantial enhancement in system efficiency achieved by adding a recuperator to the cycle.

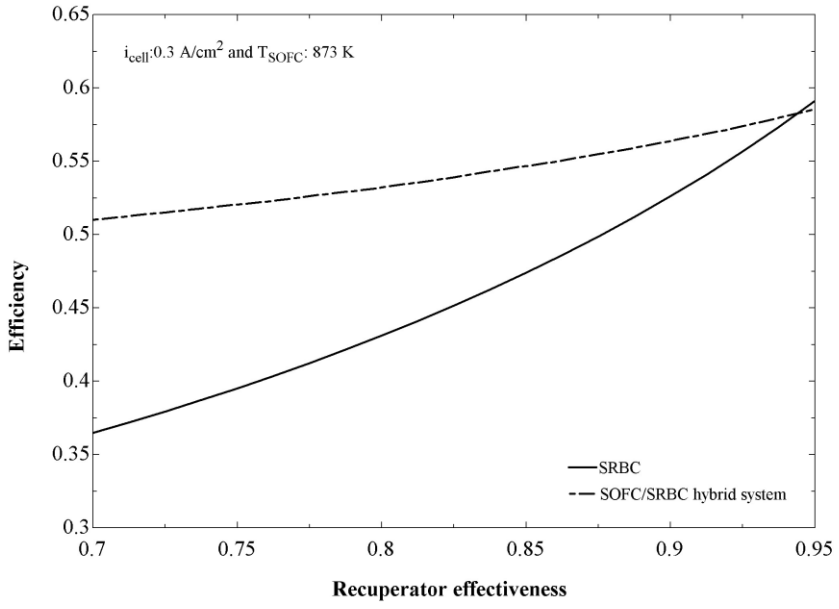

Figure 6.12 Variation of the efficiency of SRBC and SOFC/SRBC hybrid system according to the change of recuperator effectiveness (i_{cell}=0.3 A/cm^2, T_{SOFC}=873 K)

In the SRBC, the recuperator plays a crucial role, with higher exergy destruction in heat exchangers compared to turbomachinery (Sharma, Kaushik, & Manjunath, 2017). According to studies referenced in the literature (Al-Sulaiman & Atif, 2015; de la Calle, Bayon, & Too, 2018), the assessment of heat exchanger effectiveness within the S-CO_2 Brayton cycle spans from 70% to 95%. In Figure 6.12, the impact of recuperator effectiveness on the cycle and hybrid system efficiency was investigated within this specified range. With a recuperator effectiveness of 0.7, the SRBC efficiency is calculated as 0.3646. Increasing the recuperator effectiveness to 0.95 enhances the SRBC efficiency to 0.5913, resulting in a remarkable 29.29% increase in the Brayton cycle's efficiency. The same analysis was extended to the SOFC/SRBC hybrid system. With a recuperator effectiveness of 0.7, the hybrid system's efficiency is 0.5102. Further increasing the recuperator effectiveness to 0.95 improves the hybrid system's efficiency to 0.5856. This indicates a 7.54% enhancement in the hybrid system's efficiency resulting from an improved recuperator efficiency coefficient.

6.4 SRCBC and SOFC/ SRCBC Hybrid System

Another approach to increase efficiency through the utilization of waste heat is the SRCBC. The waste heat from the IT-SOFC was evaluated using the SRCBC, and its mass flow rate change demonstrated a behavior similar to the previously discussed cycles. As calculated using the Eq (5.34-5.46), under typical operating conditions of IT-SOFC (0.3 A/cm^2, 873 K), the mass flow rate of the SRCBC is found to be 2.628 kg/s, with an inlet temperature to the HEX at 654.2 K. The values specified for the SRBC are 2.502 kg/s for mass flow rate and 643.5 K for temperature, as mentioned in Table 5.5. Comparing the inlet temperatures of the HEX, it noticed which heat recovery within Brayton cycle is higher in the SRCBC than in the SRBC.

Figure 6.13 illustrates the net power generated in the SRCBC and the SOFC/SRCBC hybrid system in response to changes in current density using Eq (5.48). The trends resemble those of the first two cycles, and the impact of current density and temperature has been extensively discussed in previous sections. Therefore, only the obtained data will be presented here. At current density of 0.1

A/cm^2, SRCBC generates net power of 60.42 kW at 823 K, 50.74 kW at 873 K, and 45.44 kW at 923 K. At high current density (0.8 A/cm^2), SRCBC achieves a net power of 855.3 kW at 823 K, 717 kW at 873 K, and 611.4 kW at 923 K. At the determined operating condition of the SOFC (0.3 A/cm^2, 873 K), the power produced by SRCBC is 199.8 kW. Under the same current density, this value is 236.9 kW at 823 K and 170.6 kW at 923 K. At low current density (0.1 A/cm^2), net power from the SOFC/SRCBC hybrid system is 232.5 kW at 823 K, 255.9 kW at 873 K, and 270 kW at 923 K. Meanwhile, at high current density (0.8 A/cm^2), the power output from the SRCBC hybrid system reaches 1034 kW at 823 K, 1349 kW at 873 K, and 1601 kW at 923 K. At the specified operating conditions of the SOFC (0.3 A/cm^2, 873 K), the power produced by the hybrid system is 660.9 kW. Under the same current density, this value is 574 kW for 823 K and 732.7 kW for 923 K.

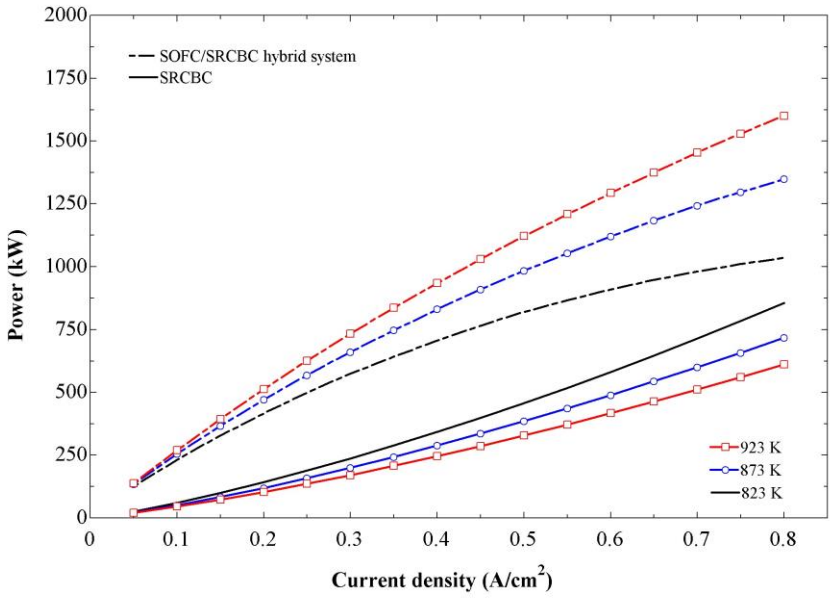

Figure 6.13 SRCBC and SOFC/SRCBC hybrid system power according to current density variation at different SOFC operating temperatures

Figure 6.14 illustrates the efficiencies of the cycle and hybrid system at various SOFC operating temperatures, which were calculated by applying Eq (5.47) and Eq (5.49) while varying the current density. Unlike the first two cycles, the efficiency of the SRCBC decreases as the SOFC operating temperature increases. Specifically, the

efficiency values for the cycle are 0.3654 at 823 K, 0.3628 at 873 K, and 0.3612 at 923 K. The important factor to take into account is the constant temperature difference of 50 K between temperature of SOFC and TIT. Namely, as SOFC temperature escalates, the TIT increases, resulting in a higher temperature at the RC inlet. In the 6.2 section, Figure 6.5 demonstrated how the work required by the compressor increases with a higher inlet temperature of the compressor, leading to a reduction in net power output. In accordance with calculations, at SOFC operating temperature of 823 K, the inlet temperature to the RC in SRCBC is 360.9 K. This temperature then increases to 376.2 K at 873 K, and further to 392.1 K at 923 K. The power consumption of the RC is measured at 97.41 kJ/kg at 823 K, 105.7 kJ/kg at 873 K, and 113.6 kJ/kg at 923 K. Due to the presence of multiple variable parameters, the power is expressed in kJ/kg rather than the power rate (kW) in order to provide a clearer understanding of the outcome. This choice is motivated by the fact that the flow rate decreases as the SOFC temperature increases, as previously explained in Figure 6.7 in the preceding sections. Taking these factors into consideration, it is concluded which increase in the SOFC operating temperature results in higher work requirements for the RC and, consequently, a decrease in overall efficiency.

Under the specified SOFC operating conditions (0.3 A/cm^2, 873 K), the SRCBC achieves an efficiency of 36.28%, while the efficiencies of SBBC and SRCB are 15.14% and 47.4%, respectively. Notably, the efficiency of SRCBC surpasses that of SBBC by 21.06% but falls 11.12% short of the efficiency achieved by SRBC. The significant difference in efficiency between SRCBC and SRBC might be related to addition of a second compressor in SRCBC and necessity for optimization in terms of temperature, split ratio, and heat exchanger effectiveness.

At low current density (0.1 A/cm^2), SOFC/SRCBC hybrid system achieves efficiencies of 0.5264 at 823 K, 0.5784 at 873 K, and 0.6095 at 923 K. Meanwhile, at high current density (0.8 A/cm^2), the efficiencies are 0.2927 at 823 K, 0.3812 at 873 K, and 0.4516 at 923 K. For the medium current density of 0.3 A/cm^2, SOFC/SRCBC hybrid system achieves efficiencies of 0.4332 at 823 K, 0.498 at 873 K, and 0.5513 at 923 K. Under typical operating conditions of the IT-SOFC (873 K, 0.3 A/cm^2), the efficiency of the SOFC stack alone is 34.75%. When evaluating the

waste heat of the SOFC in the SRCBC, the efficiency of the newly created hybrid system is 49.8%. By utilizing waste heat of SOFC, efficiency increases by 15.05%. However, in the SOFC/SRBC hybrid system, this increase is 19.91%, and in the SOFC/SBBC hybrid system, it is 9.18%. Comparatively, the SOFC/SRBC hybrid system exhibits greater efficiency and less system complexity than the SOFC/SRCBC hybrid system, making it more advantageous and preferable under these operating conditions. Another significant point is that the highest efficiency for the SRCBC is achieved at 823 K, indicating that the SRCBC is more efficient at mid-low SOFC operating temperatures (<873 K). In contrast, the SRBC achieves its highest efficiency at 923 K. The crucial role of the recuperator in the SRBC makes it more sensitive to temperature changes, resulting in increased efficiency with rising temperatures. Therefore, the SRBC is advantageous in terms of efficiency at medium-high SOFC operating temperatures (873 K<).

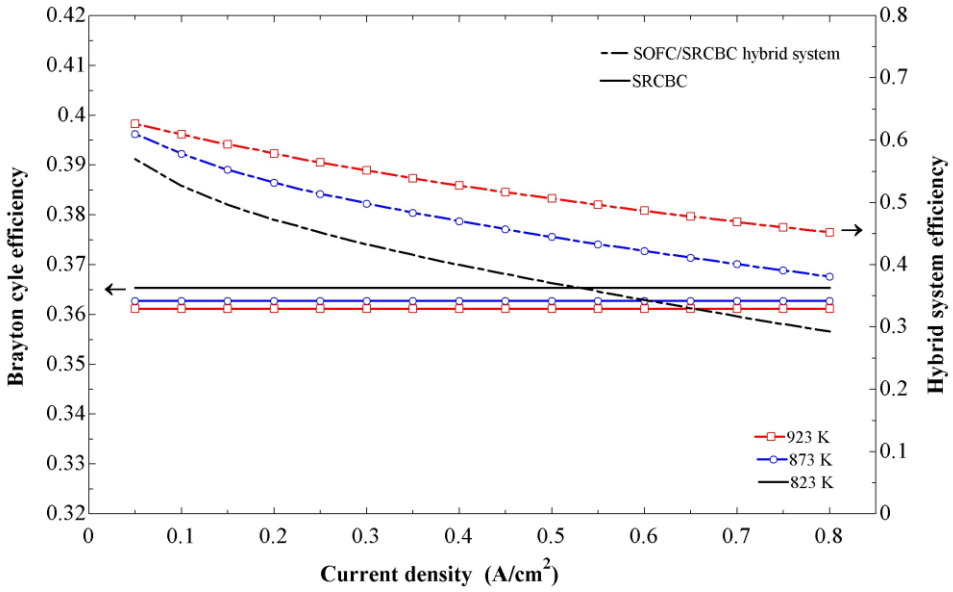

Figure 6.14 Efficiency of SRCBC and SOFC/SRCBC hybrid system according to current density variation at different SOFC operating temperatures

In Figure 6.15, the impact of the RC split rate on efficiency is explored. The input parameters in Table 5.2 are held constant, and only the split rate is considered variable, falling between 0 and 0.5 (Dyreby, Klein, Nellis, & Reindl, 2014). As the

split rate increases, an enhancement in cycle efficiency is evident (Dyreby, Klein, Nellis, & Reindl, 2014). For a split rate of 0.1, the cycle efficiency is 0.329, while at a split rate of 0.5, it increases to 0.3814.

A fraction of fluid exiting LTR is directed to RC, while another segment passes through the cooler and is conveyed to the MC. When the fluid that does not traverse the cooler directly enters the RC, a decrease in heat extraction from the system occurs, leading to an increment in heat retention in system. Consequently, the heat absorbed from the source (Q_{in}) decreases. According to the efficiency formula in Eq (5.47), a decrease in Q_{in} causes an enhancement in efficiency. In calculations, it was found that when the split rate is 0.1, Q_{in} is 597 kW, and when it is 0.5, Q_{in} is 535.2 kW. The effect of altering split rate on efficiency of the SOFC/SRCBC hybrid system is fairly limited. With adjustments made to the split rate from 0.1 to 0.5, the efficiency of the hybrid system experiences a slight improvement, increasing from 49.55% to 50.13%.

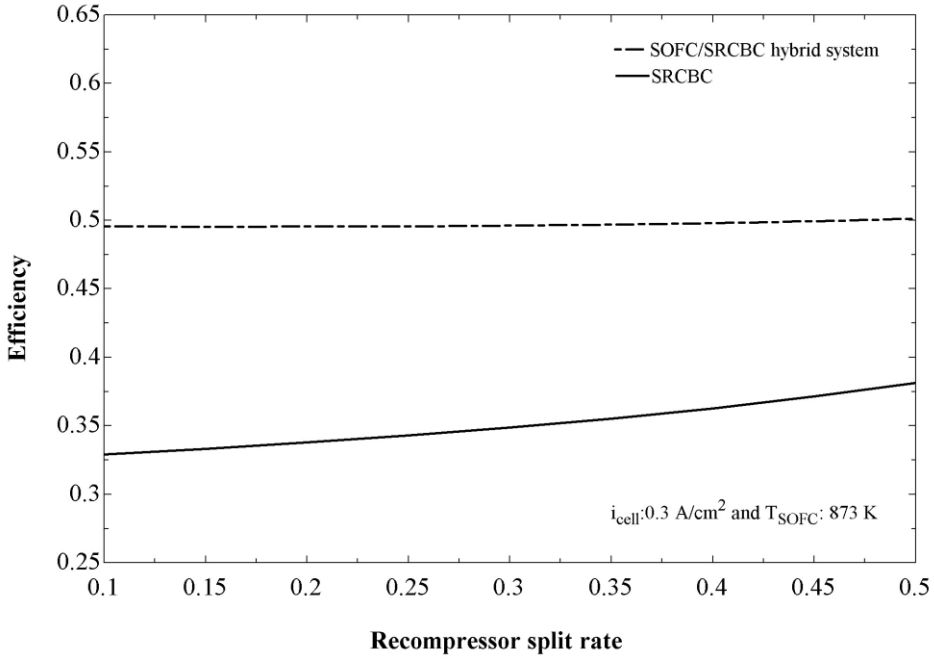

Figure 6.15 Variation of SRCBC and SOFC/SRCBC hybrid system efficiency according to RC split rate change (i_{cell}=0.3 A/cm^2, T_{SOFC}=873 K)

6.5 Comparing Hybrid Systems: SOFC Power Share and Hybrid System Efficiency

Figure 6.16 presents the distribution of power among SOFC and Brayton cycle within specified current density range and at a constant SOFC operating temperature of 873 K. As the current density increases, the share of power attributed to the SOFC also decreases. As mentioned in previous sections, increasing current density leads to higher energy levels for the products exiting the SOFC due to both the increased amount of hydrogen reacting in the fuel cell and the irreversibility within the cell. Consequently, the Brayton cycle's power share of the total hybrid system power increases with rising current density, resulting in a decrease in the SOFC power share.

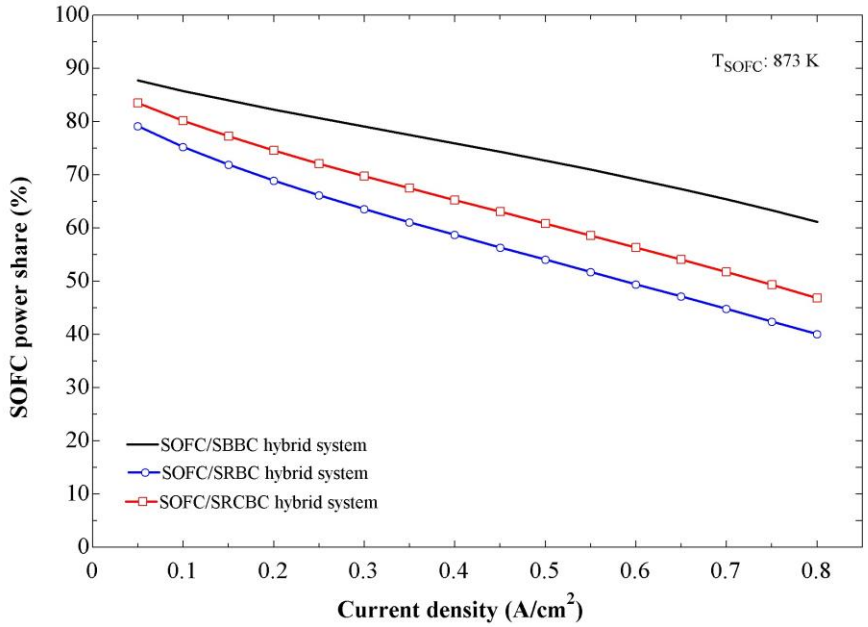

Figure 6.16 SOFC power share in different hybrid systems according to current density change

At a 0.3 A/cm^2 SOFC current density, the power share of the SOFC is as follows: 79.1% in SOFC/SBBC hybrid system, 63.57% in SOFC/SRBC hybrid system, and 69.78% in SOFC/SRCBC hybrid system. Namely, power distribution of Brayton efficiencies in the total hybrid system power is 20.9% for SBBC, 36.43% for SRBC,

and 30.22% for SRCBC. From this, it can be concluded that SOFC/SRBC is particularly superior in converting waste heat into useful work when compared to the other two Brayton cycles.

Figure 6.17 provides a comparative analysis of the efficiencies of different hybrid systems as current density varies, all while maintaining a constant SOFC operating temperature of 873 K. The results show that the SOFC/SRBC hybrid system consistently exhibits higher efficiency across all current densities. At typical temperature and current density of SOFC (873 K, 0.3 A/cm^2), the efficiencies are as follows: the SOFC/SBBC hybrid system at 43.93%, the SOFC/SRBC hybrid system at 54.66%, and the SOFC/SRCBC hybrid system at 49.8%. While the efficiency distinction among SOFC/SRBC hybrid system and SOFC/SRCBC hybrid system is marginal, it is important to consider that the SRCBC system involves a more intricate structure, which can be seen as a drawback in practical applications. Therefore, based on efficiency and performance, SOFC/SRBC hybrid system appears to be more practical and suitable choice for integration with the SOFC system when compared to others.

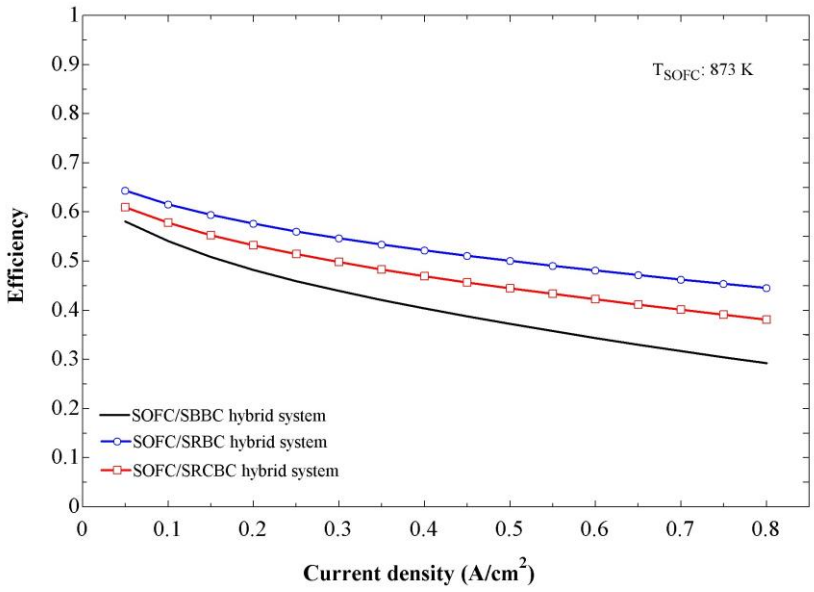

Figure 6.17 Hybrid system efficiencies according to current density change

CHAPTER SEVEN
CONCLUSION AND RECOMMENDATIONS

In this comprehensive study, the integration of IT-SOFCs with different Brayton cycle configurations was rigorously examined to optimize energy utilization and enhance system efficiency. By means of thorough analysis and simulation, details were obtained regarding the performance characteristics of each hybrid system under varying operating conditions. The investigation spanned various aspects, from SOFC behavior to the impact of recuperator effectiveness and split ratios on cycle efficiency. The findings provide a comprehensive understanding of the potential of different hybrid systems.

The analysis of IT-SOFC behavior revealed the intricate interplay of current density, temperature, cell voltage, power density, and efficiency. Activation and ohmic polarizations emerged as critical factors influencing cell voltage and power density. Operating temperature was identified as an important factor of efficiency, with higher temperatures leading to reduced polarization losses and improved efficiency. The study also underscored the importance of optimizing operating conditions to attain the highest power output and efficiency from IT-SOFCs. At the standard operational conditions of the IT-SOFC (873 K, 0.3 A/cm^2), the efficiency of the standalone IT-SOFC stack is measured at 34.75%.

An investigation delved into the characteristics of S-CO_2 fluid, prior to examining impacts of SOFC temperature and current density on S-CO_2 Brayton cycle and SOFC/S-CO_2 Brayton cycle hybrid systems. This study focused on how varying compressor inlet pressure and temperature impacted efficiency, compressor work, and net power of the SBBC. Notably, the system's efficiency peaks around critical pressure and temperature because of characteristic features of S-CO_2. These preliminary insights are crucial for the subsequent analysis, emphasizing the need for optimization around critical values for superior system performance and efficiency.

The mass flow rate of the SBBC shows sensitivity to changes in current density and temperature, with a notable decrease in the Brayton cycle mass flow rate at higher temperatures due to reduced polarizations in the SOFC. The power outputs of SBBC and SOFC/SBBC hybrid system exhibit variability with alterations in current

density and SOFC operating temperatures. Higher current densities contribute to increased power outputs, as the heightened reaction in the fuel cell results in greater energy in the output products, subsequently enhancing overall power generation. The net power from the SOFC/SBBC hybrid system demonstrates a positive correlation with both current density and SOFC operating temperature. Notably, temperature exerts a more substantial influence on power output at high current densities. Under typical SOFC conditions (0.3 A/cm^2, 873 K), the SOFC/SBBC hybrid system exhibits a promising net power of 583 kW, emphasizing the significant role of the SOFC hybrid systems in enhancing overall power output.

The efficiency of the SRBC, particularly influenced by the recuperator, demonstrates a significant boost with higher recuperator effectiveness. At 0.7 effectiveness, the SRBC efficiency is 0.3646, and at 0.95 effectiveness, it rises to 0.5913, marking a substantial 29.29% increase. This effect extends to the SOFC/SRBC hybrid system, where a recuperator effectiveness increases from 0.7 to 0.95 leads to a 7.54% improvement, elevating the efficiency from 0.5102 to 0.5856.

The SRCBC, utilizing waste heat from the IT-SOFC, exhibits characteristics similar to other discussed cycles. The cycle's efficiency, however, decreases with higher SOFC operating temperatures due to increased work requirements for the compressor, reaching 36.28% under specified conditions. Despite surpassing SBBC in efficiency by 21.06%, SRCBC falls short of SRBC by 11.12%, emphasizing the need for optimization in the presence of additional components.

An intriguing and noteworthy revelation arose in relation to the temperature preferences exhibited by different cycles. The SRCBC cycle demonstrated optimal efficiency at lower temperatures (<873 K), while the SRBC cycle excelled at medium to high temperatures (>873 K). This intriguing trend could be attributed to the SRBC recuperator's heightened sensitivity to temperature variations, further underscoring the intricate interplay of system components and their impact on efficiency optimization.

As current density rises, the share of power from the SOFC decreases, influenced by increased hydrogen reactivity and irreversibility. At 0.3 A/cm^2, the power share of the SOFC is 79.1% in the SOFC/SBBC, 63.57% in the SOFC/SRBC, and 69.78% in

the SOFC/SRCBC systems. The power distribution of Brayton efficiencies in the total hybrid system power shows superiority for SOFC/SRBC in converting waste heat into useful work compared to SBBC and SRCBC.

At the standard operating conditions of the IT-SOFC (873 K, 0.3 A/cm^2), the efficiencies stand at 43.93% for the SOFC/SBBC hybrid system, 54.66% for the SOFC/SRBC hybrid system, and 49.8% for the SOFC/SRCBC hybrid system. While the efficiency distinction among SOFC/SRBC hybrid system and SOFC/SRCBC hybrid system is minimal, it is important to consider that the SRCBC system involves a more complex system, which can be seen as a drawback in practical applications. As a synthesis of these findings, the SOFC/SRBC hybrid system emerges as the optimal choice for leveraging the waste heat potential of the IT-SOFC. Its robust efficiency gains and simplified configuration make it a pragmatic solution for practical implementation, showcasing its potential to enhance energy conversion efficiency and promote sustainable energy utilization.

Based on the findings and insights obtained from this study, several recommendations can be made to further enhance the integration of SOFCs with Brayton cycle configurations:

- Optimal Operating Conditions: Continuously explore operating conditions to identify the optimal combination of temperature and current density that yields maximum efficiency and power for hybrid systems.
- Recuperator Effectiveness: In the case of SRBC and SRCBC, further research could focus on optimizing recuperator effectiveness and separation ratios to achieve better efficiency and performance.
- Hybrid System Design: Consider the trade-off between system complexity and performance when choosing between different Brayton cycle configurations. The simpler design of the SOFC/SRBC hybrid system may be advantageous in practical applications.
- Thermal Management: Investigate advanced thermal management strategies to mitigate heat losses and improve overall system efficiency, especially in systems where the waste heat is a crucial component.

- Economic Viability: Perform a comprehensive thermo-economic analysis for the different hybrid systems, considering factors such as materials, manufacturing, maintenance, and potential revenue streams, to determine their economic viability.
- Dynamic Operation Strategies: Develop dynamic control strategies that optimize SOFC and S-CO_2 Brayton cycle operations under varying load conditions, ensuring adaptability and stability.
- Environmental impact analysis: Due to the use of hydrogen considered fuel in SOFC and the closed design of the S-CO_2 Brayton cycle, it is necessary to analyze the environmental impact of system to evaluate whether it is environmentally friendly.

In conclusion, this investigation offers a thorough examination of SOFC system integrated with diverse S-CO_2 Brayton cycle configurations, providing a foundation for developing efficient and sustainable energy systems. The insights gained and recommendations here contribute to improve clean energy technologies and their practical application in the quest for a more sustainable energy future.

REFERENCES

Ahn, Y., Bae, S. J., Kim, M., Cho, S. K., Baik, S., Lee, J. I., & Cha, J. E. (2015). Review of supercritical CO_2 power cycle technology and current status of research and development. *Nuclear Engineering and Technology*, *47*(6), 647-661.

Akroot, A. (2018). *Process Modelling and Optimization of a Planar Solid Oxide Fuel Cell-Micro Gas Turbine Hybrid Power System*. [PhD Thesis]. Ondokuz Mayıs University.

Al-Sulaiman, F. A., & Atif, M. (2015). Performance comparison of different supercritical carbon dioxide Brayton cycles integrated with a solar power tower. *Energy, 82*, 61-71.

Andersson, M. (2009). *SOFC modeling considering mass and heat transfer, fluid flow with internal reforming reactions*. [PhD Thesis]. Lund University.

Andersson, M., Yuan, J., & Sunden, B. (2011). SOFC modeling considering electrochemical reactions at the active three phase boundaries. *International Journal of Heat and Mass Transfer, 55*(2012), 773-788.

Arabacı, S. (2008). *Fırst and Second Law Analyses of a Biomass Fuelled Solid Oxide Fuel Cell- Micro Turbine Hybrid System*. [MSc Thesis]. Middle East Technical Universty.

Arnaiz del Pozo, C., Sánchez Orgaz, S., Rodríguez Martín, J., Jiménez Alvaro, Á., López Paniagua, I., González Fernández, M. C., & Nieto Carlier, R. (2019). Thermal and exergy efficiency analysis of a solar-driven closed brayton power plant with helium & S-CO_2 as working fluids. *17th International Conference on Renewable Energies and Power Quality (ICREPQ'19)*, (pp. 383-389). Tenerife, España.

Aydın, O. (2017). *Elaboration of Spatial Current and Temperature Variations in Microtubular Solid Oxide Fuel Cells by Experimental and Numerical Techniques*. [PhD Thesis] Kyushu University.

Aydın, U. (2018). *Fabrication and Microstructural Investigation of Anode Supported Microtubular Solid Oxide Fuel Cell*. [MSc Thesis], Niğde Omer Halisdemir University.

Beygul, S., & Kalinci, Y. (2022). Thermodynamic analysis of a supercritical CO_2 Brayton cycle integrated with solid oxide fuel cell. *The International Conference on Energy, Environment And Storage of Energy*, (pp. 240-247). Kayseri, Turkiye.

Blennow, P., Hjelm, J., Klemenso, T., Persson, A., Brodersen, K., Srivastava, A., & Mogensen, M. (2009). Development of planar metal supported SOFC with novel cermet anode. *ECS Transactions, 25*(2), 701.

Boaro, M., & Aricò, A. S. (2017). *Advances in medium and high temperature solid oxide fuel cell technology* (Vol. 574). Springer International Publishing.

Bove, R., & Ubertini, S. (2008). *Modeling solid oxide fuel cells: methods, procedures and techniques.* Siprenger Science & Business Media.

BP. (2023). *Statistical Review of world energy 2023.*

Braun, R. J. (2002). *Optimal design and operation of solid oxide fuel cell systems for small-scale stationary applications.* [PhD thesis]. The University of Wisconsin-Madison.

Buonomano, A., Calise, F., d'Accadia, M. D., Palombo, A., & Vicidomini, M. (2015). Hybrid solid oxide fuel cells–gas turbine systems for combined heat and power: A review. *Applied Energy, 156*, 32-85.

Calise, F., Palombo, A., & Vanoli, L. (2006). Design and partial load exergy analysis of hybrid SOFC–GT power plant. *Journal of Power Sources, 158*(1), 225-244.

Campanari, S., & Iora, P. (2004). Definition and sensitivity analysis of a finite volume SOFC model for a tubular cell geometry. *Journal of Power Sources, 132*(1-2), 113-126.

Canavar, M. (2013). *Development of a Stack For Solid Oxide Fuel Cell*. [MSc Thesis] Niğde University.

Cano, Z. P., Banham, D., Ye, S., Hintennach, A., Lu, J., Fowler, M., & Chen, Z. (2018). Batteries and fuel cells for emerging electric vehicle markets. *Nature Energy, 3*(4), 279-289.

Cao, Y., Habibi, H., Zoghi, M., & Raise, A. (2021). Waste heat recovery of a combined regenerative gas turbine-recompression supercritical CO_2 Brayton cycle driven by a

hybrid solar-biomass heat source for multi-generation purpose: 4E analysis and parametric study. *Energy, 236*, 121432.

Celik, A. N. (2018). Three-dimensional multiphysics model of a planar solid oxide fuel cell using computational fluid dynamics approach. *International Journal of Hydrogen Energy, 43*(42), 19730-19748.

Ceylan, V., & Özgur, A. E. (2021). Süperkritik Brayton Çevriminin Termodinamik Analizi. *Mehmet Akif Ersoy Üniversitesi Fen Bilimleri Enstitüsü Dergisi, 12*(1), 500-509.

Chan, S. H., Ho, H. K., & Tian, Y. (2003). Multi-level modeling of SOFC–gas turbine hybrid system. *International Journal of Hydrogen Energy, 28*(8), 889-900.

Chan, S. H., Low, C. F., & Ding, O. L. (2002). Energy and exergy analysis of simple solid-oxide fuel-cell power systems. *Journal of Power Sources, 103*(2), 188-200.

Cheddie, D. F., & Munroe, N. D. (2007). A dynamic 1D model of a solid oxide fuel cell for real time simulation. *Journal of Power Sources, 171*(2), 634-643.

Cheddie, D. F., & Murray, R. (2010). Thermo-economic modeling of a solid oxide fuel cell/gas turbine power plant with semi-direct coupling and anode recycling. *International Journal of Hydrogen Energy, 35*(20), 11208-11215.

Cheng, W. L., Huang, W. X., & Nian, Y. L. (2017). Global parameter optimization and criterion formula of supercritical carbon dioxide Brayton cycle with recompression. *Energy Conversion and Management, 150*, 669-677.

Cicek, Y. (2015). *Development of Anode For Direct Methane Solid Oxide Fuel Cell.* [MSc Thesis]. Niğde University.

Colpan, C. O., Hamdullahpur, F., & Dincer, I. (2010). Heat-up and start-up modeling of direct internal reforming solid oxide fuel cells. *Journal of Power Sources, 195*(11), 3579-3589.

Da Rosa, A. V., & Ordóñez, J. C. (2021). *Fundamentals of renewable energy processes.* Academic Press.

Damo, U., Ferrari, M., Turan, A., & Massardo, A. (2019). Solid Oxide Fuel Cell Hybrid System: A Detailed Review of an Environmentally Clean and Efficient Source of Energy. *Energy, 168*, 235-246.

de la Calle, A., Bayon, A., & Too, Y. C. (2018). Impact of ambient temperature on supercritical CO_2 recompression Brayton cycle in arid locations: Finding the optimal design conditions. *Energy, 153*, 1016-1027.

Deepika, P., Kumar, M., & Sivasankar, P. (2018). A review: Bloom Box- A Solid Oxide Fuel Cell. *International Research Journal of Engineering and Technology, 5*(3), 1562-1567.

Deng, Q. H., Wang, D., Zhao, H., Huang, W. T., Shao, S., & Feng, Z. P. (2017). Study on performances of supercritical CO_2 recompression Brayton cycles with multi-objective optimization. *Applied Thermal Engineering, 114*, 1335-1342.

Doshi, R., Richards, V. L., Carter, J. D., Wang, X., & Krumpelt, M. (1999). Development of solid-oxide fuel cells that operate at 500° C. *Journal of the Electrochemical Society, 146*(4), 1273.

Dyreby, J., Klein, S., Nellis, G., & Reindl, D. (2014). Design considerations for supercritical carbon dioxide Brayton cycles with recompression. *Journal of Engineering for Gas Turbines and Power, 136*(10).

Evcimen, S. (2019). *Development of Anode/ Cathode Electrodes for Solid Oxide Fuel Cells Working at Medium Temperatures*. [MSc Thesis] Nıgde Omer Halisdemir University.

Eyiler, E. (2008). *Heat and Power Integration for a Natural Gas Feed Tubular Solid Oxide Fuel Cell System*. [MSc Thesis]. Gebze Technical University.

Faleh, S., Khir, T., & Ben Brahim, A. (2017). Energetic performance optimization of a SOFC–GT hybrid power plant. *Arabian Journal for Science and Engineering, 42*, 1505-1515.

Fedakar, S. (2012). *Experimental and Simulation Studies of a Grid Connected Solid Oxide Fuel Cell*. [MSc Thesis]. Meliksah University.

Ferrari, M. L., Damo, U. M., Turan, A., & Sánchez, D. (2017). *Hybrid systems based on solid oxide fuel cells: modelling and design.* John Wiley & Sons.

Garg, P., Kumar, P., & Srinivasan, K. (2013). Supercritical carbon dioxide Brayton cycle for concentrated solar power. *The Journal of Supercritical Fluids, 76*, 54-60.

Gumus, E. (2019). Gemi Dizel Motoruna Alternatif: sCO_2 Güç Çevrimi. *Journal of ETA Maritime Science, 7*(2), 117-126.

Hart, D., Jones, S., Houghton, T., Cordobes, X., & Lewis, J. (2022). *The Fuel Cell Industry Review 2021.* E4tech. Retrieved from https://fuelcellindustryreview.com/

Haseli, Y. (2018). Maximum conversion efficiency of hydrogen fuel cells. *International Journal of Hydrogen Energy, 43*(18), 9015-9021.

Haseli, Y., Ibrahim, D., & Naterer, G. F. (2008). Thermodynamic modeling of a gas turbine cycle combined with a solid oxide fuel cell. *International Journal of Hydrogen Energy, 33*(20), 5811-5822.

Huang, Y., & Turan, A. (2020). Mechanical equilibrium operation integrated modelling of hybrid SOFC–GT systems: Design analyses and off-design optimization. *Energy, 208*(118334).

Hui, S. R., Yang, D., Wang, Z., Yick, S., Decès-Petit, C., Qu, W., . . . Ghosh, D. (2007). Metal-supported solid oxide fuel cell operated at 400–600° C. *Journal of Power Sources, 167*(2), 336-339.

IEA. (2022). *World energy outlook 2022.* Paris, France: IEA.

Ilbas, M., & Kumuk, B. (2019). Numerical modelling of a cathode-supported solid oxide fuel cell (SOFC) in comparison with an electrolyte-supported model. *Journal of the Energy Institute, 92*(2019), 682-692.

Ilbas, M., Cımen, F. M., & Kumuk, B. (2021). Numerical comparison of planar and micro- tubular sold oxide fuel cells. *Journal of Polytechnic, 24*(2).

IPCC. (2022). *Climate Change 2022: Impacts, Adaptation, and Vulnerability.*

Isık, R. (2019). *Numerical And Experimental Invetigation of The Effect of Flow Type On Performance And Temperature Distribution in Solid Oxide Fuel Cell.* [MSc thesis] Nigde University.

Jin, Q., Xia, S., & Chen, L. (2023). A modified recompression S–CO_2 Brayton cycle and its thermodynamic optimization. *Energy, 263*, 126015.

Jin, Q., Xia, S., Li, P., & Xie, T. (2022). Multi-objective performance optimization of regenerative S-CO_2 Brayton cycle based on neural network prediction. *Energy Conversion and Management, X*(14), 100203.

Kalinci, Y., & Dincer, I. (2018). Analysis and performance assessment of NH_3 and H_2 fed SOFC with proton-conducting electrolyte. *International Journal of Hydrogen Energy, 43*(11), 5795-5807.

Kaya, M. (2012). *Numerical modelling anode supported tubular solid oxide fuel cell performance analysis*. [MSc Thesis]. Erciyes University.

Kaya, M. (2021). *Development of thermodynamic model of a solid oxide fuel cell integrated gas turbine system*. [MSc Thesis]. Gebze Technical University.

Khan, M. Y. (2019). *Performance Analysis of Solid Oxide Fuel Cell- Gas Turbine Hybrid System.* [MSc Thesis] Sabancı University.

Krüger, M. (2019). Process development for integrated coal gasification solid oxide fuel cells hybrid power plants – Investigations on solid oxide fuel cells/gas turbine hybrid power plants run on clean coal gas. *Applied Energy, 250*, 19-31.

Kumuk, B. (2018). *Mathematical Modelling Analysis of Cathode Supported Solid Oxide Fuel Cell*. [MSc Thesis]. Gazi University.

Kundu, P. P., & Dutta, K. (2016). Hydrogen fuel cells for portable applications. In *In Compendium of Hydrogen Energy* (pp. 111-131). Woodhead Publishing.

Kupecki, J. (Ed.). (2018). *Modeling, Design, Construction, and Operation of Power Generators with Solid Oxide Fuel Cells: From Single Cell to Complete Power System.* Springer.

Le Moullec, Y. (2013). Conceptual study of a high efficiency coal-fired power plant with CO_2 capture using a supercritical CO_2 Brayton cycle. *Energy, 49*, 32-46.

Leah, R. T., Bone, A., Selcuk, A., Corcoran, D., Lankin, M., Dehaney-Steven, Z., & Whalen, P. (2011). Development of Highly Robust, Volume-Manufacturable Metal-Supported SOFCs for Operation Below 600°. *ECS Transactions, 35*(1), 351.

Leah, R. T., Brandon, N. P., & Aguiar, P. (2005). Modelling of cells, stacks and systems based around metal-supported planar IT-SOFC cells with CGO electrolytes operating at 500–600° C. *Journal of Power Sources*, *145*(2), 336-352.

Lee, H. L., Han, N. G., Kim, M. S., Kim, Y. S., & Kim, D. K. (2022). Studies on the effect of flow configuration on the temperature distribution and performance in a high current density region of solid oxide fuel cell. *Applied Thermal Engineering, 206*, 118120.

Lee, J., Lee, J. I., Yoon, H. J., & Cha, J. E. (2014). Supercritical carbon dioxide turbomachinery design for water-cooled small modular reactor application. *Nuclear Engineering and Design*(270), 76-89.

Li, A., Song, C., & Lin, Z. (2017). A Multiphysics fully coupled modelling tool for the design and operation analysis of planar solid oxide fuel cell stacks. *Applied energy, 190*, 1234-1244.

Li, H., Ju, Y., & Zhang, C. (2022). Optimization of supercritical carbon dioxide recompression Brayton cycle considering anti-condensation design of centrifugal compressor. *Energy Conversion and Management, 254*, 115207.

Li, Q., Erqi, E., Qiu, Y., Wang, J., & Zhang, Y. (2022). Conceptual design of novel He-SCO_2 Brayton cycles for ultra-high-temperature concentrating solar power. *Energy Conversion and Management, 260*, 115618.

Li, X. (2007). Thermodynamic performance of fuel cells and comparison with heat engines. *Advances In Fuel Cells, 1*, 1-46.

Liu, M., Lanzini, A., Halliop, W., Cobas, V. R., Verkooijen, A. H., & Aravind, P. V. (2013). Anode recirculation behavior of a solid oxide fuel cell system: A safety analysis and a performance optimization. *International Journal of Hydrogen Energy, 38*(6), 2868-2883.

Liu, Y., Han, J., & You, H. (2019). Performance analysis of a CCHP system based on SOFC/GT/CO_2 cycle and ORC with LNG cold energy utilization. *International Journal of Hydrogen Energy, 44*(56), 29700-29710.

Liu, Y., Wang, Y., & Huang, D. (2019). Supercritical CO_2 Brayton cycle: A state-of-the-art review. *Energy, 189*, 115900.

Luo, X. J., & Fong, K. (2016). Development of 2D dynamic model for hydrogen-fed and methane-fed solid oxide fuel cells. *Journal of Power Sources, 328*(2016), 91-104.

Lv, X., Ding, X., & Weng, Y. (2019). Effect of fuel composition fluctuation on the safety performance of an IT-SOFC/GT hybrid system. *Energy, 174*, 45-53.

Ma, Y., Liu, M., Yan, J., & Liu, J. (2017). Thermodynamic study of main compression intercooling effects on supercritical CO_2 recompression Brayton cycle. *Energy, 140*, 746-756.

Marchionni, M., Bianchi, G., Sayad Saravi, S., & Tassou, S. A. (2019). Modelling and performance analysis of a supercritical CO_2 system for high temperature industrial heat to power conversion at off-design conditions. *3rd European supercritical CO_2 Conference.* Paris, France.

Marra, D., Sorrentino, M., Pianese, C., & Mennella, A. (2015). A one-dimensional modelling approach for planar cylindrical solid oxide fuel cell. *International Conference on Fuel Cell Science, Engineering and Technology, 56611*, V001T05A005.

Massardo, A. F., & Lubelli, F. (2000). Internal reforming solid oxide fuel cell- gas turbine combined cycles (IRSOFC-GT). PartA: cell model and cycle thermodynamic analysis. *ASME Trans J Eng Gas Turbines Power, 122*, 27-35.

McVay, D. (2014). Integration of an Absorption Chiller with a High-Temperature Fuel Cell for Polygeneration of cooling, Heating, Power, and Hydrogen. *University of California*, MSc Thesis.

Mehrpooya, M., Bahramian, P., Pourfayaz, F., & Rosen, M. A. (2016). Introducing and analysis of a hybrid molten carbonate fuel cell-supercritical carbon dioxide Brayton cycle system. *Sustainable Energy Technologies and Assessments, 18*, 100-106.

Mench, M. M. (2008). *Fuel cell engines.* John Wiley & Sons.

Merle, G., Wessling, M., & Nijmeijer, K. (2011). Anion exchange membranes for alkaline fuel cells: A review. *Journal of Membrane Science, 377*(1-2), 1-35.

Ni, M. (2012). Modeling of SOFC running on partially pre-reformed gas mixture. *International Journal of Hydrogen Energy, 37*(2), 1731-1745.

Ni, M. (2013). Modeling and parametric simulations of solid oxide fuel cells with methane carbon dioxide reforming. *Energy and Management, 70*(2013), 116-129.

Njodzefon, J. C., Klotz, D., Kromp, A., Weber, A., & Ivers-Tiffée, E. (2013). Electrochemical modeling of the current-voltage characteristics of an SOFC in fuel cell and electrolyzer operation modes. *Journal of the Electrochemical Society, 160*(4), F313.

Oishi, N., Atkinson, A., Brandon, N. P., Kilner, J. A., & Steele, B. C. (2005). Fabrication of an anode-supported gadolinium-doped ceria solid oxide fuel cell and its operation at 550° C. *Journal of the American Ceramic Society, 88*(6), 1394-1396.

Olabi, A. G., Wilberforce, T., & Abdelkareem, M. A. (2021). Fuel cell application in the automotive industry and future perspective. *Energy, 214*, 118955.

Pan, M., Zhu, Y., Bian, X., Liang, Y., Lu, F., & Ban, Z. (2020). Theoretical analysis and comparison on supercritical CO_2 based combined cycles for waste heat recovery of engine. *Energy Conversion and Management, 219*, 113049.

Pasch, J. J., Fleming, D. D., & Rochau, G. E. (2012). *Supercritical CO_2 recompression Brayton cycle: completed assembly description.* Albuquerque, NM, and Livermore, CA (United States): Sandia National Laboratories (SNL).

Pirkandi, J., Mahmoodi, M., & Ommian, M. (2017). An optimal configuration for a solid oxide fuel cell-gas turbine (SOFC-GT) hybrid system based on thermo-economic modelling. *Journal of Cleaner Production, 144*, 375-386.

Que, Y., Hu, Z., Ren, S., & Jiang, Z. (2022). Thermodynamic Analysis of a Combined Recompression Supercritical Carbon Dioxide Brayton Cycle With an Organic Flash Cycle for Hybrid Solar-Geothermal Energies Power Generation. *Frontiers in Energy Research*, 834.

Rabuni, M. F., Li, T., Punmeechao, P., & Li, K. (2018). Electrode design for direct-methane micro-tubular solid oxide fuel cell (MT-SOFC). *Power Sources, 384*, 287-294.

Ramli, Z. A., Shaari, N., & Saharuddin, T. S. (2022). Progress and major BARRIERS of nanocatalyst development in direct methanol fuel cell: A review. *International Journal of Hydrogen Energy*.

Ranasinghe, S. N., & Middleton, P. H. (2017). Modelling of single cell solid oxide fuel cells using COMSOL multiphysics. *IEEE International Conference on Environment and Electrical Engineering and 2017 IEEE Industrial and Commercial Power Systems Europe* (pp. 1-6). EEEIC/I&CPS Europe.

Rashid, N. L., Samat, A. A., Jais, A. A., Somalu, M. R., Muchtar, A., Baharuddin, N. A., & Isahak, W. N. (2019). Review on zirconate-cerate-based electrolytes for proton-conducting solid oxide fuel cell. *Ceramics International, 45*(6), 6605-6615.

Ritchie, A. J. (2016). *Design, reliability and availability of an SOFC system for data centers.* [MSc Thesis]. University of California.

Sadeghi, M., Mahmoudi, S. M., & Rosen, M. A. (2022). Thermoeconomic analysis of two solid oxide fuel cell based cogeneration plants integrated with simple or modified supercritical CO_2 Brayton cycles: A comparative study. *Energy, 259*, 125038.

Saebea, D., Authayanun, S., Patcharavorachot, Y., & Arpornwichanop, A. (2016). Effect of anode–cathode exhaust gas recirculation on energy recuperation in a solid oxide fuel cell-gas turbine hybrid power system. *Energy, 94*, 218-232.

Saeed, M., Khatoon, S., & Kim, M. H. (2019). Design optimization and performance analysis of a supercritical carbon dioxide recompression Brayton cycle based on the detailed models of the cycle components. *Energy Conversion and Management, 196*, 242-260.

Salogni, A., Iora, P., & Campanari, S. (2009). Dynamic analysis and control of a planar IT-SOFC system. *In International Conference on Fuel Cell Science. 48814*, pp. 879-887. Engineering and Technology.

Sammes, N., Bove, R., & Stahl, K. (2004). Phosphoric acid fuel cells: Fundamentals and applications. *Current Opinion In Solid State and Materials Science, 8*(5), 372-378.

Sánchez, D., Chacartegui, R., Jiménez-Espadafor, F., & Sánchez, T. (2009). A new concept for high temperature fuel cell hybrid systems using supercritical carbon dioxide. *Journal of Fuel Cell Science and Technology, 6*(2), 021306.

Sarı, D. (2017). *Combınatorıal Development of LSC-113/LSC-214 Cathode Materials For Intermediate Temperature Solid Oxide Fuel Cells*. [MSc Thesis] Middle East Technical University.

Sarkar, J. (2009). Second law analysis of supercritical CO_2 recompression Brayton cycle. *Energy, 34*(9), 1172-1178.

Sazali, N., Wan Salleh, W. N., Jamaludin, A. S., & Mhd Razali, M. N. (2020). New perspectives on fuel cell technology: A brief review. *Membranes, 10*(5), 99.

Schöffer, S., Klein, S., Aravind, P., & Pecnik, R. (2021). A Solid Oxide Fuel Cell-Supercritical Carbon Dioxide Brayton Cycle Hybrid System. *Applied Energy, 283*, 115748.

Shao, Z., & Tadé, M. O. (2016). *Intermediate-temperature solid oxide fuel cells* (Vol. 37). Chem. Soc. Rev.

Sharma, O. P., Kaushik, S. C., & Manjunath, K. (2017). Thermodynamic analysis and optimization of a supercritical CO_2 regenerative recompression Brayton cycle coupled with a marine gas turbine for shipboard waste heat recovery. *Thermal Science and Engineering Progress, 3*, 62-74.

Shi, J., & Xue, X. (2010). CFD analysis of a symmetrical planar SOFC with heterogeneous electrode properties. *Electrochimica Acta, 55*(18), 5263-5273.

Soydan, A. M. (2015). *Manufacturing and Development of a 100 Watt Micro Tubular Solid Oxide Fuel Cell System*. [PhD Thesis]. Gebze Technical University.

Spallina, V., Mastropasqua, L., Iora, P., Romano, M. C., & Campanari, S. (2015). Assessment of finite volume modelling approaches for intermediate temperature Solid Oxide Fuel Cells working with CO-rich syngas fuels. *International Journal of Hydrogen Energy, 40*(43), 15012-15031.

Srinivasan, S. (2006). *Fuel cells: from fundamentals to applications.* Springer Science & Business media.

Staniforth, J., & Ormerod, M. (2002). Imlications for using biogas as fuel source for solid oxide fuel cells: internal dry reforming in a small tubular solid oxide fuel cell. *Catalysis Letters, 81*(1-2), 19-23.

Stout, S. D. (2015). *Design and characterization of intermediate temperature solid oxide fuel cells with a honeycomb structure: Operation, research, and opportunities*. [MSc Thesis]. Southern Illinois University.

Tarroja, B., Mueller, F., Maclay, J., & Brouwer, J. (2010). Parametric thermodynamic analysis of a solid oxide fuel cell gas turbine system design space. *Journal of Engineering for Gas Turbines and Power, 132*(7).

Timurkutluk, B. (2007). Performance anaylsıs of an intermediate temperature solid oxide fuel cell. *Mıddle East Technical University*, MSc Thesis.

Timurkutluk, C. (2019). *Devolopment of Micro-Tubular Solid Oxide Fuel Cell Membrane Electrode Assembly for Mobile Applications.* [PhD Thesis] Nigde Omer Halisdemir University.

Tseronis, K., Kookos, I. K., & Theodoropoulos, C. (2008). Modelling mass transport in solid oxide fuel cell anodes: a case for a multidimensional dusty gas-based model. *Chemical Engineering Science, 63*(23), 5626-5638.

Ugartemendia, J., Ostolaza, J. X., & Zubia, I. (2013). Operating point optimization of a hydrogen fueled hybrid solid oxide fuel cell-steam turbine (SOFC-ST) plant. *Energies, 6*(10), 5046-5048.

Utamura, M., Hasuike, H., Ogawa, K., Yamamoto, T., Fukushima, T., Watanabe, T., & Himeno, T. (2012). Demonstration of supercritical CO_2 closed regenerative Brayton cycle in a bench scale experiment. *In Turbo Expo: Power for Land, Sea, and Air, 44694*, 155-164.

Van Biert, L., Woudstra, T., Godjevac, M., Visser, K., & Aravind, P. V. (2018). A thermodynamic comparison of solid oxide fuel cell-combined cycles. *Journal of Power Sources, 397*, 382- 396.

Wang, L., Pan, L. M., Wang, J., Chen, D., Huang, Y., & Hu, L. (2019). Investigation on the temperature sensitivity of the S-CO_2 Brayton cycle efficiency. *Energy, 178*, 739-750.

Weber, A. Z., & Lipman, T. E. (2019). *Fuel cells and hydrogen production.* New York, NY: Springer.

Welaya, Y. M., Mosleh, M., & Ammar, N. R. (2013). Thermodynamic analysis of a combined gas turbine power plant with a solid oxide fuel cell for marine applications. *International Journal of Naval Architecture and Ocean Engineering, 5*(4), 529-545.

Wilberforce, T., Alaswad, A., Palumbo, A., Dassisti, M., & Olabi, A. G. (2016). Advances in stationary and portable fuel cell applications. *International Journal of Hydrogen Energy, 37*, 16509-16522.

Wright, S. A., Conboy, T. M., & Suo-Anttila, A. J. (2011). *Summary of the Sandia Supercritical CO_2 Development Program.* Albuquerque, NM (United States): Sandia National Lab.(SNL-NM).

Yakabe, H., Ogiwara, T., Hishinuma, M., & Yasuda, I. (2001). 3-D model calculation for planar SOFC. *Journal of Power Sources, 102*((1-2)), 144-154.

Yari, M., Mehr, A. S., Mahmoudi, S. M., & Santarelli, M. (2016). A comparative study of two SOFC based cogeneration systems fed by municipal solid waste by means of either the gasifier or digester. *Energy, 114*, 586-602.

Yılmaz, S. (2010). *Solid Oxide Fuel Cell Stack Modeling with Prereformed Natural Gas*. [MSc Thesis]. Ege University.

Zhang, F., Liao, G., Jiaqiang, E., Chen, J., & Leng, E. (2021). Comparative study on the thermodynamic and economic performance of novel absorption power cycles driven by the waste heat from a supercritical CO_2 cycle. *Energy Conversion and Management, 228*, 113671.